



8-2016

Optimal Design of a Thermoelectric Cooling/ Heating System for Car Seat Climate Control (CSCC)

Abdulmunaem H. Elarusi

Western Michigan University, menem1986_juventus@yahoo.com

Follow this and additional works at: http://scholarworks.wmich.edu/masters_theses

 Part of the [Aerospace Engineering Commons](#), and the [Automotive Engineering Commons](#)

Recommended Citation

Elarusi, Abdulmunaem H., "Optimal Design of a Thermoelectric Cooling/Heating System for Car Seat Climate Control (CSCC)" (2016). *Master's Theses*. 720.

http://scholarworks.wmich.edu/masters_theses/720

This Masters Thesis-Open Access is brought to you for free and open access by the Graduate College at ScholarWorks at WMU. It has been accepted for inclusion in Master's Theses by an authorized administrator of ScholarWorks at WMU. For more information, please contact maira.bundza@wmich.edu.



OPTIMAL DESIGN OF A THERMOELECTRIC COOLING/HEATING SYSTEM FOR
CAR SEAT CLIMATE CONTROL (CSCC)

by

Abdulmunaem H. Elarusi

A thesis submitted to the Graduate College
in partial fulfillment of the requirements
for the degree of Master of Science (Mechanical)
Mechanical and Aerospace Engineering
Western Michigan University
August 2016

Thesis Committee:

HoSung Lee, Ph.D., Chair
Chris Cho, Ph.D.
Claudia Fajardo, Ph.D.

OPTIMAL DESIGN OF A THERMOELECTRIC COOLING/HEATING SYSTEM FOR CAR SEAT CLIMATE CONTROL (CSCC)

Abdulmunaem H. Elarusi, M.S.E.

Western Michigan University, 2016

In this work, optimal design of a thermoelectric device itself (element length, cross section area and number of thermoelements) applied in a car seat climate control (CSCC) is studied analytically using our newly developed optimization method. This method, which is based on the thermoelectric ideal equations along with dimensional analysis allows us to simultaneously obtain the best combination of the thermoelectric parameters in order to improve the performance of the thermoelectric device regarding the cooling/heating power and the coefficient of performance (COP). First, this method was implemented to investigate the optimal design of a readily existing air-to-air thermoelectric system. Then, a new system design which includes a fan, a thermoelectric device, and under-seat channels, was designed and tested toward the high system efficiency to validate the analytical model. Several experiments were conducted based on the optimal design model including heating and cooling operating conditions. This design also includes the initial (transient) startup warming and cooling before the car HVAC is active in the cabin. Although this approach is based on the simple thermoelectric ideal equations, the calculated results indicate a good agreement with the experiment.

© 2016 Abdulmunaem H. Elarusi

ACKNOWLEDGEMENTS

Firstly, I would like to express my sincere gratitude to my advisor, Prof. HoSung Lee, for his continuous support of my Master study and related research, for his patience, motivation, and immense knowledge. His guidance helped me in all the time of research and writing of this thesis. I could not have imagined having a better advisor and mentor for my Master study.

Besides my advisor, I would like to thank the rest of my thesis committee: Prof. Chris Cho, and Prof. Claudia Fajardo, for their insightful comments and encouragement, but also for the hard question which incited me to widen my research from various perspectives.

My sincere thanks also goes to Dr. Alaa Attar, who helped me with his experience and knowledge in this field. Without his precious support, it would not be possible to conduct this research.

Last but not the least, I would like to thank my family: my parents and to my brothers and sisters and my friends for supporting me spiritually throughout writing this thesis and my life in general.

Abdulmunaem H. Elarusi

TABLE OF CONTENTS

ACKNOWLEDEMENTS	ii
LIST OF TABLES	vi
LIST OF FIGURES	vii
NOMENCLATURE	x
CHAPTER	
I. INTRODUCTION AND BACKGROUND	1
1.1 Introduction	1
1.1.1 Thermoelectric Climate Control in Car Seats.....	2
1.1.2 Current Work in Thermoelectric Car Seat Climate Control	4
1.2 Background	5
1.2.1 Thermoelectric Governing Effects.....	6
1.2.2 Figure of Merit.....	8
1.2.3 Thermoelectric Ideal Equations	10
1.2.4 Thermoelectric Generator	14
1.2.5 Thermoelectric Cooler	19
1.2.6 Thermal and Electrical Contact Resistances:.....	24
1.2.7 Thermoelectric System	27

Table of contents - continued

CHAPTER		
1.2.8	Heat Sink Design and Optimization	29
II	PROJECT OBJECTIVE AND LITERATURE REVIEW	31
2.1	Problem Statement and Objectives	31
2.2	Literature Review	33
2.2.1	Thermoelectric Cooler for Car Seat Comfort	33
2.2.2	Optimal Design of a Thermoelectric Cooler.....	37
2.2.3	Experimental Investigation of Thermoelectric Systems.....	38
III	ANALYTICAL APPROACH AND EXPERIMENTAL METHOD.....	41
3.1	Calculating the Effective Material Properties	42
3.2	Optimal Design of a Thermoelectric Cooler Using Dimensional Analysis	44
3.3	Optimization of Heat Sink for the Thermoelectric System.....	49
3.4	Experimental Method.....	52
3.4.1	Experimental Overview	53
3.4.2	Experimental Setup.....	54
IV	RESULTS AND DISCUSSION.....	63
4.1	Effective Material Properties	63
4.2	Study of Feher's VTS.....	67
4.3	Feher's VTS Optimal Design.....	72

Table of contents - continued

CHAPTER	
4.4	New Design of the CSCC 77
4.5	Experimental Validation of the New Design 87
4.6	Cooling Mode Experimental Validation 87
4.6.1	Heating Mode Experimental Validation 91
V	CONCLUSIONS AND FUTURE WORK..... 96
5.1	Conclusions 96
5.2	Future Work 98
6	REFERENCES 99

LIST OF TABLES

4.1	Comparison of the Properties and Dimensions of the Commercial Products of Thermoelectric Modules.	64
4.2	Compression Between Feher's VTS Heat Pump Data and The Present Prediction for Cooling and Heating Modes.	70
4.3	Compression Between Feher's VTS Heat Pump Predicted Data and Optimal Design.	75
4.4	Summary of The New CSCC Optimal Design.	83
4.5	Compression of The New CSCC Optimal Design with Feher's VTS Heat Pump Predicted Data and Its Optimal Design.	84
4.6	Optimal Design Performance for Different ZT Values for Cooling Mode.	85
4.7	Optimal Design Performance for Different ZT Values for Heating Mode.....	86
4.8	Comparison Between the Experiment, Prediction, and Optimum Design Results for the Cooling Mode.	90
4.9	Comparison between the Experiment, Prediction, and Optimum Design Results for the Heating Mode.	94

LIST OF FIGURES

1.1 Seebeck Effect.....	6
1.2 Peltier and Thomson Effects [17].....	8
1.3 Dimensionless Figure of Merits for Various Nanocomposite Thermoelectric Materials.....	9
1.4 Cross-section of P-type and n-type Thermocouple.....	12
1.5 Cutaway of Thermoelectric Generator Module.....	14
1.6 Electric Circuit for One Thermocouple with p- and n-type.....	15
1.7 Normalized Chart of TEG with $T_c/T_h = 0.75$ and $ZT = 1$ Used.....	19
1.8 Thermoelectric Cooler with One Thermocouple (p-type and n-type).....	20
1.9 Normalized Chart for Thermoelectric Coolers with $ZTh = 0.75$ Used.....	23
1.10 A Section of a Real Thermoelectric Couple $T_2 > T_1$	24
1.11 Cooling Power Per Unit Area and COP as a Function of Thermoelement Length for Different Values of r and when $s = 0.1mm$, $\psi = 0.2$, $k = 1.5W/mK$, $lc =$ $0.1mm$, $T_1 = 275K$, $T_2 = 300K$, and $Z = 3 \times 10^{-3}K^{-1}$ [17].....	27
1.12 Thermoelectric System (Thermoelectric Cooler Module Attached to Two Heat Sinks).....	28
1.13 Multiple Array Heat Sink.....	29
2.1 Typical Thermoelectric Cooler Module [24].....	32
3.1 (a) Cooling Mode and (B) Heating Mode of the Car Seat Climate Control.....	42
3.2 (a) Thermoelectric Cooler Attached to Two Heat Sinks, and (B) Schematic of a Thermocouple.....	45

List of Figures - continued

3.3 Schematic of the Unit Cell Configuration.....	46
3.4 Schematic of Plate Fin Heat Sink.....	50
3.5 Schematic of the Experimental Setup.	55
3.6 Schematic of the Experimental Setup.	56
3.7 Temperature Extrapolation.....	57
3.8 Test Stand Power Supplies.....	58
3.9 Flowchart of the Experimental Procedure.....	61
3.10 Data Acquisition VI's Front Panel.....	62
4.1 For Module TE-127-1.4-1.15 by TE-Technology, the Comparison Between Calculations with Effective Material Properties and Commercial Data. (A) Cooling Power Versus Temperature Difference as a Function of Current, (B) Cooling Power Versus Input Current as a Function of Temperature Difference, and (C) Cooling Power Versus Temperature Difference as a Function of Voltage.....	67
4.2 Schematic diagram of Feher's VTS Heat Pump. (a) Cooling Mode and (b) Heating Mode.....	68
4.3 Cooling/Heating Power and COP Versus Input Power for Feher's Work and Present Prediction for (a) Cooling Mode and (b) Heating Mode.....	72
4.4 Cooling and Input Power Versus (a) Thermoelement Geometric Ratio and (b) Input Current.	74
4.5 Cooling/Heating Power, Temperature Difference and COP Versus Input Current at Variable Ambient Temperature. (A) Cooling Power Versus Input Current, (B) Heating Power Versus Input Current, (C) Cooling Temperature Difference Versus Input Current, (D) Heating Temperature.....	77
4.6 Schematic of the New CSCC Heat Pump. (A) Cooling Mode and (B) Heating Mode.....	78

List of Figures - continued

4.7 Schematic of the New CSCC Design. (A) The Air Flow Venting System, (B) the Car Seat with the Occupant Seated.	79
4.8 Total Heat Transfer Rate Versus Fin Thickness for (A) Cold Heat Sink and (B) Hot Heat Sink.	80
4.9 Cooling Power, Input Power and COP Versus (A) Dimensionless Input Current and (B) Dimensionless Thermal Conductance.	82
4.10 Cold and Hot Junction Temperatures Versus Current. The Symbols are Measurements and the Lines are Predictions.	88
4.11 Comparison between Experimental and Analytical (A) Cooling Power and (B) COP vs. Input Power.	89
4.12 For Cooling Mode, a Comparison between Experiment, Prediction and Optimal Design COP and Cold Air Temperature Difference as Function of Input Power.	91
4.13 Hot and Cold Junction Temperatures Versus Current. The Symbols are Measurements and the Lines are Predictions.	92
4.14 Comparison between Experimental and Analytical (A) Heating Power and (B) COP as a Function of Input Power.	93
4.15 For Heating Mode, a Comparison between Experiment, Prediction and Optimal Design COP and Hot Air Temperature Difference as Function of Input Power.	95

NOMENCLATURE

A_m	Cross-sectional area of thermoelectric module (mm^2)
A_c	Total heat transfer area at cold heat sink (mm^2)
A_h	Total heat transfer area at heat sink (mm^2)
$A_{s,c}$	Total base area of cold heat sink (mm^2)
$A_{s,h}$	Total base area of hot heat sink (mm^2)
b_c	Profile length of cold heat sink (mm)
b_h	Profile length of hot heat sink (mm)
COP	Coefficient of performance
c_p	Specific heat (J/kgK)
DMU	Driver's Metabolic Unit (%)
G_e	Geometric ratio (mm)
h_c	Convection coefficient of cold fluid (W/m^2K)
h_h	Convection coefficient of hot fluid (W/m^2K)
I	Current (A)
\vec{j}	Electric current density vector (A/m^2)
k	Thermal conductance (W/mK)
l_e	Thermoelement length (mm)
n	Number of thermocouples

Nomenclature—Continued

n_c	Number of fins for the cold heat sink
n_h	Number of fins for hot heat sink
N_c	Ratio of enthalpy flows
N_M	Ratio of enthalpy flow at the cold heat sink to the convection conductance
N_k	Dimensionless thermal conductance
N_I	Dimensionless current
N_h	Ratio of thermal convectance
Nu	Nusselt number
q_x	The rate of heat transfer around the differential element
Q_c	Cooling power (W)
Q_h	Heating power (W)
P_{in}	Input power (W)
PD	Power density (W/cm^2)
R	Electrical resistance (Ω)
T_c	Cold junction temperature (K)
T_h	Hot junction temperature (K)
$T_{\infty c,in}$	Cold fluid inlet temperature (K)
$T_{\infty h,in}$	Hot fluid inlet temperature (K)
$\Delta T_{cooling}$	Cold side temperature difference (K)

Nomenclature—Continued

$\Delta T_{heating}$	Hot side temperature difference (K)
t_c	Fin thickness of cold heat sink (mm)
t_h	Fin thickness of hot heat sink (mm)
V_c	Cold fluid volume flow rate (cfm)
V_h	Hot fluid volume flow rate (cfm)
\dot{W}	Electrical power (W)
x	Direction along the length of the element
Z	Figure of merit ($1/K$)
z_c	Fin spacing of cold heat sink (mm)
z_h	fin spacing of hot heat sink (mm)

Greek symbols

α	Seebeck coefficient (V/K)
ρ	Electric resistivity (Ωcm)
η_c	Total fin efficiency of cold heat sink
η_h	Total fin efficiency of hot heat sink
Π	Peltier coefficient
τ	Thomson coefficient

Nomenclature—Continued

Subscripts

<i>c</i>	Cold
<i>e</i>	Thermoelement
<i>h</i>	Hot
<i>n</i>	n-type element
<i>P</i>	p-type element
opt.	Optimal quantity

Superscript

*	Dimensionless quantity
---	------------------------

CHAPTER I

INTRODUCTION AND BACKGROUND

1.1 Introduction

Thermoelectrics is the science associated with two essential forms of energy; the thermal energy, and the electrical energy. Physically, the thermoelectric effect is the conversion of the thermal energy to electrical energy and vice versa due to the reversibility of the thermoelectric process. In the mode of the cooling or heating, a thermoelectric device (TED) converts the electrical energy represented in the input current into a temperature difference on its hot and cold sides. While in the mode of power generating, TED converts the thermal energy (manifested as the temperature difference across the device) into electrical energy. Thermoelectric devices have become highly attractive because of their solid-state mechanism that does not require any moving parts or working fluids, which decreases mechanical failure. Another advantage of TEDs is that they allow quite cooling/heating and power generating operations unlike the conventional compressor-based refrigerator and fuel-based electric generating systems. Such advantages make TEDs on demand in multiple of applications. Thermoelectric coolers (TECs) are highly involved in heating, ventilations and cooling systems (HVAC) and electronic cooling [1, 2]. TECs also can be seen in many other applications such as in sensitive equipment as medical tools and microprocessors due to their high manufacturability and reliability in the temperature controlling and stabilizing [3]. Thermoelectric generators (TEGs) also have various

applications such as converting the thermal energy in the exhaust waste into electrical energy in automobile and low-grade applications [4, 5]. Also, in solar energy, TEGs converts the thermal energy from the sunlight into electricity that can be used in many other areas [6].

1.1.1 Thermoelectric climate control in car seats

As mentioned above, thermoelectric usage has become well seen in many applicable areas. Nowadays, people are spending huge amounts of money and time on their cars, so a comfortable environment has become one of the priorities in the automobile industry. It was found that the interior temperature of the vehicle is one of the key factors that determines the level of comfort within the car's environment. Human bodies are highly sensitive to the surrounding temperature especially car seats as their closeness and large contact area with the occupants. For example, in the summer, the temperature of the car seats increases as they are exposed to the direct sun or the hotness of the ambient, while in the winter, their temperature decreases because of the coldness. Thus, when driving a car in the hot summer, seats prevent the radiation coming out from occupants' bodies so that they may experience sweating especially during the long-term driving. In contrast, in the winter, the reverse process may occur. Cold seats are usually difficult to warm up due to the contact with the occupants' bodies. Consequently, drivers and passengers are displeased with this disturbance coming from the seats. To avoid coldness, temperature controllers employing electric wires have been used to warm up the car seat, but car seat cooling systems are rarely used. The most wished for car seat would be that which can produce coldness and warmth as a response to the vehicle interior temperature.

Various types of climate control systems have been implemented in car seats. One of the well-known designs is seat covers which are placed on the top of the car seats to provide cooling or heating. However, these systems may not be efficient as they depend on the passive air flow which is not capable of settling the sweating problem mentioned above. Other systems use conditioned air supplied by the main air conditioner in the vehicle (HVAC) and redirect it to the car seats, providing the occupants with the desired conditions. From the early twentieth century, it was found that the car seat with aerated system increase the thermal human comfort [7, 8]. In 2001, climate chamber tests for different types of seats indicated that ventilated perforated material improved the comfort [9]. Also, it is shown that placing seat temperature control unit in series with the automotive HVAC module for humidity control increased body comfort [8]. However, the first time a thermoelectric device was applied to a car seat comfort was in 1990 [9]. Later, thermoelectric cooler for initial startup cooling and heating was applied in a temperature-controlled car seat in 2003 [10]. Recently, a novel disclosed system including a thermoelectric device configured to pump heat for car seat ventilation was reported in 2013 [11]. Currently, Gentherm is one of the leading companies considering this technology, providing their customers with a wide range of thermally controlled car seats (heated, cooled, and ventilated) [12].

One of the features of thermoelectric coolers is that they can provide temperature difference on their two sides which can be switched by reversing the direction of the applied current. The high and the low temperatures on both sides of the TEC can be used to realize a cooler in the summer and heater in the winter. The occupant can easily change from the cooling mode to the heating mode and vice versa by a touch of a button. Therefore,

thermoelectric climate controls for car seats have become more and more competitive, moving from optional to standard vehicle equipment.

1.1.2 Current work in thermoelectric car seat climate control

The analysis or modeling of car seat cooling/heating is rarely discussed in the scientific literature, which infers the inventors' proprietary information. Such analysis is found to be very challenging for some reasons. First, the manufacturers provide the performance curves of their thermoelectric coolers at constant junction temperatures, assuming no thermal resistance between the device and the fluid. This is unrealistic in real applications. Second, the optimization of thermoelectric coolers needs to be done by optimizing several parameters simultaneously using the approach of the iterative method which is analytically very complicated and requires advanced simulating programs. Thus, system designers may face great difficulty to choose suitable thermoelectric modules for their different designs among the wide variety of commercial options available in the market

Recently, Lee (2013) [13] developed a new optimization method based on the dimensionless analysis technique allowing thermoelectric parameters to be optimized simultaneously. The current work employs this optimization method on the thermoelectric car seat climate control to study any possibilities to improve the performance of such system regarding cooling power and the coefficient of performance (COP). Two key factors within the thermoelectric device can be optimized to enhance the performance: the applied current, and the thermoelement geometric ratio (or the number of the thermocouples). However, two technical obstacles should be considered when applying the optimum design method. The first is that the ideal equation used in the optimization method

are formed based on the presumption that the thermal and electrical contact resistances are negligible. Second, the thermoelectric material properties are unknown, and the manufacturers do not usually provide them due to their proprietary information. These two conflicts can be resolved by using the *effective material properties* determined by using the maximum parameters of the thermoelectric device [14]. These maximum parameters are usually provided in the data sheets as modules specifications.

Optimal design is a general analytical approach that requires being validated through measurements. Thus, constructing and experimentally testing the optimized air-to-air thermoelectric car seat climate control is needed to obtain the validity of the optimized analytical model. Based on the optimization of a unit cell, the accuracy of the theoretical model could be obtained by comparing it with the realistic design. Consequentially, this work investigates the optimal design of a single thermoelectric cooler used in car seat climate control, and experimentally validates the performance of the device.

1.2 Background

The thermoelectric phenomenon was discovered in the early 1800s when a German physicist called Thomas Seebeck noticed that an electromotive potential (electrical voltage) was produced within a circuit of two dissimilar materials that had two different temperatures on both sides. This electromotive force was known later as Seebeck effect. Three decades after the discovery of Seebeck effect, a French physicist named Jean Peltier found that Seebeck effect is a reversible process. This means that applying voltage potential through the circuit produces temperature difference on both junctions (one side becomes colder and the other hotter).

1.2.1 Thermoelectric Governing Effects

Seebeck Effect

The Seebeck effect is the conversion of the temperature difference between the two sides of any thermoelectric material into electric current. On both sides of the semiconductor material more electrons and holes become free, and that cause an electrical current to flow through the semiconductor, as shown in Figure 1.1 [15]. The voltage produced is proportional to the temperature, which can be formulated as following,

$$V = \alpha \Delta T \quad (1.1)$$

Where α is now as the Seebeck coefficient, and ΔT is the temperature difference across the thermoelectric material.

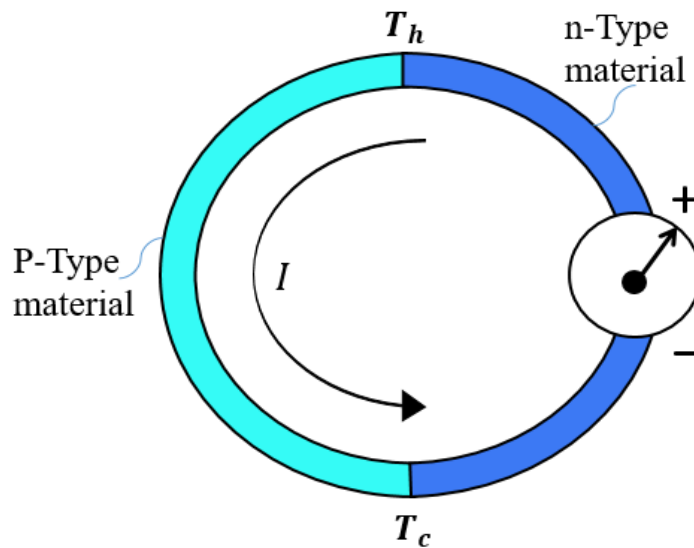


Figure 1.1 Seebeck effect

Peltier Effect

In 1834, a French physicist named Jean Peltier discovered that When current is passes through a junction between two conductors, heat must be released on one side and absorbed on the other side to maintain the temperature of the junction constant (see Figure 1.2) [16]. The heat flux flowing across the junction is a function of the current, which can be written as,

$$Q_{Peltier} = \Pi * I \quad (1.2)$$

Where $Q_{Peltier}$ is the amount of heat liberated or absorbed, Π is the Peltier coefficient, and I is the current passing through the junction.

Thomson Effect

The last effect is Thomson effect which is similar to Peltier effect in which heat is released or absorbed when an electric current is passing through a thermoelectric material, but in this effect temperature gradient is needed to complete the process (see Figure 1.2) [17]. The heat flux due to Thomson effect is proportional to the current and the temperature difference, which leads to,

$$Q_{Thomson} = \tau I \Delta T \quad (1.3)$$

Where $Q_{Thomson}$ is the heat flux, τ is Thomson coefficient, I is the flowing current, and ΔT is the temperature difference in the junction.

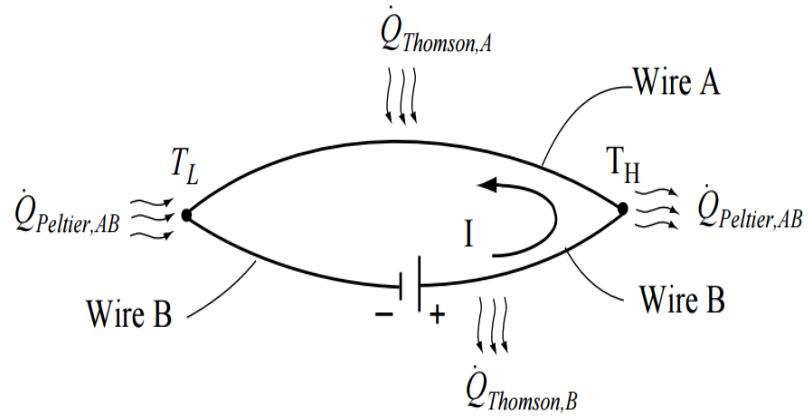


Figure 1.2 Peltier and Thomson effects [17].

1.2.2 Figure of Merit

The performance of any thermoelectric material is usually referred to as the figure of merit (Z) of that material, which can be defined mathematically as following,

$$Z = \frac{\alpha^2}{\rho k} \quad (1.4)$$

Where ρ is the electrical resistivity and k is the thermal conductivity. These three material properties are temperature dependent. Thus, for convenience, the dimensionless figure of merit is represented by multiplying in the average operating temperature \bar{T} which is given as $\bar{T} = \frac{T_c + T_h}{2}$. Materials that have higher a figure of merit values are considered to be good thermoelectric materials. As seen from Equation (1.4), there are potentials to improve the Z value either by increasing the Seebeck coefficient and the electrical resistivity (the power factor $PF = \alpha^2/\rho$) or by decreasing the thermal conductivity of the material. However, increasing one of the PF components may cause the other component to increase because they are proportionally related to each other.

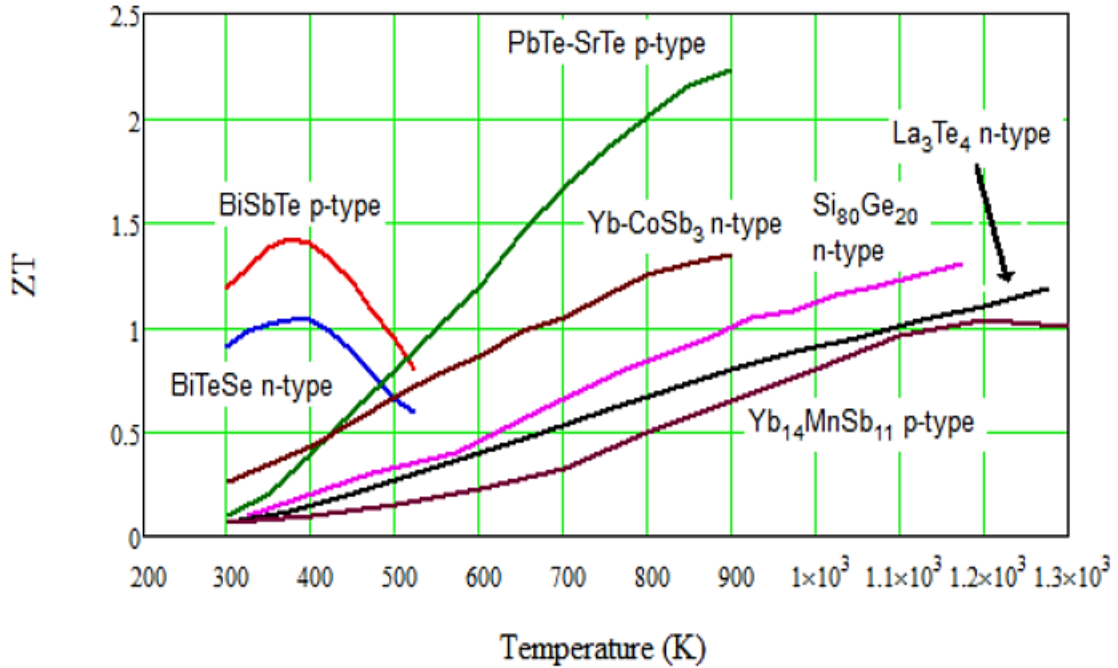


Figure 1.3 Dimensionless figure of merits for various nanocomposite thermoelectric materials [18].

Figure 1.3 indicates the most recent updated ZT values for several commonly used semiconductors versus the operating temperature. As shown in this figure, Bismuth telluride (Bi_2Te_3) has the highest ZT (about 1.4) value at room temperature, which makes it the best favorable semiconductor for cooling applications and low-grade waste heat recovery. On the other hand, at higher operating temperature as in the exhaust waste heat recovery, lead telluride (PbTe) materials have the higher ZT value (about 2.1). At a temperature exceeding 1000 K, it is found that materials like silicon germanium (SiGe) and lanthanum telluride (La_3Te_4) materials are the best.

There has been an enormous amount of research dedicated to enhancing the Z value. One of the most promising technology to increase the ZT value is nanotechnology,

which is focusing on limiting the thermal conductivity by manipulating the electron and phonon scattering through reducing the scattering mean free path [19, 20].

1.2.3 Thermoelectric Ideal Equations

General Ideal Equations:

Assuming a non-uniformly heated material with isotropic properties, the continuity equation for a constant current can be written as,

$$\vec{\nabla} \cdot \vec{j} = 0 \quad (1.5)$$

Where $\vec{\nabla}$ is the differential operation on length, and \vec{j} is the current factor. According to Ohm's Law and the Seebeck effect, the electric field, which is mostly effected by the temperature gradient $\vec{\nabla}T$ and the flowing current \vec{j} , can be expressed as,

$$\vec{E} = \vec{j}\rho + \alpha\vec{\nabla}T \quad (1.6)$$

The heat flow is also affected by the temperature gradient $\vec{\nabla}T$ and the electric field \vec{E} . Thus, the heat flow density can be defined using the Thomson relationship and the Onsager's principle [21], as following,

$$\vec{q} = \alpha T \vec{j} - K \vec{\nabla}T \quad (1.7)$$

Where $\alpha T \vec{j}$ is the Peltier heat contribution, T is the temperature of the junction through which the heat flux flows, and $K \vec{\nabla}T$ is the heat transfer from the Fourier's Law of conduction. The general form of the rate of heat diffusion is given by,

$$-\vec{\nabla} \cdot \vec{q} + \dot{q} = \rho C_p \frac{\partial T}{\partial t} \quad (1.8)$$

Where \dot{q} is the heat flow by unit volume, ρ is the density of the material through which the heat flowing, C_p is the specific heat capacity, and $\frac{\partial T}{\partial t}$ is the rate of change in temperature with respect to time. Thus, for steady state condition ($\frac{\partial T}{\partial t} = 0$), Equation (1.8) is reduced to,

$$\dot{q} = \vec{\nabla} \cdot \vec{q} \quad (1.9)$$

The heat flux can be defined as a function of the electric power as,

$$\dot{q} = \vec{E} \cdot \vec{j} = j^2 \rho + \vec{j} \cdot \alpha \vec{\nabla} T \quad (1.10)$$

Substituting Equations (1.3) and (1.7) into Equation (1.6) yields to,

$$\vec{\nabla} \cdot (K \vec{\nabla} T) + j^2 \rho - T \frac{d\alpha}{dT} \vec{j} \cdot \vec{\nabla} T = 0 \quad (1.11)$$

Where $\tau = T \frac{d\alpha}{dT}$ is known as Thomson coefficient. The second term of Equation (1.11) is the Joule heating, and the third term is the Thomson heat. As mentioned above, assuming that the material properties are temperature independent, which means that the Thomson coefficient is equal to zero. Previous studies have indicated the disparity between the exact solution including the Thomson effect and the exact solution neglecting the Thomson effect is very small and can be neglected. As such, this work considers negligible Thomson effect [22, 23].

Considering a steady state one-dimensional thermoelectric module which consists of n number of p-type and n-type thermocouples as shown in Figure 1.4, and assuming that the thermal and electrical contact resistances have slight effect and can be neglected, and

there are no radiation or convection heat losses through the boundaries, Equation (1.11) can be reduced to,

$$\frac{d}{dx} \left(kA \frac{dT}{dx} \right) + I^2 \frac{\rho}{A} = 0 \quad (1.12)$$

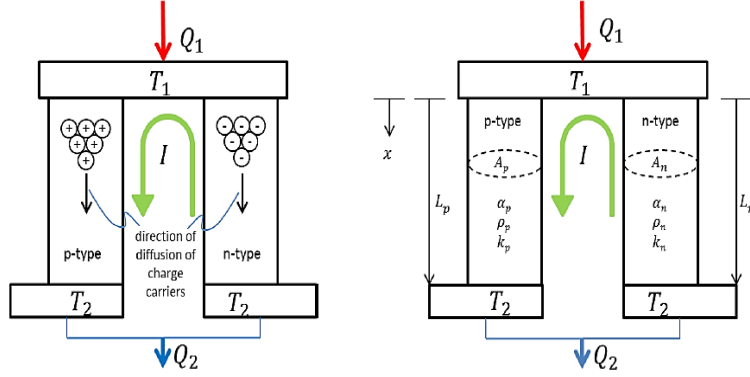


Figure 1.4 Cross-section of P-type and n-type thermocouple.

To solve Equation (1.12), which is a differential equation, a set of boundary conditions is required. These boundary conditions can be defined as functions of position (x) from *Figure 1.4* as ($T_{x=0} = T_h$ and $T_{x=L} = T_c$). Therefore, after integrating Equation (1.12) and applying the boundary conditions, the solution is expressed as following,

$$\left. \frac{dT}{dx} \right|_{x=0} = \frac{(T_2 - T_1)}{L} + I^2 \frac{\rho L}{2kA^2} \quad (1.13)$$

$$\left. \frac{dT}{dx} \right|_{x=L} = \frac{(T_2 - T_1)}{L} - I^2 \frac{\rho L}{2kA^2} \quad (1.14)$$

Consequently, Equation (1.7) is expressed for either p-type or n-type as,

$$q_{p_{x=0}} = \alpha_p T_1 I - \frac{1}{2} \rho_p \frac{L}{A} I^2 + \frac{Ak_p}{L} (T_1 - T_2) \quad (1.15)$$

$$q_{n_{x=0}} = -\alpha_n T_1 I - \frac{1}{2} \rho_n \frac{L}{A} I^2 + \frac{A k_n}{L} (T_1 - T_2) \quad (1.16)$$

Similarly, the heat flux equation is carried out at $x = L$ for the p-type and the n-type as following,

$$q_{p_{x=L}} = \alpha_p T_1 I + \frac{1}{2} \rho_p \frac{L}{A} I^2 + \frac{A k_p}{L} (T_1 - T_2) \quad (1.17)$$

$$q_{n_{x=L}} = -\alpha_n T_1 I + \frac{1}{2} \rho_n \frac{L}{A} I^2 + \frac{A k_n}{L} (T_1 - T_2) \quad (1.18)$$

Taking the summation of Equations (1.15), (1.16), (1.17), and (1.18), the total heat flux at positions 1 and 2 can be formulated as,

$$Q_1 = n[(\alpha_p - \alpha_n) T_1 I - \frac{1}{2} I^2 \left(\frac{\rho_p L_p}{A_p} + \frac{\rho_n L_n}{A_n} \right) + \left(\frac{k_p A_p}{L_p} + \frac{k_n A_n}{L_n} \right) (T_1 - T_2)] \quad (1.19)$$

$$Q_2 = n[(\alpha_p - \alpha_n) T_2 I + \frac{1}{2} I^2 \left(\frac{\rho_p L_p}{A_p} + \frac{\rho_n L_n}{A_n} \right) + \left(\frac{k_p A_p}{L_p} + \frac{k_n A_n}{L_n} \right) (T_1 - T_2)] \quad (1.20)$$

Where again n is the number of thermocouples within the thermoelectric module.

Equations (1.19) and (1.20) can be reduced to,

$$Q_1 = n[\alpha T_1 I - \frac{1}{2} R I^2 + K(T_1 - T_2)] \quad (1.21)$$

$$Q_2 = n[\alpha T_2 I + \frac{1}{2} R I^2 + K(T_1 - T_2)] \quad (1.22)$$

Where,

$$\alpha = \alpha_p - \alpha_n \quad (1.23)$$

$$R = \frac{\rho_p L_p}{A_p} + \frac{\rho_n L_n}{A_n} \quad (1.24)$$

$$K = \frac{k_p A_p}{L_p} + \frac{k_n A_n}{L_n} \quad (1.25)$$

α , R and K are the total Seebeck coefficient, electric resistance, and thermal conductance, respectively.

1.2.4 Thermoelectric Generator

A thermoelectric generator is a device which converts the thermal energy represented by the temperature gradient through the thermoelectric device into electric power. Figure 1.5 shows a cutaway of thermoelectric generator module that consists of many p-type and n-type thermocouples connected thermally in parallel and electrically in series.

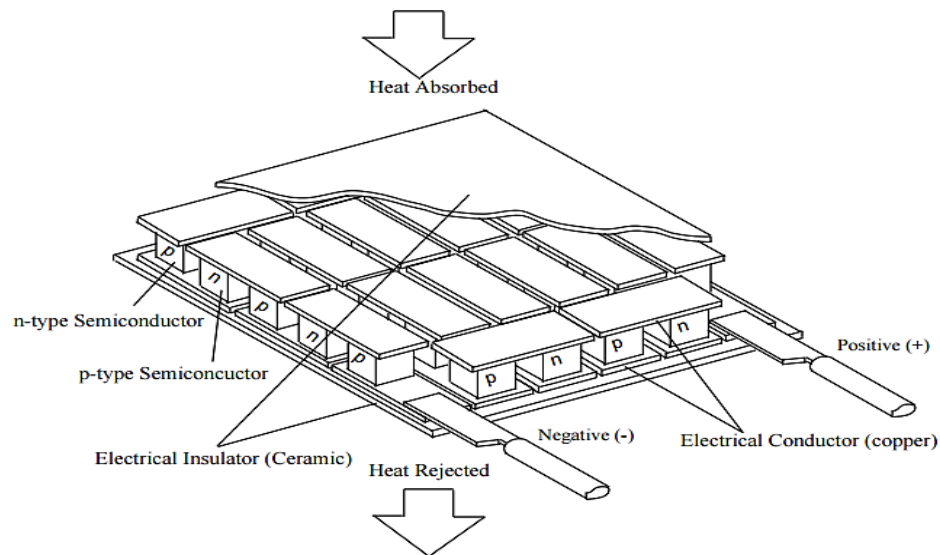


Figure 1.5 Cutaway of thermoelectric generator module.

For the thermoelectric generator, the 1 and 2 states in Equations (1.21) and (1.22) are replaced with the h and c for hot and cold sides, respectively, as shown in Figure 1.6. Thus, the thermoelectric ideal equations for thermoelectric generator can be modified using the respective hot and cold junction temperatures as following,

$$Q_h = n[\alpha T_h I - \frac{1}{2} R I^2 + K(T_h - T_c)] \quad (1.26)$$

$$Q_c = n[\alpha T_c I + \frac{1}{2} R I^2 + K(T_h - T_c)] \quad (1.27)$$

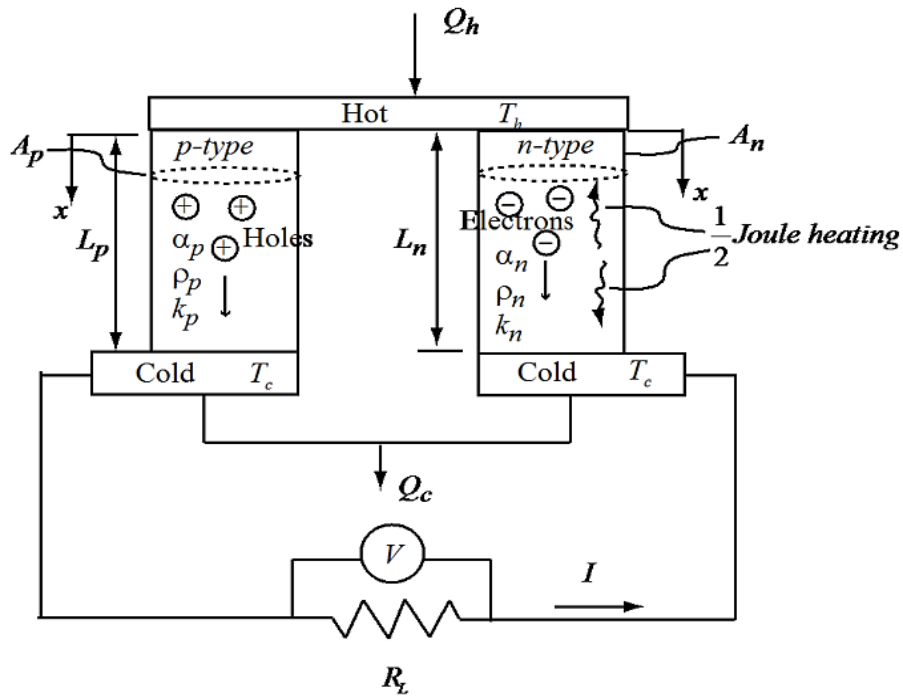


Figure 1.6 Electric circuit for one thermocouple with p- and n-type elements.

From the 1st law of Thermodynamics, the total power for a thermoelectric module is given by $W_{in} = Q_h - Q_c$, or it can be expressed in terms of the internal properties as,

$$W_{in} = n[\alpha I(T_h - T_c) - I^2 R] \quad (1.28)$$

Or, in terms of the external load resistance (R_L) as,

$$W_{\dot{n}} = nI^2R_L \quad (1.29)$$

Also, from Ohm's Law we have,

$$V_n = nIR_L = n[\alpha(T_h - T_c) - IR] \quad (1.30)$$

Rearranging Equation (1.30) the current is given as,

$$I = \frac{\alpha(T_h - T_c)}{R_L + R} \quad (1.31)$$

Consequently, Equation (1.30) can be re-represented independent of the current as following,

$$V_n = \frac{n\alpha(T_h - T_c)}{\frac{R_L}{R} + 1} \left(\frac{R_L}{R}\right) \quad (1.32)$$

Inserting Equation (1.31) into Equation (1.29) gives,

$$W_{\dot{n}} = \frac{n\alpha^2(T_h - T_c)^2}{R} \left[\frac{\frac{R_L}{R}}{\left(\frac{R_L}{R} + 1\right)^2} \right] \quad (1.33)$$

From the definition of the thermal efficiency ($\eta_{th} = \frac{W_{\dot{n}}}{Q_{\dot{h}}}$), the thermal efficiency of a thermoelectric generator can be obtained by inserting Equation (1.26) and (1.29) into the thermal efficiency equation as,

$$\eta_{th} = \frac{\left(1 - \frac{T_c}{T_h}\right) \frac{R_L}{R}}{\left(1 - \frac{R_L}{R}\right) - \frac{1}{2} \left(1 - \frac{T_c}{T_h}\right) + \frac{1}{2Z\bar{T}} \left(1 - \frac{R_L}{R}\right)^2 \left(1 + \frac{T_c}{T_h}\right)} \quad (1.34)$$

Where $1 - \frac{T_c}{T_h}$ is known as Carnot cycle efficiency, and $\bar{T} = \frac{T_h + T_c}{2}$ is the average temperature.

To obtain the maximum conversion efficiency, we differentiate Equation (1.34) with respect to $\frac{R_L}{R}$ and equate the result to zero, which gives,

$$\frac{R_L}{R} = \sqrt{1 + Z\bar{T}} \quad (1.35)$$

Inserting Equation (1.35) into Equation (1.34) leads to,

$$\eta_{max} = \left(1 - \frac{T_c}{T_h}\right) \frac{\sqrt{1 + Z\bar{T}} - 1}{\left(\sqrt{1 + Z\bar{T}} + \frac{T_c}{T_h}\right)} \quad (1.36)$$

Similarly, for the maximum power output, Equation (1.33) is differentiated with respect to the resistance ratio $\frac{R_L}{R}$ and equating the result to zero resulting in $\frac{R_L}{R} = 1$, which reduces Equation (1.33) to,

$$W_{max} = \frac{n\alpha^2(T_h - T_c)^2}{4R} \quad (1.37)$$

At the maximum power output, there is also a maximum power efficiency which can be obtained by letting $\frac{R_L}{R} = 1$ in Equation (1.34), which results in,

$$\eta_{mp} = \frac{\left(1 - \frac{T_c}{T_h}\right)}{2 - \frac{1}{2}\left(1 - \frac{T_c}{T_h}\right) + \frac{2}{Z\bar{T}}\left(1 + \frac{T_c}{T_h}\right)} \quad (1.38)$$

The maximum current, which occurs at the short circuit ($R_L = 0$), and maximum voltage, which occurs at the open circuit ($I = 0$), they can be defined as,

$$I_{max} = \frac{\alpha(T_h - T_c)}{R} \quad (1.39)$$

$$V_{max} = n\alpha(T_h - T_c) \quad (1.40)$$

The normalized parameters of a thermoelectric generator can be obtained by dividing the performance parameters by the maximum parameters. The normalized current is formulated by dividing Equations (1.31) by Equation (1.39) as,

$$\frac{I}{I_{max}} = \frac{1}{\frac{R_L}{R} + 1} \quad (1.41)$$

Equations (1.32) and (1.40) give the maximum voltage as,

$$\frac{V}{V_{max}} = \frac{\frac{R_L}{R}}{\frac{R_L}{R} + 1} \quad (1.42)$$

The normalized power output is obtained from Equations (1.33) and (1.37) as,

$$\frac{W}{W_{max}} = \frac{4 \frac{R_L}{R}}{\left(\frac{R_L}{R} + 1\right)^2} \quad (1.43)$$

Equations (1.43) and (1.36) give the normalized thermal efficiency as,

$$\begin{aligned} \frac{\eta_{th}}{\eta_{max}} &= \frac{\frac{R_L}{R} \left(\sqrt{1 + Z\bar{T}} + \frac{T_c}{T_h} \right)}{\left[\left(\frac{R_L}{R} + 1 \right) - \frac{1}{2} \left(1 - \frac{T_c}{T_h} \right) + \frac{1}{2Z\bar{T}} \left(\frac{R_L}{R} + 1 \right)^2 \left(1 + \frac{T_c}{T_h} \right) \right] \left(\sqrt{1 + Z\bar{T}} - 1 \right)} \end{aligned} \quad (1.44)$$

Figure 1.7 shows a plot of the normalized parameters of a thermoelectric generator. This chart was created using Equations (1.41) - (1.44). As seen from this figure, the maximum power output occurs at the resistance ratio of 1, and the normalized efficiency has the same trend in the curve as the normalized power output. However, the maximum

normalized efficiency occurs at a higher value of the resistance ratio (about 1.5). Note that this chart is created at $\frac{T_c}{T_h} = 0.75$ and $Z\bar{T} = 1$ [24].

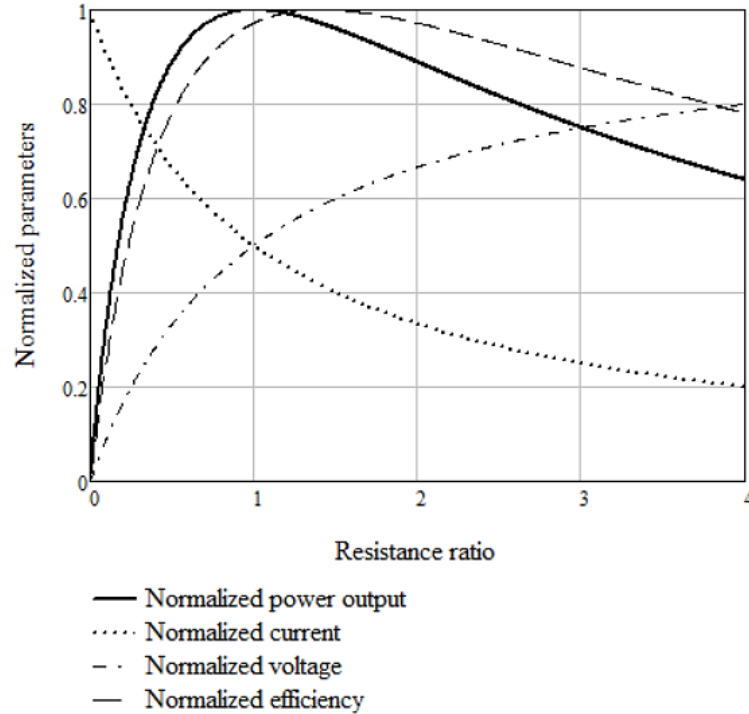


Figure 1.7 Normalized chart of TEG with $\frac{T_c}{T_h} = 0.75$ and $Z\bar{T} = 1$ used.

1.2.5 Thermoelectric Cooler

As mentioned above, the Seebeck effect is reversible. In other words, if electrical current is passed through a thermocouple, this will cause one side to be cooled and the other to be heated. In such case, heat will be absorbed from the cold side and released from the hot side, as shown in Figure 1.8.

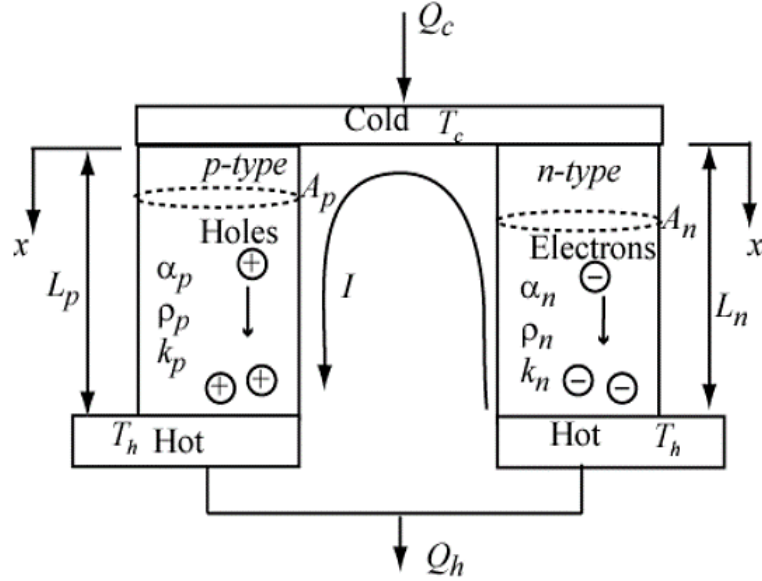


Figure 1.8 Thermoelectric cooler with one thermocouple (p-type and n-type).

For the thermoelectric cooler, states 1 and 2 in Equations (1.21) and (1.22) represent the cold and the hot junctions, respectively, which gives,

$$Q_c = n \left[\alpha T_c I - \frac{1}{2} R I^2 - K(T_h - T_c) \right] \quad (1.45)$$

$$Q_h = n \left[\alpha T_h I + \frac{1}{2} R I^2 - K(T_h - T_c) \right] \quad (1.46)$$

Applying the 1st law of Thermodynamics for the thermocouple leads to,

$$W_n = Q_h - Q_c \quad (1.47)$$

Inserting Equations (1.45) and (1.46) in Equation (1.47) gives,

$$W_n = n[\alpha I(T_h - T_c) + I^2 R] \quad (1.48)$$

We also have,

$$V_n = n I R_L = n[\alpha(T_h - T_c) + I R] \quad (1.49)$$

For a thermoelectric cooler, the coefficient of performance (COP) is defined as the ratio of the cooling power over the power input as the thermoelectric device, which means,

$$COP = \frac{Q_c}{W_i} = \frac{n \left[\alpha T_c I - \frac{1}{2} R I^2 - K(T_h - T_c) \right]}{n[\alpha I(T_h - T_c) + I^2 R]} \quad (1.50)$$

For the maximum cooling power, the maximum current can be found by differentiating Equation (1.45) with respect to the current and set the result to be zero as,

$$\frac{dQ_c}{dI} = \alpha T_c - IR = 0 \quad (1.51)$$

Or,

$$I_{mp} = \frac{\alpha T_c}{R} \quad (1.52)$$

Similarly, the current at the maximum COP can be expressed by differentiating Equation (1.50) with respect to the current and setting it to zero as,

$$\frac{dCOP}{dI} = 0 \rightarrow I_{COP} = \frac{\alpha \Delta T}{R \left[(1 + Z\bar{T})^{\frac{1}{2}} - 1 \right]} \quad (1.53)$$

Where,

$$\Delta T = T_h - T_c \quad (1.54)$$

The maximum current I_{max} usually occurs when the temperature difference is at the maximum value, which always happens when the cooling power is zero. Thus, from Equation (1.52), I_{mp} is represented in terms of T_h and ΔT_{max} as,

$$I_{max} = \frac{\alpha(T_h - \Delta T_{max})}{R} \quad (1.55)$$

Equivalently, I_{max} can be obtained by taking the derivative of ΔT with respect to the current and setting it to zero, which gives,

$$I_{max} = \frac{\alpha}{R} \left[\sqrt{\left(T_h + \frac{1}{Z}\right)^2 - T_h^2} - \frac{1}{Z} \right] \quad (1.56)$$

Now, equating Equations (1.55) and (1.56) and solving for ΔT_{max} gives,

$$\Delta T_{max} = \left(T_h + \frac{1}{Z}\right) - \sqrt{\left(T_h + \frac{1}{Z}\right)^2 - T_h^2} \quad (1.57)$$

The maximum cooling power, which occurs at $\Delta T = 0$ and $I = I_{max}$, can be found from Equation (1.45) by replacing T_c with T_h , and I with I_{max} and solving for $Q_{c,max}$. The maximum cooling power for a thermoelectric cooler is given by,

$$Q_{c,max} = \frac{n\alpha^2(T_h^2 - \Delta T_{max}^2)}{2R} \quad (1.58)$$

The maximum voltage is associated with the voltage that gives the maximum temperature difference ΔT_{max} at the maximum current I_{max} . Thus, the maximum voltage is obtained from Equation (1.49) as,

$$V_{max} = n\alpha T_h \quad (1.59)$$

The normalized parameters for a thermoelectric cooler can be derived by dividing the active performance parameters with the maximum parameters. For example, the normalized cooling power can be obtained by dividing Equation (1.45) by Equation (1.58), which is

$$\frac{Q_c}{Q_{c,max}} = \frac{n \left[\alpha(T_h - \Delta T)I - \frac{1}{2}RI^2 - K\Delta T \right]}{n\alpha^2(T_h^2 - \Delta T_{max}^2)/2R} \quad (1.60)$$

The normalized voltage is

$$\frac{V}{V_{max}} = \frac{\Delta T}{\Delta T_{max}} \frac{\Delta T_{max}}{T_h} + \left(1 - \frac{\Delta T_{max}}{T_h}\right) \frac{I}{I_{max}} \quad (1.61)$$

The normalized current is,

$$\frac{I}{I_{max}} = \frac{\frac{\Delta T}{\Delta T_{max}} \frac{\Delta T_{max}}{T_h}}{\left(1 - \frac{\Delta T_{max}}{T_h}\right) \left((1 + Z\bar{T})^{\frac{1}{2}} - 1\right)} \quad (1.62)$$

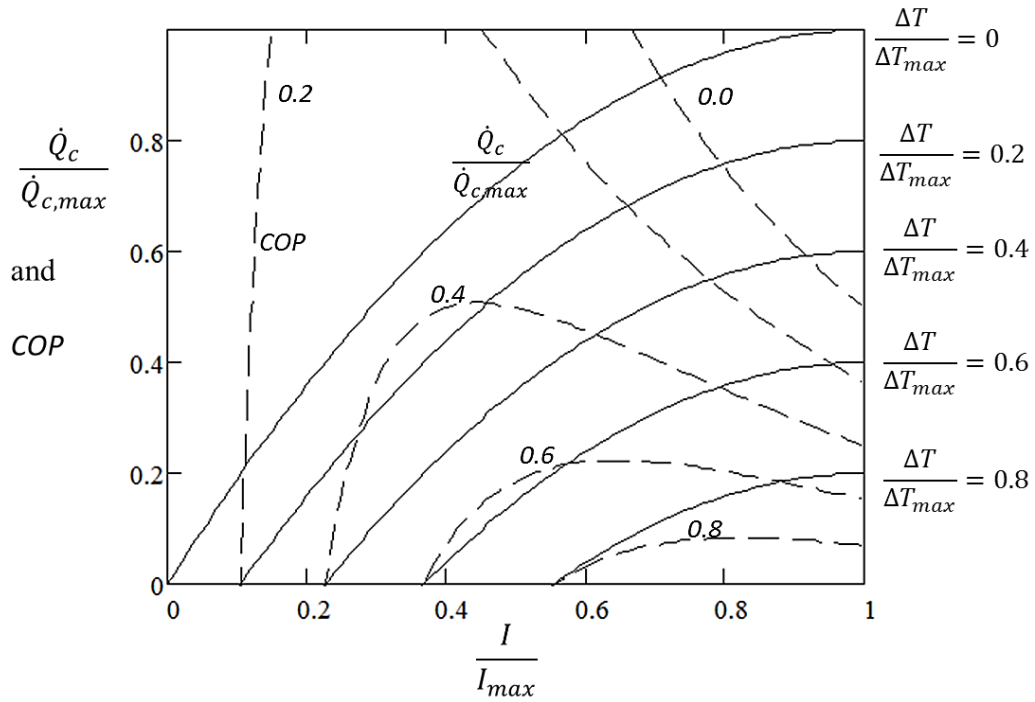


Figure 1.9 Normalized chart for thermoelectric coolers with $ZT_h = 1$.

Figure 1.9 shows the normalized parameters (cooling power and COP) versus the normalized current. From this chart, the normalized cooling power (solid lines) and COP (dashed lines) are inversely proportional to each other, especially in the low-temperature difference. Moreover, the cooling power increases with the increase of the temperature

difference and the supplied current. However, increasing the current may negatively affect the COP, so the current should be arranged and optimized to result in a well suitable combination of the cooling power and COP. Also, taking into account safety, larger currents are not desirable nor may be possible with current vehicle electrical system

1.2.6 Thermal and Electrical Contact Resistances:

In this section, we consider a realistic case of a thermocouple in a TEC module to study the influence of the thermal and electrical contact resistances. This thermocouple is connected electrically in series by conductors with the neighboring thermocouples, which are all thermally connected in parallel using ceramic plates or other electrical insulators with high thermal conductivity (see Figure 1.10). These different conductors add to the system two resistances: electrical and thermal resistances, which cause some discrepancies between the real case and the ideal model [17].

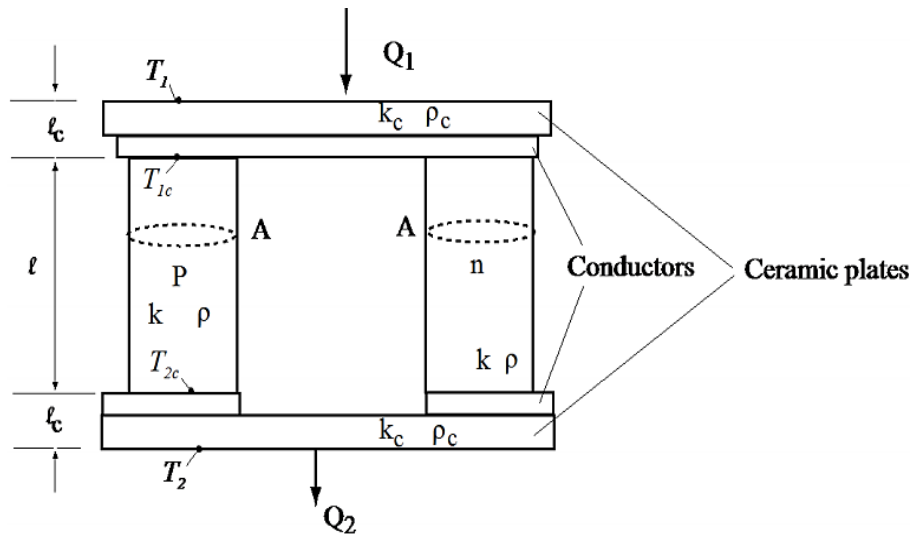


Figure 1.10 A section of a real thermocouple ($T_2 > T_1$).

The heat balance assuming steady state conditions is given as,

$$\dot{Q}_1 = \frac{Ak_c}{l_c} (T_1 - T_{1c}) \quad (1.63)$$

$$\dot{Q}_1 = \alpha T_{1c} I - \frac{1}{2} R I^2 + \frac{Ak}{l} (T_{1c} - T_{2c}) \quad (1.64)$$

$$\dot{Q}_2 = \alpha T_{2c} I + \frac{1}{2} R I^2 + \frac{Ak}{l} (T_{1c} - T_{2c}) \quad (1.65)$$

$$\dot{Q}_2 = \frac{Ak_c}{l_c} (T_{2c} - T_2) \quad (1.66)$$

Where $\alpha = \alpha_p - \alpha_n$ and $k = k_p - k_n$ are the Seebeck coefficient and the thermal conductivity of the thermocouple, respectively, k_c is the thermal contact conductivity, which includes the thermal conductivity of the ceramic plates and the electric conductors, l is the length of the thermoelement, and l_c is the thickness of the conductors. The electric resistance consists of two electric resistances: the electric resistance of the thermocouple and the electrical resistance of the contact.

$$R = R_o + R_c = \frac{\rho l}{A} + \frac{\rho_c}{A} = \frac{\rho l}{A} \left(1 + \frac{s}{l}\right) \quad (1.67)$$

Where $\rho = \rho_p + \rho_n$ is the electrical resistivity of the thermocouple, ρ_c is the electrical resistance of the contact, and s is the ratio of the electrical contact resistivity and the electrical resistivity ($s = \rho_c/\rho$). Equations (1.63) - (1.66) are combined and rearranged to solve for the cooling power and the COP in terms of the two ideal junction temperatures (T_1 and T_2) as,

$$\frac{Q_{1n}}{nA} = \frac{kT_1}{l} \left[\frac{2Z\bar{T}\xi_{TEC} \left(\frac{T_2}{T_1} + 1\right)^{-1} \left(\frac{T_2}{T_1} - 1\right)}{\psi \left(1 + \frac{s}{l}\right) \left(1 - mr \frac{l_c}{l}\right)} - \frac{2Z\bar{T} \left(\frac{T_2}{T_1} + 1\right)^{-1} \left(\frac{T_2}{T_1} - 1\right)^2}{\xi_{TEC}} - \frac{\left(\frac{T_2}{T_1} - 1\right)}{\left(1 - mr \frac{l_c}{l}\right)} \right] \quad (1.68)$$

COP

$$= \frac{\xi_{TEC} \left(1 - mr \frac{l_c}{l}\right)}{\frac{T_2}{T_1} - 1} \frac{\left[\psi - \frac{\left(\frac{T_2}{T_1} - 1\right)}{2\xi_{TEC} \left(1 - mr \frac{l_c}{l}\right)} - \frac{\psi^2 \left(\frac{T_2}{T_1} + 1\right) \left(1 + \frac{s}{l}\right)}{2Z\bar{T}\xi_{TEC}} \right]}{\psi + 1} \quad (1.69)$$

Where,

$$r = \frac{k}{k_c} \quad (1.70)$$

$$m = 2 \left(\frac{Z\bar{T}}{\psi \left(1 + \frac{s}{l}\right)} - 1 \right) \quad (1.71)$$

$$\psi = \sqrt{1 + Z\bar{T}} - 1 \quad (1.72)$$

$$\xi_{TEC} = \frac{T_{1c}}{T_1} = \frac{1 + \frac{l_c}{l} \frac{Z\bar{T} \left(\frac{T_2}{T_1} + 1\right)^{-1} \left(\frac{T_2}{T_1} - 1\right)^2}{\psi^2 \left(1 + \frac{s}{l}\right) \left(1 - mr \frac{l_c}{l}\right)^2} + r \frac{l_c}{l} \frac{\left(\frac{T_2}{T_1} - 1\right)}{\left(1 - mr \frac{l_c}{l}\right)} \quad (1.73)$$

$$= \frac{1 + 2r \frac{l_c}{l} \frac{Z\bar{T} \left(\frac{T_2}{T_1} + 1\right)^{-1} \left(\frac{T_2}{T_1} - 1\right)}{\psi \left(1 + \frac{s}{l}\right) \left(1 - mr \frac{l_c}{l}\right)}$$

One of the important findings in this section is that the effect of the contact resistances increases with the decrease of the leg length of the thermoelement. Figure 1.11 shows the cooling power and COP change with the leg length for four different values of r . It is important to notice that at high contact resistance values, the performance of the TEC is low compared with that at smaller contact resistance values. Also, it is clear that at large leg lengths, the effect of the contact resistances becomes small, while at short leg lengths (less than 1mm), the difference between the performances with the ideal equations ($r = 0, s = 0$) and the real case becomes greater.

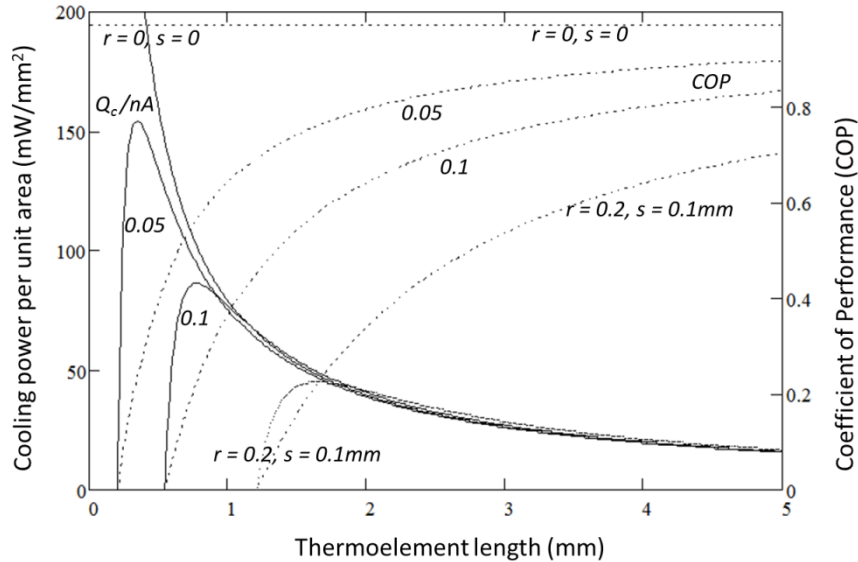


Figure 1.11 Cooling power per unit area and COP as a function of thermoelement length for different values of r and when $s = 0.1\text{mm}$, $\psi = 0.2$, $k = 1.5\text{W/mK}$, $l_c = 0.1\text{mm}$, $T_1 = 275\text{K}$, $T_2 = 300\text{K}$, and $Z = 3 \times 10^{-3}\text{K}^{-1}$ [17].

1.2.7 Thermoelectric System

Let us consider a case where we have a thermoelectric cooler sandwiched between two heat sinks (hot and cold) as shown in Figure 1.12. Both heat sinks face fluid flow with temperature T_∞ . Subscript 1 and 2 represent cold and hot quantities, respectively. In such

setup, there will be two thermal resistances between the two junctions and the fluids, constructing the thermoelectric device. It is assumed that the thermal and electrical contact resistances are negligible, the material properties are temperature dependent, and that the thermoelectric cooler is perfectly isolated [13].

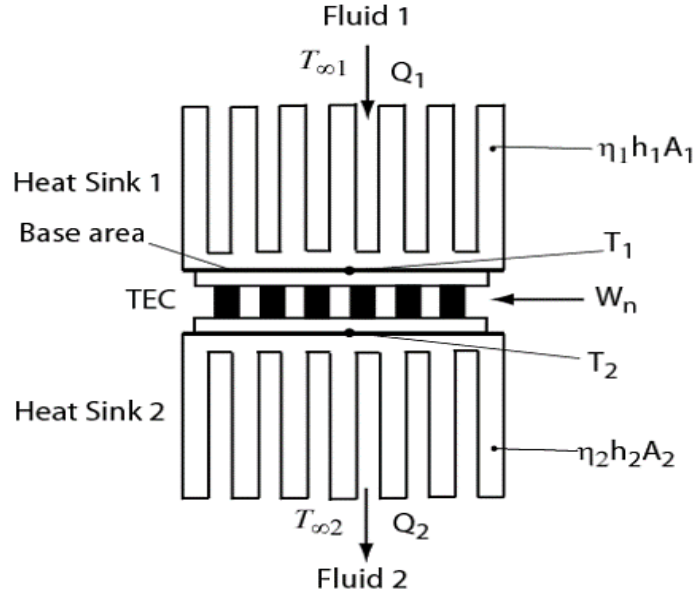


Figure 1.12 Thermoelectric system (thermoelectric cooler module attached to two heat sinks).

Consequently, two more equations will be considered with the two thermoelectric ideal equations discussed earlier, which give the following basic equations for any thermoelectric cooler with given heat sinks,

$$\dot{Q}_1 = \eta_1 h_1 A_1 (T_{\infty 1} - T_1) \quad (1.74)$$

$$\dot{Q}_1 = n \left[\alpha T_1 I - \frac{1}{2} R I^2 + K (T_1 - T_2) \right] \quad (1.75)$$

$$\dot{Q}_2 = n \left[\alpha T_2 I + \frac{1}{2} R I^2 + K (T_1 - T_2) \right] \quad (1.76)$$

$$\dot{Q}_2 = \eta_2 h_2 A_2 (T_2 - T_{\infty 2}) \quad (1.77)$$

Where $\eta_1 h_1 A_1$, and $\eta_2 h_2 A_2$ are the convection conductance for each heat sink (i.e. η_1 is the heat sink efficiency, h_1 is the convection coefficient, and A_1 is the total heat transfer area of the heat sink). Also, T_1 and T_2 are the thermoelectric module junction temperatures which are equal to the heat sinks base temperatures [13].

1.2.8 Heat Sink Design and Optimization

The key factor in the heat sink optimization is to have the highest rate of heat transfer from the fins. Thus, for a given heat sink with width (W) and length (L) and profile length (b) as shown in Figure 1.13, the fin thickness (t_f) and fin spacing (z_f) should be optimized [17].

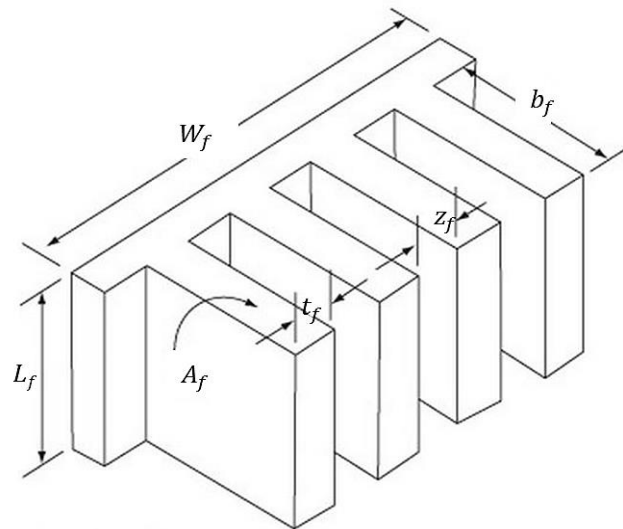


Figure 1.13 Multiple array heat sink.

The single fin efficiency is given by,

$$\eta_f = \frac{\tanh\left(b_f \left(\frac{2h}{k_f t_f}\right)^{\frac{1}{2}}\right)}{b_f \left(\frac{2h}{k_f t_f}\right)^{\frac{1}{2}}} \quad (1.78)$$

Where k_f is the fin thermal conductivity, and h is the convection heat transfer coefficient which can be determined from the Nusselt number correlation as,

$$h = \frac{k_{fluid}}{L_f} Nu \quad (1.79)$$

where k_{fluid} is the fluid thermal conductivity and L_f is the length of the heat sink, which can be replaced by the hydraulic diameter (D_h) in the case of channel flow. The total heat transfer area is given as,

$$A = n_f [2(L_f + t_f) + L_f z_{f,opt}] \quad (1.80)$$

Where n_f is the number of fins, and $z_{f,opt}$ is the optimum spacing which can be determined from,

$$z_{f,opt} = L_f Re_L^{-1/2} Pr^{-1/4} \quad (1.81)$$

Where Re_L is the Reynolds number for a flow over a flat plate and Pr is Prandtl number.

Once the optimum fin spacing is found, the fin thickness can be optimized to give the maximum heat transfer rate given by the following,

$$q_f = \eta_f h A (T_\infty - T_b) \quad (1.82)$$

Where T_∞ and T_b are the fluid and the base temperatures, respectively.

CHAPTER II

PROJECT OBJECTIVE AND LITERATURE REVIEW

2.1 Problem Statement and Objectives

As thermoelectric devices are being used in a wide range of applications, the commercialization of these devices have become widespread in today's thermal comfort and energy conversion. However, designers of thermal systems who would include thermoelectric devices in their designs are still struggling with the difficult task of finding a suitable thermoelectric module that meets their system cooling or heating requirements among many commercial options available.

Manufacturers of thermoelectric modules usually provide their customers with some information which is very often in the form of performance curves at certain operating conditions (maximum or minimum performance at constant high and low junction temperatures). In such case, designers may find it difficult to compare the performance of different modules because these curves are not standardized. For instance, one TEC company may provide the performance charts of their products as the cooling power versus the applied current while the other one may give the cooling power versus the temperature difference curves [25].

A typical thin thermoelectric cooler (refers to by Figure 2.1) with short thermoelement leg length is favorable to decrease the Joule heating. However, this may

revoke the heat back from the hot side to the cold side by the thermal conduction. Thus, it is not clear whether the short leg length is beneficial or not until the optimization of the thermoelectric cooler for certain application is taken into account. Furthermore, another challenging task designers may face when optimizing thermoelectric cooling devices is that manufacturers usually do not provide their modules thermoelectric properties due to their proprietary information. Also, the contact resistances (thermal and electrical) are unknown and even complicated to treat within the optimum design.

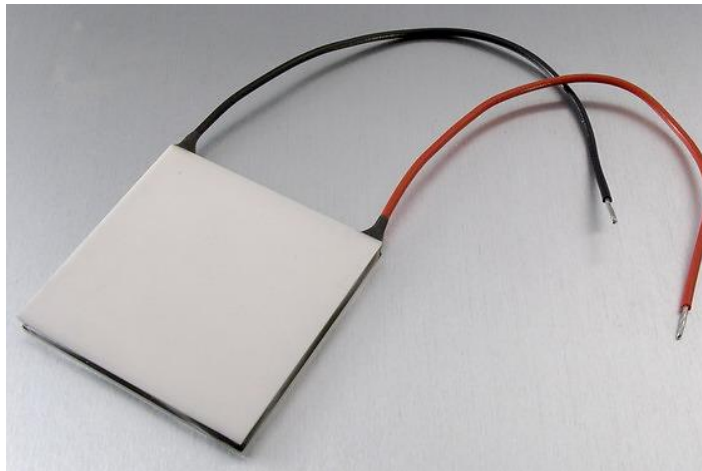


Figure 2.1 Typical thermoelectric cooler module [26].

There are very few published studies about the car seat climate control design which will be discussed in the literature survey section, but none of these studies have shown the optimum design regardless how powerful and efficient the studied design is. The optimization of the thermoelectric module can be obtained through series of experimental evaluation tests which are usually laborious, costly and time-consuming to the designers. An alternative way to optimize the design of thermoelectric cooler would be analytically, using the simple ideal equations discussed in CHAPTER I. Recently, an optimization

method was developed by Lee [13] to evaluate and examine the optimum design of thermoelectric modules (coolers and generators). This approach was modified and implemented in this work to find a simple technique to optimize the TEC parameters for a car seat climate control. One of the goals of this study was to develop and experimentally validate the optimum design of a thermoelectric cooler for a car seat climate control by comparing the experimental performance with the analytical model-calculated results. Therefore, after finding the optimum parameters (number of thermocouples and geometric ratio), a thermoelectric cooler with similar geometry was branched and tested in our lab.

Thus, the aims of the current study can be summarized as:

- Providing an analytical approach for the optimal design of a thermoelectric cooler applied in a car seat climate control using dimensional techniques along with the standard thermoelectric ideal equations.
- Experimentally validate the accuracy of the optimum design approach by conducting several performance tests to compare experimental results with the analytical model calculations.

2.2 Literature Review

2.2.1 Thermoelectric Cooler for Car Seat Comfort

At present, very few researchers have carried out investigations of using thermoelectric coolers in car seat climate control. For instance, Feher [27] employed a thermoelectric cooler in a variable temperature seat (VTS) to increase the vehicle occupant thermal comfort and decrease fuel/energy consumption. The aim of his study was to remove the heat from the occupant body directly instead of the entire vehicle space. His

system consists of one thermoelectric cooler sandwiched between two heat sinks supplied with ambient air by two auxiliary fans and one main blower. Experimental data showed that at a vehicle interior temperature of 300.4 K , his VTS was able to pump about $10.2 \frac{\text{m}^3}{\text{h}}$ of air at a temperature difference of 10 K in the cooling mode, which can be converted to approximately 33.3 W of heat subtracted from the seat. While in the heating mode, the VTS has the capacity to pump the same volume flow rate of air at ambient temperature of 257.04 K with temperature difference close to 14.4 K , which is equivalent to 56.5 W of heating power. This design will be discussed further in this work seeking any possible rooms for improvement.

The same author, but in a different study [28], designed and tested a stirling air conditioned variable temperature seat (SVTS) and compared its performance with the thermoelectric VTS. He concluded that the SVTS has the higher efficiency than the VTS, where at the same volume flow rate of 8 CFM and ambient temperature of 297.1 K the SVTS provides conditioned air with temperature difference of 10.2 K at the performance of coefficient (COP) of 2.32 , while the VTS pumps the same amount of air at the same temperature difference but at COP of about 0.5 . Also, he found that the SVTS is more efficient at a greater temperature difference with lower levels of noise because it does not need as much air as the VTS. However, in terms of manufacturing costs and reliability, the VTS showed extreme reliability and low maintenance expenses over the SVTS.

Menon et al. [29] presented the iterative learning control of shape memory alloy actuators with thermoelectric temperature regulation for a multifunctional car seat to provide the occupant with thermal comfort, rapid cooling/heating and massaging. Their

architecture was built using a series of two layer thermoelectric devices close to the seat surface to increase the efficiency of heat pumping to meet their functional requirements. The cooling ability of their system was tested using prototype assembly. The system was heated to around 50 °C and then was let to cool down by two methods. In the first method, the thermoelectric coolers were used, and in the second method, the assembly was let to cool naturally. Their results showed that the Peltier cooling system has the advantage of speed up the cooling to about 6 °C in only five minutes.

Choi et al. [30] analyzed the characteristic of a thermoelectric cooler used to control the temperature of a car seat surface (cooling and heating). Besides the thermoelectric device (HM3930), their conditioning system was composed of a fan and duct to cool down the warm side of the thermoelectric device, and to control the temperature of the seat, a robust control algorithm based on a sliding mode control was applied. To control the temperature of the car seat, they analytically modeled their system employing the thermoelectric equations such as Equation (1.45) and (1.49). After installing two temperature control modules, each consisting of two thermoelectric coolers, in a car seat, the test results showed that with an applied voltage of 6 V for each thermoelectric device the cooling temperature reduced from 28 °C to about 10 °C by the control system. Similarly, the warming temperature converged to about 50 °C in an acceptable response time.

Vinoth et al. [31] designed and tested an automated car safety seat cooling system using a thermoelectric cooler to minimize the danger that children are exposed to when left alone in a parked vehicle at high surrounding temperature. After studying and measuring the temperature variation inside a car parked in different weather conditions using a thermal

gun, they selected the proper thermoelectric cooler and heatsinks that meet their operation conditions. Then, the specifications of the TEC were mathematically modeled using Equation (1.48) to determine the power supply, Equation (1.45) to calculate the cooling power, as well as Equation (1.50) to determine the performance of coefficient. To meet the cooling requirements, two thermoelectric coolers connected to PIR and LM35 sensors were employed to their system which was installed in a child seat. As the sensors detect a higher temperature close to a threshold value, the thermoelectric coolers start to work cooling down the surrounding air and providing thermal comfort to the child. Furthermore, an alert message is sent to the mobile number stored in the system. Test results indicate that the TECs could maintain the surrounding temperature at 32 °C to 25.8 °C within a stabilizing time of 3 minutes.

DU et al. [32] designed a temperature-controlled car seat powered by an exhaust thermoelectric generator to enhance the riding comfort through adjusting the seat surface temperature. The characteristics of the selected thermoelectric cooler (TEC1-12706) were investigated, then the optimum operating conditions were determined theoretically using the simple thermoelectric ideal equation. The optimum current was evaluated by Equation (1.52) at constant operating temperature, material properties, and geometrical dimensions, which led to the optimum current of 3.7 A. The simulation for the air ducts resulted in lower power of 12 W with duct inlet air velocity of $2.55 \frac{m}{s}$. To validate their theoretical scheme, multiple experimental tests including real vehicle tests were conducted. Two thermoelectric coolers at 12 V DC were installed at the inlet of the air duct, which resulted in seat surface temperature of 23.5 °C at lap ambient temperature of 25.1 °C. On the other hand, the real vehicle tests indicated that after 10 minutes of running the thermoelectric

system, the temperature of the seat surface was reduced from 36.61 °C to 31.27 °C, while the temperature of the seat rest was reduced from 36.24 °C to 32.19 °C.

At present, very few researchers have established a link between the thermoelectric cooler and the heat sinks, constructing the thermoelectric system, considering the concrete optimum design of the temperature controlled seat. As for heat sink optimization, Lee [17] established a comprehensive work which provides a clear guideline for finding the optimum heat sink geometry (fin thickness and spacing). Also, the Nusselt number correlations based on experimental investigations can be used as reliable methods even for very complicated systems [33]. For instance, Teertstra et al. [34] developed a theoretical model to calculate the Nusselt number for flow in parallel plate channel combining fully-developed and developing flow. Their correlations showed good agreement with the experimental work. In similar fashion, Zhimin et al. [35] provided an analysis methodology of the optimum thermal design of microchannel heat sink. For both laminar and turbulent flow, they defined two correlations to calculate the Nusselt number for developing and fully-developed flow in three and four sided-heated channels. Their analytical results were then compared with some experimental values with good agreement. These studies on heat sink optimization and Nusselt number correlations can be applied in the present study to determine the best thermal design of the system.

2.2.2 Optimal Design of a Thermoelectric Cooler

Studies on the optimal design of thermoelectric coolers used in different applications are hardly found in the literature. Furthermore, none of the states of art designs related to car seat climate control mentioned above have provided a precise method of how to optimize the system, particularly the thermoelectric device. In different areas, however,

the literature shows some techniques for analyzing the optimization of thermoelectric parameters regarding the number of thermocouples and the geometric ratio. Yamanashi [36] first introduced the dimensionless parameters for the thermoelectric cooler to obtain the optimum cooling power. Despite the complexity of Yamanashi's technique to find the optimum thermoelectric parameters, other researchers were able to adopt and apply his method achieve practical and accurate results. As such, Xuan [37] and Pan et al. [38] implemented Yamanashi's method to study the optimum a thermoelectric leg length and the optimum cooling power for a thermoelectric cooler, respectively.

Recently, Lee [13] developed a new optimum design method using the thermoelectric ideal equations and the dimensional technique for both thermoelectric coolers and generators. He defined a set of dimensionless parameters such as dimensionless current and dimensionless thermal conductance to reduce the parameters, which allowed him to optimize these parameters simultaneously at given material properties, ambient temperature, and heat sink geometry. Attar et al. [39] applied this optimization method to study the optimum design of Gentherm air-to-liquid and air-to-air automotive thermoelectric air conditioning system (TEAC) investigating any possible improvements in the COP. Same technique then was used to study the optimum design of the air-to-air TEAC system. Their air-to-air optimization results showed excellent agreement with the experimental data [40, 41].

2.2.3 Experimental Investigation of Thermoelectric Systems

Most of the literature has discussed the theoretical approach of studying the optimal design of thermoelectric systems. Experimental work is, thus, needed to validate the accuracy of these analytical studies. The literature has shown several experimental works

in multiple of applications. For instance, Chang et al. [42] tested a thermoelectric cooler for electronic device air-cooling, where a good agreement was noticed with the thermoelectric ideal equations. To obtain their module thermoelectric properties, they conducted another experiment using the same thermoelectric module, which later were used in their performance calculations. Similarly, Liu et al. [43] proposed a thermoelectric mini cooler coupled with micro thermosiphon for CPU cooling system. They conducted full-scale experiments to investigate the effect of the operating voltage on the thermoelectric system performance. As a way to study the impact of the thermal resistance of the system on the performance, Huang et al. [44] did a similar experiment with fair agreement with prediction.

Furthermore, Riffat et al. [45] carried out tests to investigate the potential application of thermoelectric refrigeration with heat pipes and phase change materials. They designed and tested a thermoelectric refrigeration prototype for two different configurations: the first one was with a conventional heat sink (finned heat sink) on the cold side of the thermoelectric device, and the second configuration used an encapsulated phase change material (PCM) instead of the heat sink unit. The experimental results showed that by using the conventional heat sink system with an encapsulated PCM, the performance of the thermoelectric system as well as the cooling storage capacity are improved. Cosnier et al. [46] established an experimental study, and a numerical model of a thermoelectric system consisting of four thermoelectric cooler modules used to cool and warm airflow. They used a finned heat sink within a circulated airflow on the cold side and a water box heat exchanger at the hot side. Their experimental results were in good agreement with the numerical results.

Zhao et al. [47] experimentally evaluated a prototype thermoelectric system integrated with PCM heat storage unit for space cooling. They investigated the performance of their thermoelectric module using Equations (1.45) and (1.46) to determine the balanced operating conditions of the thermoelectric module. For their experimental setup, they used air-to-liquid configuration to evaluate the performance of the thermoelectric cooling system, which indicated that a maximum COP of 1.22 could be achieved.

Dai et al. [48] introduced an experimental investigation and analysis of a thermoelectric refrigerator driven by solar cells. Their primary interest was to test the performance of their cooling system under sunshine to study the effect of the intensity of solar insolation and the temperature difference across the thermoelectric module. They used the natural convection process to release the heat through the fin-type heat exchanger at the hot side; while the cold side of the module was set inside the refrigerator. The test results showed that the refrigerator space could be maintained at 5 – 10 °C with COP of 0.3 under given conditions.

CHAPTER III

ANALYTICAL APPROACH AND EXPERIMENTAL METHOD

Modeling of Thermoelectric Device for Car Seat Climate Control

All information in this chapter is in reference to the methodologies explained in Ref. [49, 14] with the author's contribution. This chapter focuses on the methodology used to study the optimization of a thermoelectric device applied for car seat climate control. Our newly developed optimization method was implemented to examine the optimum design [13] of a thermoelectric cooler for car seat cooling and heating purposes. A proposed schematic of the design for both cooling and heating modes is shown in Figure 3.1, where we have one thermoelectric cooler sandwiched between two hot and cold air heat sinks connected to an auxiliary fan and main blower, respectively. The primary concern of the analytical modeling is to apply this optimum design method along with the dimensional technique to simulate the performance of the thermoelectric car seat climate control.

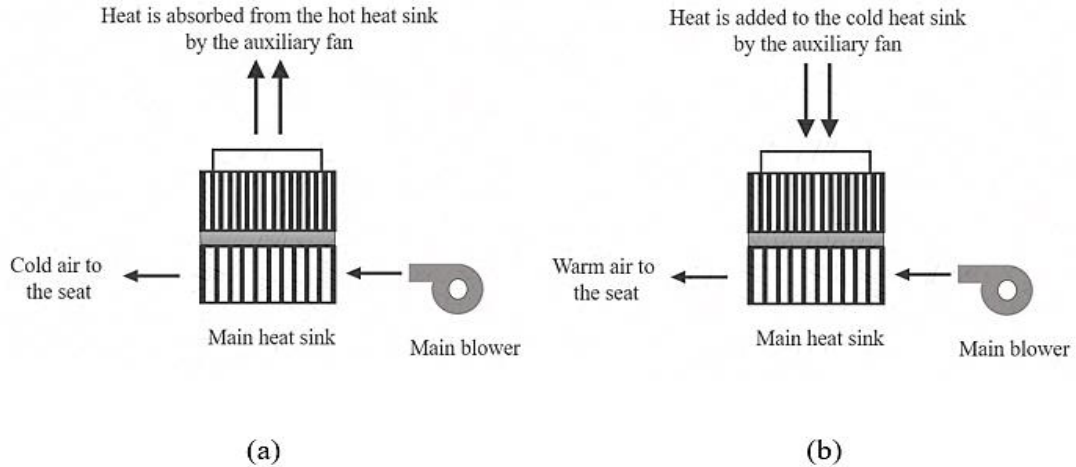


Figure 3.1 (a) Cooling mode and (b) Heating mode of the car seat climate control.

3.1 Calculating the Effective Material Properties

In order to utilize the thermoelectric ideal equation in the optimal design, it is necessary that the material properties of the thermoelectric module (α , R , and K) be known. However, as mentioned in chapter I, the material properties of the thermoelectric device are usually not available or provides to customers. Therefore, the effective material properties, which are formulated from the maximum parameters equations described in Chapter I, are discussed in this section to move forward in the optimization procedure. The maximum parameters of the thermoelectric device are usually provided by manufacturers based on real experimental measurements, which means that the material properties calculated using these manufacturer's maximum parameters should include the neglected effects (i.e. contact resistances). Thus, using the effective material properties instead of the intrinsic properties can reduce the errors associated with such effects.

The effective figure of merit is directly obtained from Equation (1.56) as,

$$Z^* = \frac{2\Delta T_{max}}{(T_h - \Delta T_{max})^2} \quad (3.1)$$

Dividing Equation (1.55) by Equation (1.57), the Seebeck coefficient can be defined as,

$$\alpha^* = \frac{2Q_{c,max}}{nI_{max}(T_h + \Delta T_{max})} \quad (3.2)$$

The effective electrical resistivity can be obtained from Equation (1.55) as,

$$\rho^* = \frac{\alpha^*(T_h - \Delta T_{max})^2 A_e / l_e}{I_{max}} \quad (3.3)$$

And finally, the effective thermal conductivity is determined from Equation (1.4) as,

$$k^* = \frac{\alpha^{*2}}{\rho^* Z^*} \quad (3.4)$$

Note that these effective material properties are defined from the ideal equations. The advantage of using such material properties lies in reducing the errors associated with the assumption of neglecting the contact resistances in the thermoelectric ideal equation. The maximum parameters are experimental values, so they already include the effects of the thermal and electrical contact resistances and Thomson effect. Therefore, there is no need to reaccount for these effects again in the thermoelectric ideal equations. In the other hand, using the intrinsic material properties, which do not include the contact resistances effects, can cause the analysis to be complicated as these affects have to be considered with the optimizations procedure. These effective properties are the total properties, so they should be divided by two to obtain the material properties of the single p-type and n-type thermocouples.

3.2 Optimal Design of a Thermoelectric Cooler Using Dimensional Analysis

The optimum design theory based on the dimensional technique developed by Lee [14] is modified and employed to determine the optimum design of the thermoelectric device (thermoelectric cooler) in conjunction with heat sinks (Figure 3.2a). From this analysis, it is found that if two fluid temperatures at the heat sinks are known, an optimum design always exists and can be determined. This method allows us to optimize the performance (Cooling power and COP) of the thermoelectric cooler by simultaneously optimizing the dimensionless current (N_I) and the dimensionless thermal conductance (N_k), which represent the applied current and the geometric ratio (or number of thermocouples), respectively, at a set of given dimensionless parameters. Such parameters reduction technique enables the six heat balance equations (Equations. 3.5– 3.10) to be converted to two dimensionless equations as seen in Equations. (3.20) and (3.21). This method assumes that the n-type and p-type thermoelectric elements (Figure 3.2b) have the same leg length and cross-sectional area.

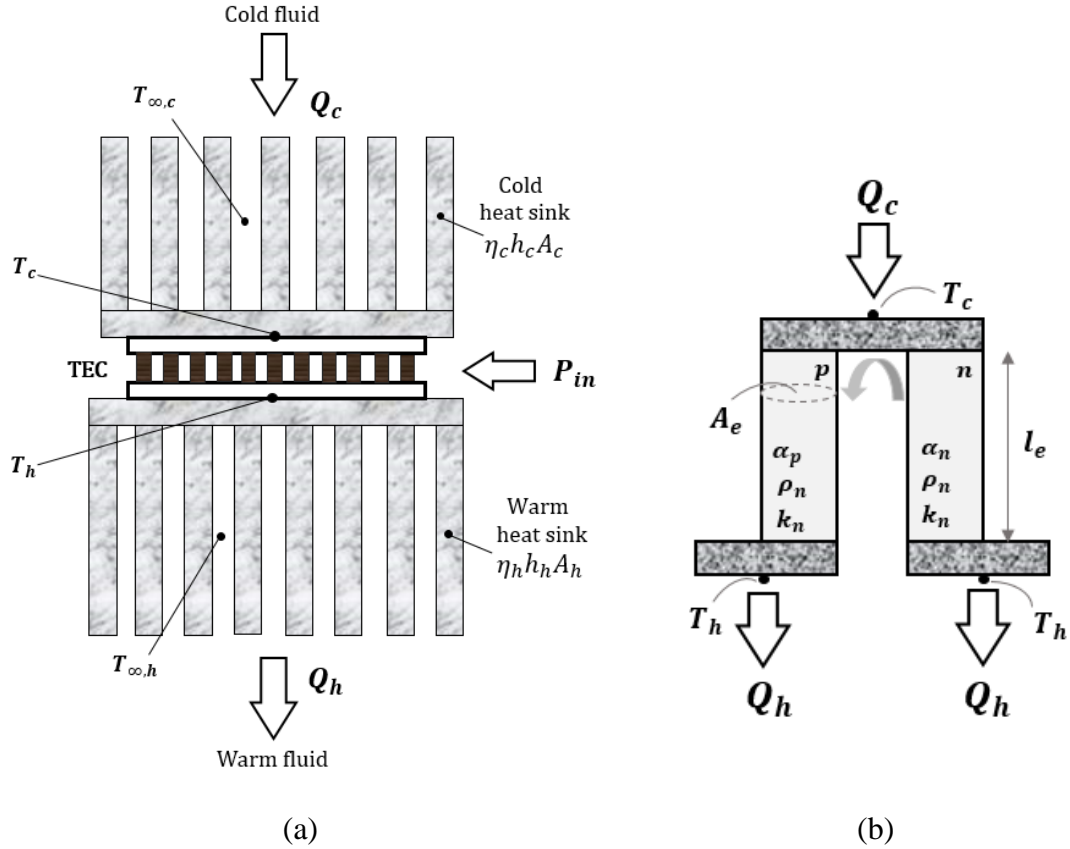


Figure 3.2 (a) Thermoelectric cooler attached to two heat sinks, and (b) schematic of a thermocouple.

This system can be converted to a set of heat equations as following,

$$\dot{Q}_c = \dot{m}_c c_{p,c} (T_{\infty,c,in} - T_{\infty,c,out}) \quad (3.5)$$

$$\dot{Q}_c = \eta_c h_c A_c (T_{\infty,c} - T_c) \quad (3.6)$$

$$\dot{Q}_c = n \left[\alpha T_c I - \frac{1}{2} R I^2 + K (T_c - T_h) \right] \quad (3.7)$$

$$\dot{Q}_h = n \left[\alpha T_h I + \frac{1}{2} R I^2 + K (T_c - T_h) \right] \quad (3.8)$$

$$\dot{Q}_h = \eta_h h_h A_h (T_h - T_{\infty h}) \quad (3.9)$$

$$\dot{Q}_h = \dot{m}_h c_{p,h} (T_{\infty h, out} - T_{\infty h, in}) \quad (3.10)$$

Where the thermal resistance at the heat sinks is defined by the reciprocal of the thermal conductance (i.e. $\eta_c h_c A_c$), where η_c is the heat sink efficiency, h_c is the convection coefficient, and A_c is the heat transfer area at the heat sink. The local ambient cold air temperature at the unit cell $T_{\infty c}$ is obtained by averaging the inlet and outlet cold air temperatures assuming linear change in the temperature of the unit cell ($T_{\infty c} = \frac{T_{\infty c, in} + T_{\infty c, out}}{2}$). Similarly, the local ambient hot liquid temperature $T_{\infty h}$ at the unit cell is obtained by averaging the inlet and outlet hot air temperature ($T_{\infty h} = \frac{T_{\infty h, in} + T_{\infty h, out}}{2}$) as shown in Figure 3.3.

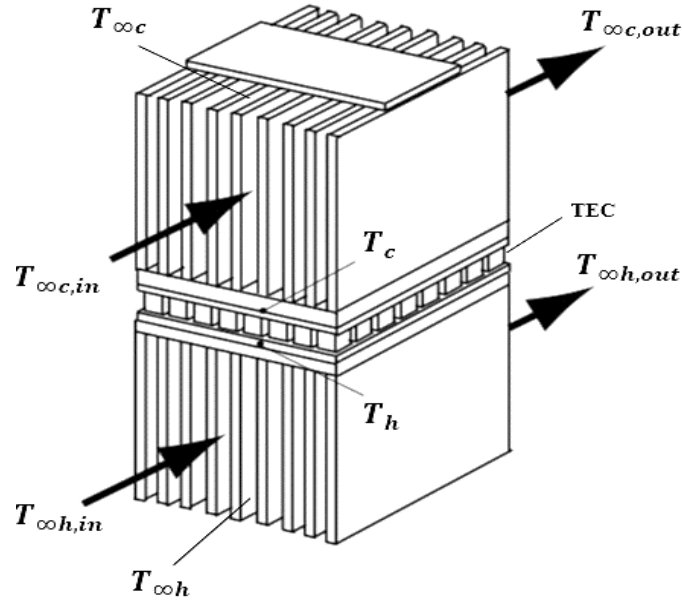


Figure 3.3 Schematic of the unit cell configuration.

This system of Equations (3.5)-(3.10) can be solved for T_c and T_h , providing the cooling power. However, optimization using these six heat balance equations can be very difficult because the high number of parameters needed to be optimized. Thus, to study the optimum design of such system, five independent dimensionless parameters, not conflicting with each another are introduced in order to minimize the parameters. The dimensionless thermal conductance, the ratio of the thermal conductance to the convection conductance of the hot side is given as,

$$N_k = \frac{n(Ak/L)}{\eta_h h_h A_h} \quad (3.11)$$

The dimensionless convection is defined as the ratio of the cold side convection conductance to the hot side convection conductance, which gives,

$$N_h = \frac{\eta_c h_c A_c}{\eta_h h_h A_h} \quad (3.12)$$

The dimensionless current is given as,

$$N_I = \frac{n\alpha I}{\eta_h h_h A_h} \quad (3.13)$$

The ratio of the enthalpy flow at the cold side to the convection conductance is defined as,

$$N_M = \frac{\dot{m}_c c_{p,c}}{\eta_h h_h A_h} \quad (3.14)$$

And the ratio of the enthalpy flow on both sides is given as,

$$N_c = \frac{\dot{m}_c c_{p,c}}{\dot{m}_h c_{p,h}} \quad (3.15)$$

The dimensionless figure of merit is defined as,

$$ZT_{\infty h, in} = \frac{\alpha^2}{\rho k} T_{\infty h, in} \quad (3.16)$$

The dimensionless temperatures are defined as,

$$T_c^* = \frac{T_c}{T_{\infty h, in}} \quad (3.17)$$

$$T_h^* = \frac{T_h}{T_{\infty h, in}} \quad (3.18)$$

$$T_{\infty, in}^* = \frac{T_{\infty c, in}}{T_{\infty h, in}} \quad (3.19)$$

It is remarkable that the dimensionless parameters are based on the convection conductance in the hot fluid $\eta_h h_h A_h$ and its inlet temperature $T_{\infty h, in}$. Therefore, they are assumed to be initially given. Using these dimensionless parameters, Equations (3.5) - (3.10) can be converted to two dimensionless equations as,

$$\frac{N_h}{1 + \frac{N_h}{2N_M}} (T_{\infty, in}^* - T_c^*) = N_I T_c^* - \frac{N_I^2}{N_h} \frac{1}{ZT_{\infty h, in}} + N_k (T_c^* - T_h^*) \quad (3.20)$$

$$\frac{1}{1 + \frac{N_c}{2N_M}} (T_h^* - 1) = N_I T_h^* - \frac{N_I^2}{2N_k} \frac{1}{ZT_{\infty h, in}} + N_k (T_c^* - T_h^*) \quad (3.21)$$

Equations (3.20) and (3.21) can be solved for T_c^* and T_h^* which are functions of five independent parameters as,

$$T_c^* = f(N_k, N_I, N_h, T_{\infty, in}^*, ZT_{\infty h, in}) \quad (3.22)$$

$$T_h^* = f(N_k, N_I, N_h, T_{\infty, in}^*, ZT_{\infty h, in}) \quad (3.23)$$

Where $T_{\infty, in}^*$ is the inlet temperature ratio and $ZT_{\infty h, in}$ is the material property, both initially known. Thus, the optimization is done with the first three dimensionless parameters N_k , N_I and N_h . Once the two dimensionless junction temperatures (T_c^* and T_h^*) are solved for, the

dimensionless rates of heat transfer at the two junctions can be determined from the following equations,

$$Q_1^* = \frac{N_h}{1 + \frac{N_h}{2N_M}} (T_{\infty, in}^* - T_c^*) \quad (3.24)$$

$$Q_2^* = \frac{1}{1 + \frac{N_c}{2N_M}} (T_h^* - 1) \quad (3.25)$$

The dimensionless input power is given by,

$$W_n^* = Q_2^* - Q_1^* \quad (3.26)$$

Thus, the coefficient of performance is defined as,

$$COP = \frac{Q_1^*}{W_n^*} \quad (3.27)$$

It is found that both N_l and N_k show the optimum value for the dimensionless cooling power, while the N_h does not. In other words, if the value of N_h is given, the optimal combination of N_l and N_k can be obtained. This allows designers to determine the operating condition. In fact, N_k is the geometry or dimension of TED, so once determined, it is permanent. But N_l represents the current, so it can be adjusted depending on the demand such as transient initial startup cooling for a short time (a few seconds to minutes) or steady cooling/heating for a longer time (minutes to hours). This dynamic behavior is usually very difficult to predict without the analysis of dimensionless parameters.

3.3 Optimization of Heat Sink for the Thermoelectric System

Heat sink optimization plays an essential role in enhancing the performance of the thermoelectric car seat climate control. The same method discussed in section 1.2.8 is

implemented to optimize the fin spacing and the fin thickness. After determining the fin spacing using Equation (1.81), the fin thickness is calculated to give the maximum rate of heat transfer (see Figure 3.4). Then, the total heat transfer area of both cold and hot heat sink surface is calculated using Equation (1.82).

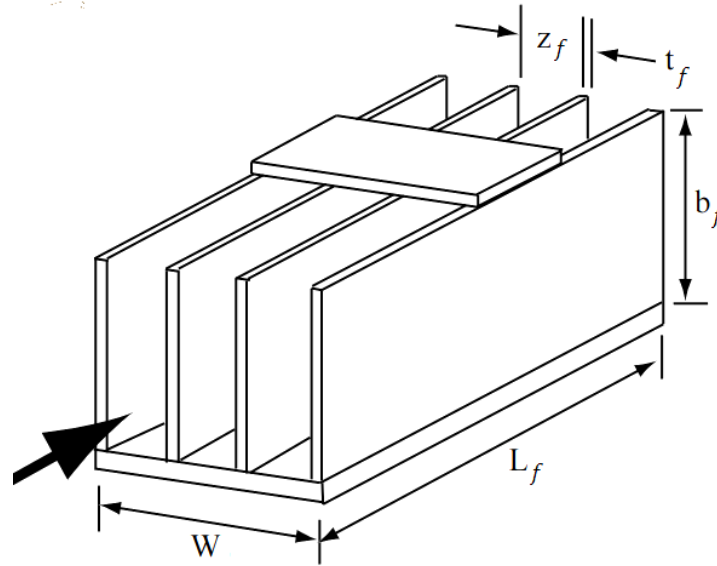


Figure 3.4 Schematic of a plate fin heat sink.

Mass flow rates can be determined using the air inlet velocities $V_{c,in}$ and $V_{h,in}$ as,

$$\dot{m}_c = \rho_c V_{c,in} A_{cross,c} \quad (3.28)$$

$$\dot{m}_h = \rho_h V_{h,in} A_{cross,h} \quad (3.29)$$

Where $A_{cross,c}$, $A_{cross,h}$ are the cold and hot cross flow areas and can be calculated as,

$$A_{cross,c} = (n_{f,c} - 1) b_{f,c} z_{f,c} \quad (3.30)$$

$$A_{cross,h} = (n_{f,h} - 1) b_{f,h} z_{f,h} \quad (3.31)$$

The Reynolds number is calculated to determine whether the flow is laminar or turbulent; thus, the hydraulic Reynolds number is given as,

$$R_{e,D} = \frac{VD}{\nu} \quad (3.32)$$

Where D is the hydraulic diameter of the rectangular channel and ν is the kinematic viscosity of air.

Furthermore, the Nusselt number is regarded as another important factor in determining the heat transfer coefficient which has a remarkable effect on the performance of the whole system. The Nusselt number correlation used in this study is explained in reference [35] for laminar flow in a long channel based on experimental work. Accordingly, for laminar flow, the Nusselt numbers in which three walls are heated is given as a function of the aspect ratio as,

$$N_{u,c} = 8.235(1 - 2.042\alpha_c^{-1} + 3.0853\alpha_c^{-2} - 2.4765\alpha_c^{-3} + 1.0578\alpha_c^{-4} - 0.1861\alpha_c^{-5}) \quad (3.33)$$

$$N_{u,h} = 8.235(1 - 2.042\alpha_h^{-1} + 3.0853\alpha_h^{-2} - 2.4765\alpha_h^{-3} + 1.0578\alpha_h^{-4} - 0.1861\alpha_h^{-5}) \quad (3.34)$$

Where α_c and α_h are the aspect ratios of the channels between fins for hot and cold sinks and given as,

$$\alpha_c = \frac{b_{f,c}}{z_{f,c}} \quad (3.35)$$

$$\alpha_h = \frac{b_{f,h}}{z_{f,h}} \quad (3.36)$$

After calculating the Nusselt number, the convection coefficient h can be determined directly from Equation (1.79). Using Equation (1.78), the total or overall fin

efficiencies for the multiple fin areas (heat sink areas) for the hot and cold heat sinks are calculated as,

$$\eta_{o,c} = 1 - n \frac{A_{f,c}}{A_{s,c}} (1 - \eta_{f,c}) \quad (3.37)$$

$$\eta_{o,h} = 1 - n \frac{A_{f,h}}{A_{s,h}} (1 - \eta_{f,h}) \quad (3.38)$$

Where $A_{f,c}$ and $A_{f,h}$ are the surface areas of single fin, which is given as,

$$A_{f,c} = 2b_{f,c}(L_{f,c} + t_{f,c}) \quad (3.39)$$

$$A_{f,h} = 2b_{f,h}(L_{f,h} + t_{f,h}) \quad (3.40)$$

Now we introduce the thermal resistance of the cold and hot heat sinks as,

$$R_{t,c} = \frac{1}{\eta_{o,c} h_c A_{s,c}} \quad (3.41)$$

$$R_{t,h} = \frac{1}{\eta_{o,h} h_h A_{s,h}} \quad (3.42)$$

Where $A_{s,c}$ and $A_{s,h}$ are the total heat transfer area at the cold and hot heat sinks, respectively.

3.4 Experimental Method

This section focuses on the experimental work as a method of verifying the analytical optimum design results. The goal was to use the theoretically obtained optimum parameters (discussed in section 3.2) and test the accuracy of the optimum performance prediction by comparing against the experimental results. Thus, the primary objective is not to evaluate the performance of a randomly chosen commercial thermoelectric cooler, but to test a thermoelectric cooler with parameters (number of thermocouples and

geometric ratio) stipulated by the optimum design calculations. This can also give the basis for comparing the analytical results with data provided by other models such as Feher's data.

3.4.1 Experimental Overview

When current is supplied to a thermoelectric cooler, heat will be absorbed and rejected at the cold and the hot sides, respectively, which results in a difference in the junctions' temperatures. To maintain this temperature gradient, heat has to be rejected from the hot side. Otherwise, the two sides will reach thermal equilibrium leading to a rise in the temperature of the cold junction. To do that, heat sinks with forced convection process using fans or blowers for air and pumps for liquid water configurations are recommended, depending on the system application. For the cold side, heat is absorbed from the air driven by fans to achieve cooling air with low temperatures. Through reversing the direction of the supplied current, heat dissipation at the hot side can also be used to produce heating by using forced air convection and heat sinks. In this case, the cold side should be as warm as possible to maximize the efficiency of heating on the hot side; this can be handled by applying forced convection at the cold side so that heat is absorbed from the ambient air to the cold heat sink to keep it warm. The volume flow rate at the two heat sinks can be easily varied by manipulating the input power to the fans, and the cooling/heating power can be changed depending on the demand by changing the input current to the thermoelectric cooler. The critical parameters when operating a thermoelectric cooler are the input current or voltage through the power supply and the cold and hot junction temperatures, which can be measured using thermocouples.

3.4.2 Experimental Setup

To assess the validity of this optimum design results, an experiment had to be conducted based on the optimum design input parameters. From the optimum design of the heat sinks, two commercial heat sinks with close geometry to the optimum values were selected to be used in the experimental work. The thermoelectric cooler also was chosen based on the optimum parameters results, and due to availability limitations, a similar module with close geometry was selected instead. The test stand accommodates two $40 \times 40 \text{ mm}$ ALPHA UB40-25B heat sinks at the cold and the hot sides and a $40 \times 40 \text{ mm}$ TB 127-1.4-1.15 thermoelectric module from TETECHNOLOGY, INC company. Figure 3.5 indicates a schematic drawing of the test stand with air flow direction while Figure 3.6 shows a photograph of the test stand with removed isolation pads. These pads are extremely important to reduce the errors associated with heat convection and radiation losses from the system.

As mentioned earlier, one of the convenient features of thermoelectric coolers is that they can provide coldness and hotness depending on the direction of the applied voltage. Therefore, exactly same experimental setup was employed to investigate the performance of the heating mode. The only difference is that the polarity of the applied voltage was switched so that the thermoelectric device produces heat at the main heat sink (cold heat sink in the previous setup). In such case, the same volume flow rates were maintained at the two sides of the thermoelectric system.

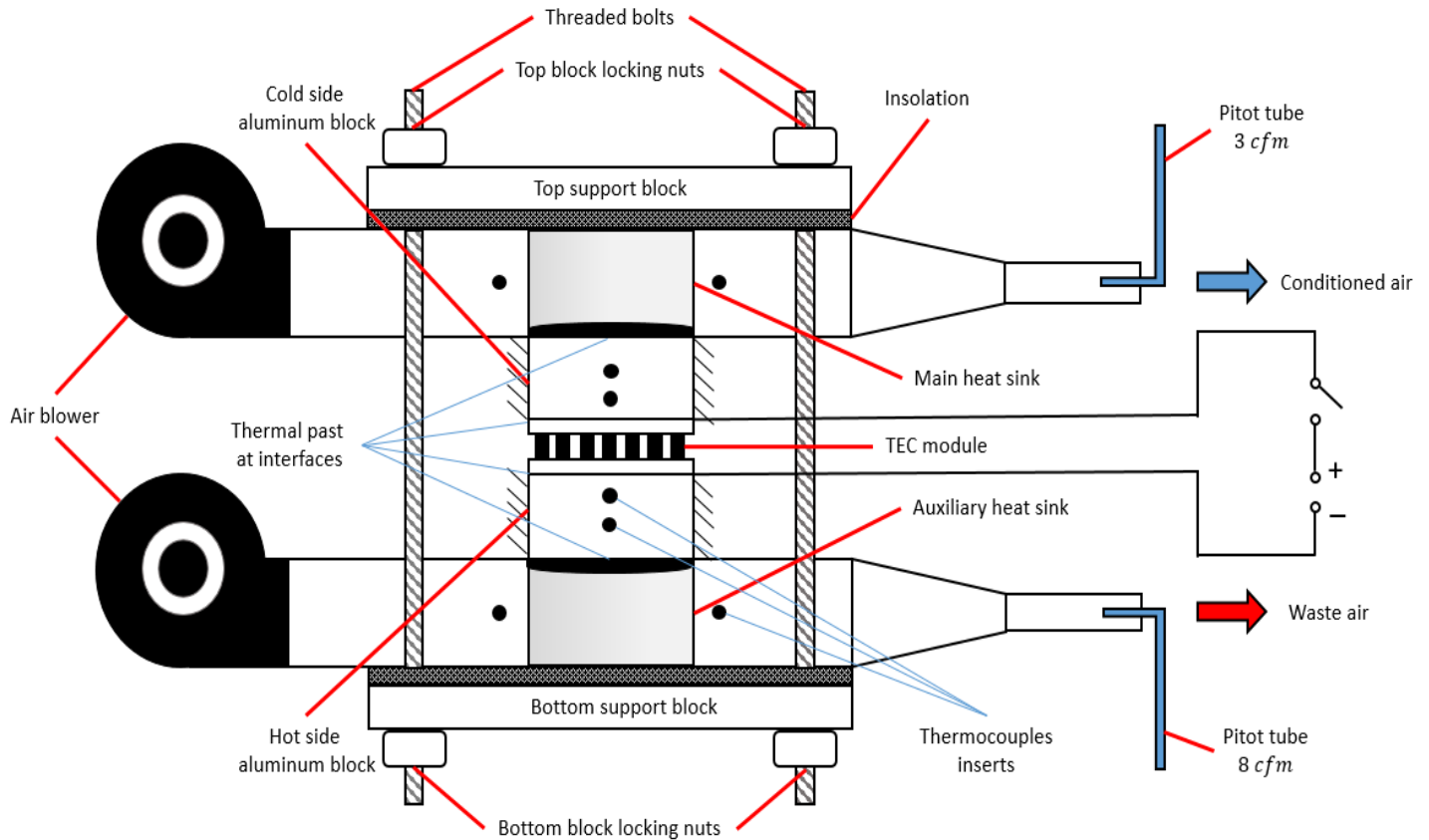


Figure 3.5 Schematic of the experimental setup.

As seen in Figure 3.6 two aluminum blocks with dimensions ($40 \times 40 \times 19.1 \text{ mm}^3$) are clamped between the heat sinks with two thermocouple inserts (with a diameter of 2 mm and depth of 20 mm) in each block. Two parallel K-type thermocouples are inserted into the center of the aluminum blocks where the average hot and cold temperatures occur. These aluminum blocks had two purposes. This first one was to measure the junction temperature occurring at the surfaces of the thermoelectric module through a linear method of extrapolation. The second purpose was to measure the heat flux accruing at the junction of the thermoelectric module. In order to efficiently blow the cold and the hot air, it is essential to design proper air ducts. The housing air ducts for both sides were fabricated using plastic sheets to minimize the heat leak along the air ducts.

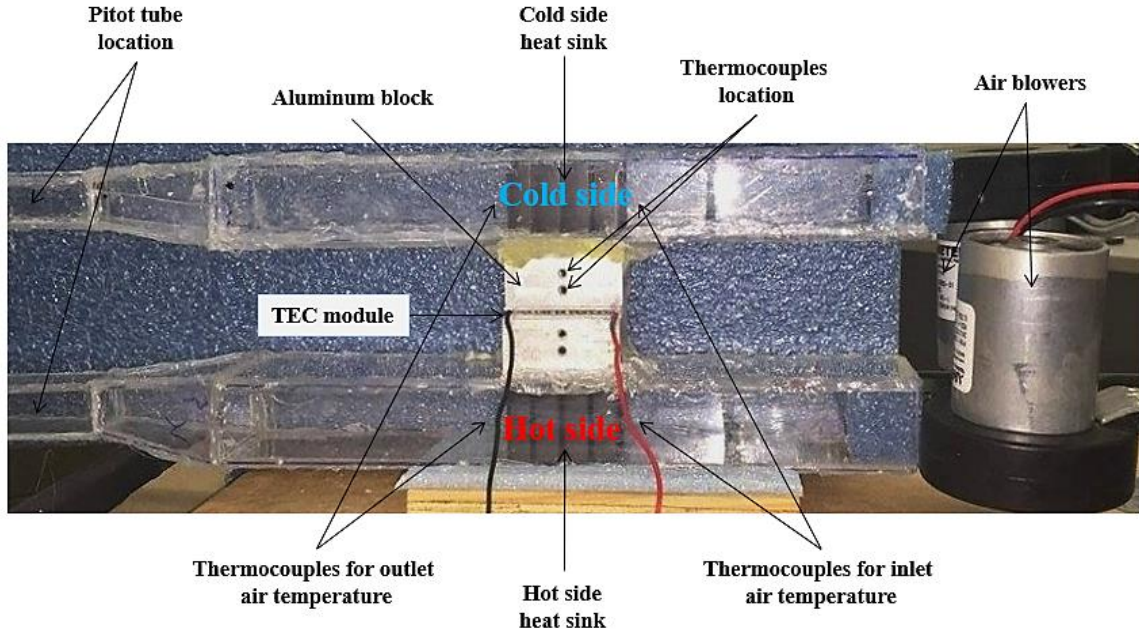


Figure 3.6 Photograph of the experimental setup.

Now, in order to obtain the junction temperature, let's consider the conduction heat transfer diagram shown in Figure 3.7. Assuming perfect insulation and perfect contact between the interfaces of the aluminum blocks and the thermoelectric module surfaces and one-dimensional uniform heat fluxes at the cold and the hot junctions, the steady state governing equation with no heat generation would be,

$$\frac{d^2T}{dx^2} = 0 \quad (3.43)$$

Where T is the temperature distribution as a function in distance x . The two boundary conditions needed to solve Equation (3.43) are the temperatures measured by the thermocouples given as,

$$T(x = x_1) = T_1 \quad (3.44)$$

$$T(x = x_2) = T_2 \quad (3.45)$$

Now, by integrating Equation (3.43) we get,

$$T(x) = C_1x + C_2 \quad (3.46)$$

Where C_1 and C_2 are the integrating constants. Applying the boundary conditions from Equations (3.44) and (3.45), Equation (3.46) can be solved for the temperature distribution as,

$$T(x) = \left(\frac{T_1 - T_2}{x_1 - x_2}\right)x + \left(T_1 - \frac{T_1 - T_2}{x_1 - x_2}x_1\right) \quad (3.47)$$

In the current case, we have $x_2 = \Delta x_{TC} + \Delta x_s$ where $\Delta x_{TC} = \Delta x_s$. This, leads to the value of the junction temperature T_s as,

$$T_s = T_1 - \left(\frac{T_2 - T_1}{\Delta x_{TC}}\right)\Delta x_s \quad (3.48)$$

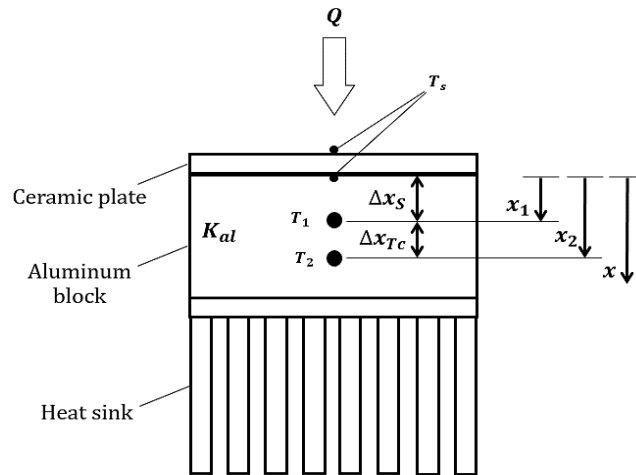


Figure 3.7 Temperature extrapolation.

Moreover, according to the assumption of neglecting the contact resistance of the ceramic plates, this surface temperature T_s can be treated as the actual junction temperature of the thermoelectric couples of the module. The advantage of this method of direct

measurement is reducing the contact resistance that may occur when using tape type thermocouples instead.

Two centrifugal blowers are used to drive the ambient air from the surrounding through the plastic duct to the cold and hot heat sinks where the volume flow rate is measured by pitot tubes fixed at the duct exit. These blowers are controlled by a TDK-Lambda EMS80-60 power supply model (Figure 3.8) with an output of up to 80 V and 60 A of DC power for a maximum power of 5 KW. The temperature of the air at the inlet and the exit of the heat sinks ($T_{\infty c,in}$, $T_{\infty h,in}$, $T_{\infty c,out}$, and $T_{\infty h,out}$) as shown in Figure 3.4b are measured using E-type thermocouples installed right at the inlets and the exits of the heat sinks. From these measurements, the average temperatures between fins are calculated as $T_{\infty c} = \frac{T_{\infty c,in} + T_{\infty c,out}}{2}$ and $T_{\infty h} = \frac{T_{\infty h,in} + T_{\infty h,out}}{2}$. The TEC input power, one the other hand, is manipulated using DC power supply TCR 10 20S30D-2-D model (Figure 3.8) with output voltage of 20 V and current of 30 A (0.6 KW of maximum power).



Figure 3.8 Test Stand power supplies.

Figure 3.9 indicates the connection of the test stand to the power supplies, electronic load and thermocouples. The power supplies and the thermocouples were connected to a data acquisition VI. The thermocouples were connected to the terminal blocks which have a high-accuracy thermistor cold and hot junction temperature sensor. The electronic load was connected directly to the computer using RS 232 serial communication, while the DAQ was connected directly to the computer. The temperature readings were set at a sampling rate of 1 Hz or 1 sample per second since the transient data are not crucial to this experiment.

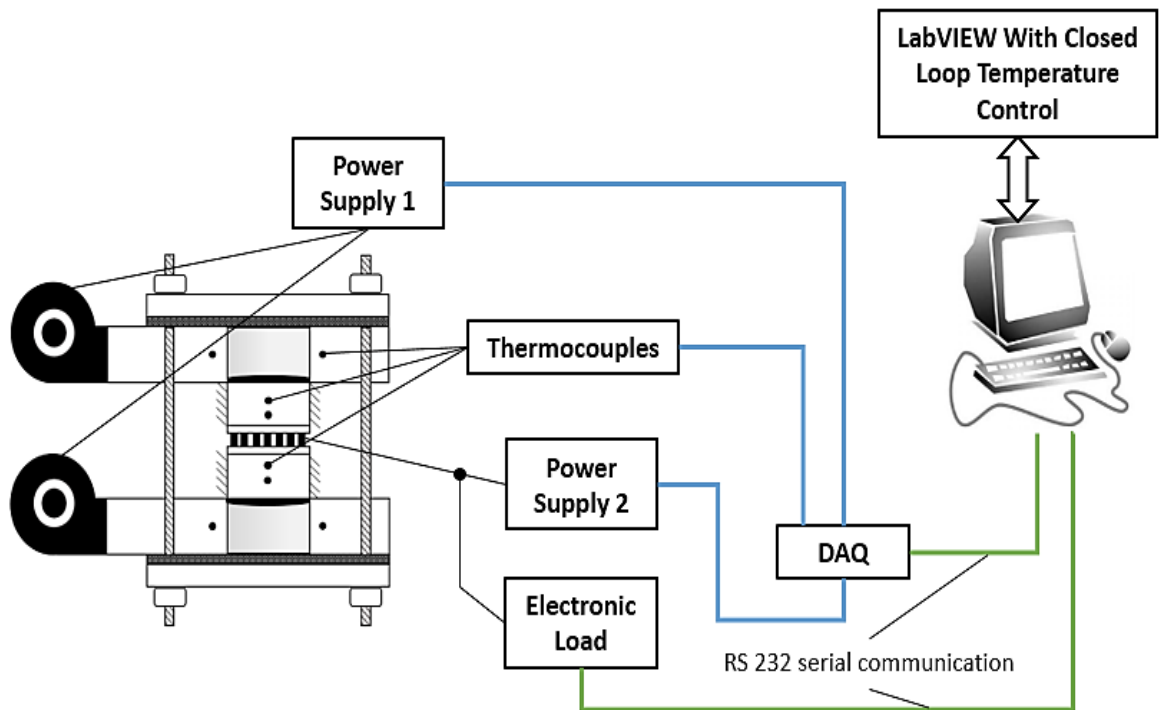


Figure 3.9 Overview of Experimental Control

Once the optimum geometric parameters and the input power of the thermoelectric cooler are obtained analytically, the experimental work is conducted to evaluate the performance of the thermoelectric system. Figure 3.10 indicates the flowchart of the

experimental process. In the first step, highly conductive thermal paste was applied to reduce the thermal resistance between the interfaces of the TEC module and the aluminum blocks. The test stand was also bolted down using locking nuts to ensure the equal pressure is applied to all pins which can reduce the thermal resistances and provide efficient heat transfer from the module to the aluminum blocks and the heat sinks. Then, the input voltage is adjusted until the steady state conditions are reached (no change in the temperature readings with time), and measurements are taken for the junctions and fluid inlet and exit temperatures at variable input voltages ranging from 0 V to the maximum voltage provided by the module manufacturer. Finally, the readings were tabulated or plotted for further analysis.

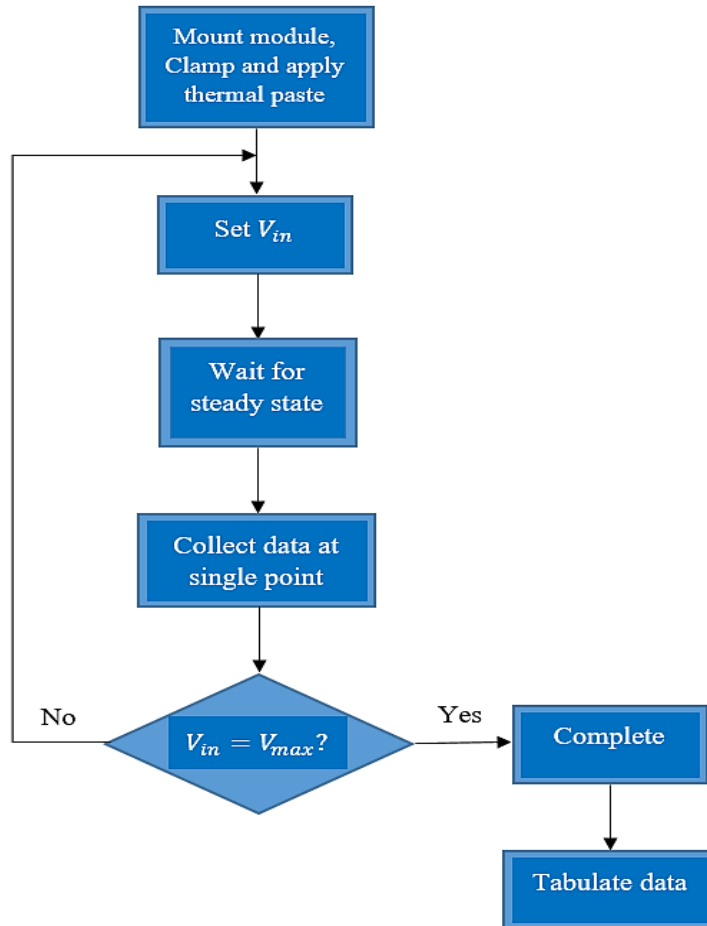


Figure 3.10 Flowchart of the experimental procedure.

Figure 3.11 shows the data acquisition VI front panel which was used to process the data collected by the thermocouples. As seen in this Figure, there are five waveform charts which are illustrating the thermocouples readings versus time. Two of these readings are for the hot and cold junction temperatures of the thermoelectric cooler. This procedure of data processing was repeated for all input voltage values. Once the junction temperatures are obtained, the cooling/heating power and coefficient of performance can be determined using Equations (3.7), (3.8) and (3.27), respectively. Finally, these experimental measurements are compared against the theoretical results in CHAPTER IV to check the

accuracy of the analytical calculations. Note that the screenshot of the data front panel was captured when the testing was still in the transient condition.

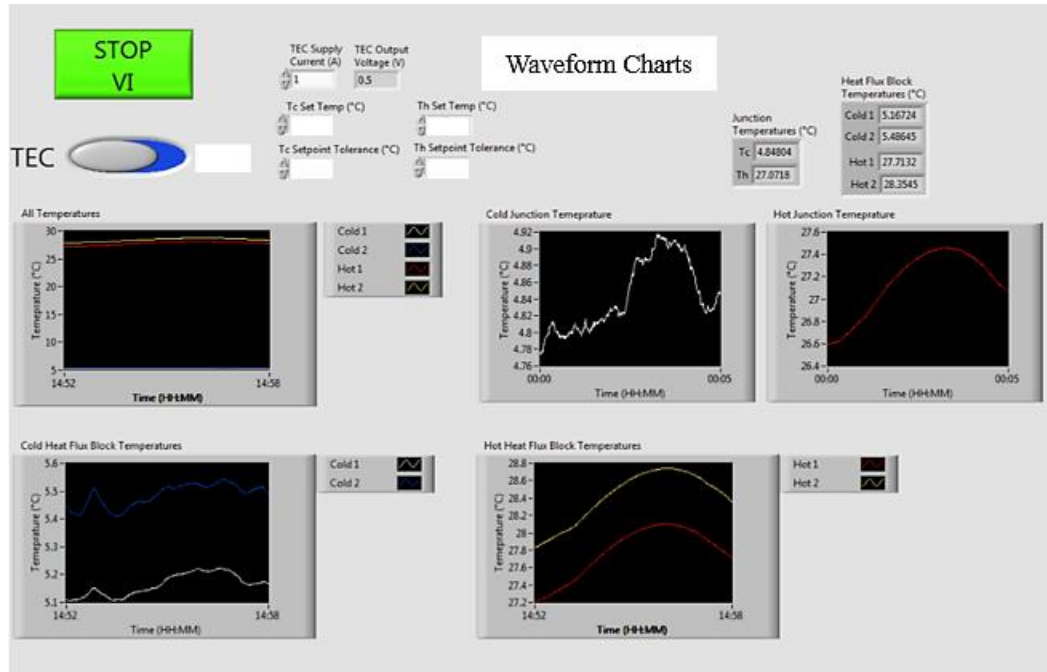


Figure 3.11 Data acquisition VI's front panel.

CHAPTER IV

RESULTS AND DISCUSSION

Most of the information in this chapter is with respect to the methodologies explained in Ref. [49] with the author's contribution. The objectives of this chapter can be summarized in four main points. First, calculating the effective material properties and comparing them with the manufacturer experimental data. Second, an existing design of air-to-air VTS heat pump is studied and validated using the thermoelectric ideal equations. The optimization of this design is investigated utilizing the dimensional technique at the same given input power and compared with the predicted performance concerning any room for improvement. Also, the optimal design of a new design of CSCC is studied analytically using the same power consumption with different overall geometry. Finally, the last portion of this chapter discusses the experimental validation which is employed to assess the accuracy of the new air-to-air CSCC theoretical model.

4.1 Effective Material Properties

In this section, the effective material properties (α^* , ρ^* and k^*) were calculated using the manufacturer's maximum parameters (Q_{max} , I_{max} and ΔT_{max}). Four different modules were chosen to check the status of the ideal equation with the effective material properties, as shown in Table 4.1. First, the effective material properties for each module were obtained using Equations (3.1) – (3.4). The cross-sectional area (A) and the leg length

(L) of the thermoelement were either measured or provided by manufacturers. As shown in Table 4.1, Equations (1.56) – (1.59) were employed to recalculate the maximum parameters (Q_{max} , I_{max} , ΔT_{max} , and V_{max}) using the calculated effective material properties. These values were compared with the manufacturers' maximum parameters. It shows good agreement except the maximum voltage which is reasonable because it was not considered in our calculations (secondary parameter).

Table 4.1 Comparison of the Properties and Dimensions of the Commercial Products of Thermoelectric Modules.

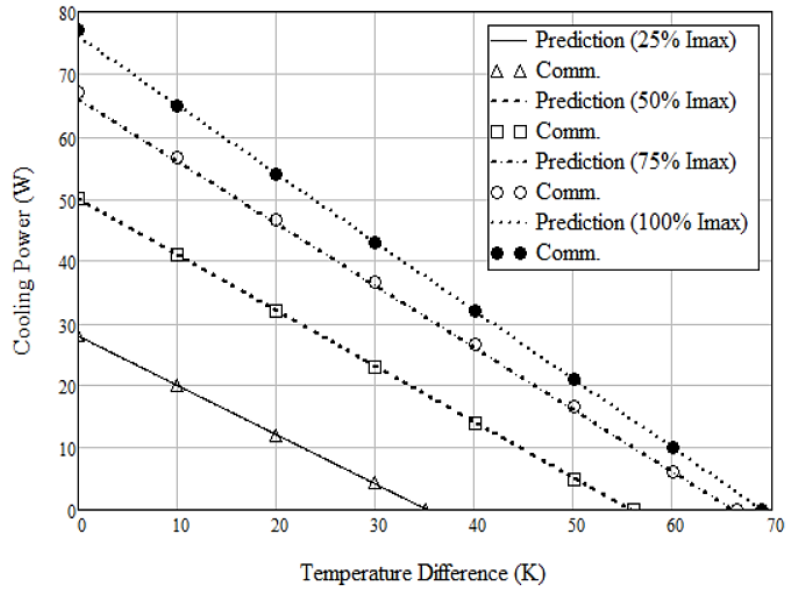
Description	TEC Modules (Bismuth Telluride)				
	Symbols	TE-127-1.4-1.15 $T_h = 27^\circ\text{C}$	RC 12-4 $T_h = 50^\circ\text{C}$	CP10-127-05 $T_h = 25^\circ\text{C}$	C2-30-1503 $T_h = 25^\circ\text{C}$
Number of thermocouples	n	127	127	127	127
Manufacturers' maximum parameters	$Q_{max}(W)$	76	39	34.3	34.1
	$I_{max}(A)$	7.9	3.7	3.9	3.5
	$\Delta T_{max}(K)$	69	74	67	68
	$V_{max}(V)$	15.9	16.4	14.4	15.5
Measured geometry of thermoelement	$A(mm^2)$	1.96	1	1	1.21
	$L(mm)$	1.15	1.17	1.25	1.66
	$G = A/L(cm)$	0.17	0.085	0.08	0.073
Dimension (W×L×H)	mm	$40 \times 40 \times 3.4$	$30 \times 30 \times 3.4$	$30 \times 30 \times 3.2$	$30 \times 30 \times 3.7$
Effective material properties (calculated using commercial Q_{max} , I_{max} , and ΔT_{max})	$\alpha^*(\mu V/K)$	205.285	208.98	189.2	208.5
	$\rho^*(\Omega cm)$	1.023×10^{-3}	1.2×10^{-3}	0.9×10^{-3}	1.0×10^{-3}
	$k^*(W/cmK)$	0.016	0.015	0.016	0.017
	ZT_h	0.776	0.77	0.744	0.758
The maximum parameters	$Q_{max}(W)$	76	39	34.3	34.1
	$I_{max}(A)$	7.9	3.7	3.9	3.5

using effective material properties	ΔT_{max} (K)	69	74	67	68
	V_{max} (V)	15.643	16.21	14.15	15.37

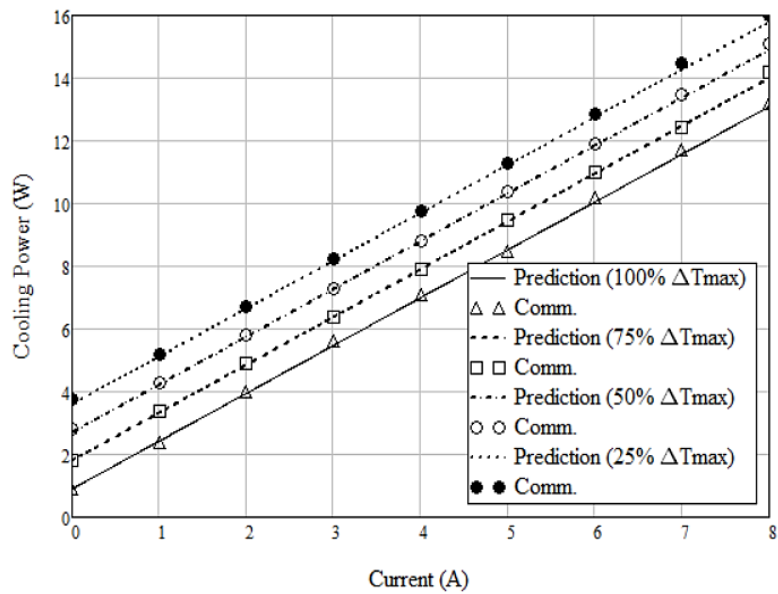
Note that the effective material properties are calculated using the thermoelectric ideal equations and the measured maximum parameters (Q_{max} , I_{max} and ΔT_{max}). Thus, they include different effects like the Thomson effect, the temperature dependence of the material properties, contact resistances, and losses due to radiation and convection during modules performance testes. This combination of maximum parameters (Q_{max} , I_{max} and ΔT_{max}) causes the errors between the present prediction with the ideal equation and the real measurements to lie within the maximum voltage as shown in Table 4.1. Such technique enables more accurate prediction of the cooling power which is in this case given priority over the voltage, because it is a crucial and common parameter.

Furthermore, the effective material properties along with the thermoelectric ideal equations, were employed to predict the performance of the used thermoelectric module (TE-127-1.4-1.15), which was compared later with the commercial performance curves provided by the manufacturer (refers to by Figure 4.1 a, b and c). Figure 4.1a indicates the cooling power calculated using Equation (1.45) and the effective material properties versus the temperature difference at variable input current. It is seen in Figure 4.1a that the analytically calculated cooling power is in good agreement with the manufacturer's performance curves. In Figure 4.1b, the estimated cooling power versus input current at various junction temperature differences is compared against the manufacturer data with fair agreement found. Figure 4.1c shows the cooling power as a function of the temperature difference various applied voltages. It is seen that the errors between the predictions and the manufacturer's data on the curves increase with larger input voltages, which is

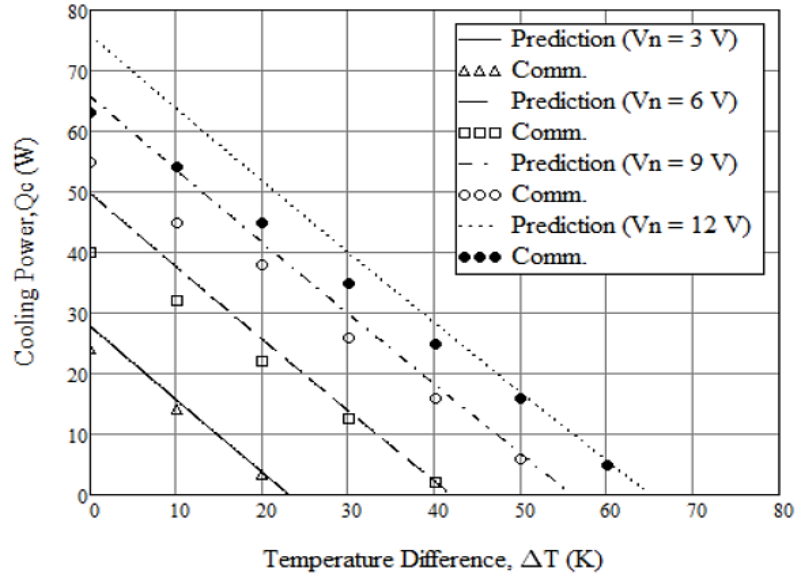
reasonable because the material properties are not temperature independent and because of the errors associated with input voltage as discussed earlier.



(a)



(b)



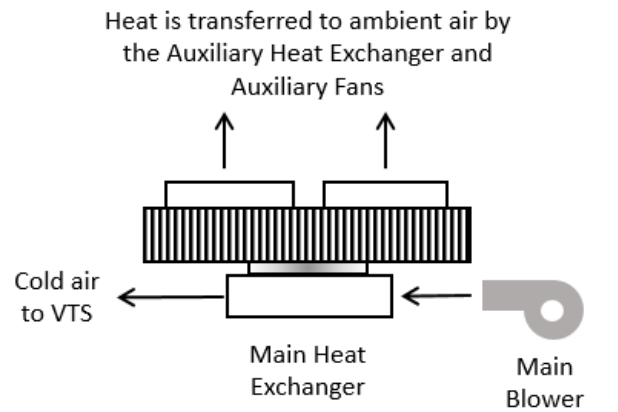
(c)

Figure 4.1 For module TE-127-1.4-1.15 by TE-Technology, the comparison between calculations with effective material properties and commercial data. (a) cooling power versus temperature difference as a function of current, (b) cooling power versus input current as a function of temperature difference, and (c) cooling power versus temperature difference as a function of voltage.

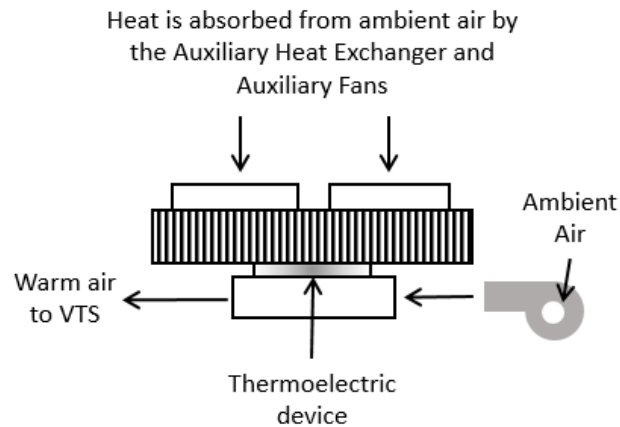
4.2 Study of Feher's VTS

In this section, the variable temperature seat (VTS) heat pump data provided by Feher is reproduced using the thermoelectric ideal equation based on Feher's inputs along with some needed assumptions for the missing information. Figure 4.2 illustrates a schematic of Feher's air-to-air VTS heat pump design. As seen, the design consists of one thermoelectric cooler clamped between two heat exchangers, which are driven by two auxiliary fans and one air blower. The auxiliary heat exchanger dissipates the heat to the ambient air by the auxiliary fans in cooling mode (Figure 4.2a) and absorbs the heat from the ambient air in heating mode (Figure 4.2b). The main heat sink regulates the air (cold or warm) pumped to the seat by the main blower. The geometric dimensions of this design

are given as 209.6 mm in length, 92.1 mm in width and 57.2 mm in height. In cooling mode at ambient temperature (T_{amb}) of 300.4 K , the system pumps about 6 cfm of cold air at a temperature difference of 10 K , which converts to about 33.3 W at input power of 82 W . In heating mode and at an ambient temperature of 257.04 K , the VTS pumps the same air flow rate at sensible heating power of 56.5 W at a temperature difference of 14.4 K .



(a)



(b)

Figure 4.2. Schematic diagram of Feher's VTS heat pump. (a) cooling mode and (b) heating mode.

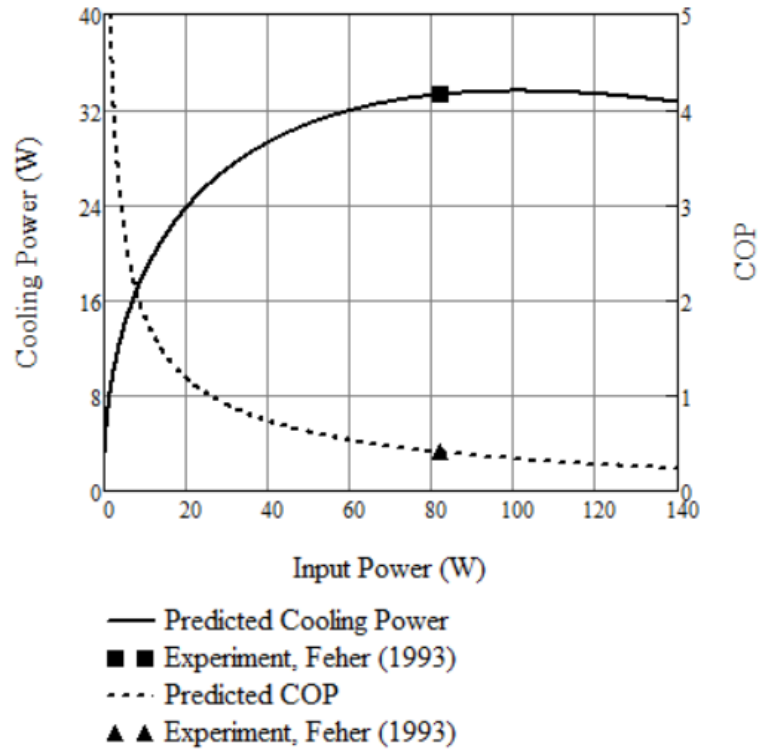
To reproduce Feher's performance data, several assumptions needed to be considered, some of which are carefully adjusted until good agreement is observed. For instance, the air flow rate at the auxiliary heat sink is 18 cfm , the heat sinks materials are aluminum, the profile length b_f of heat sinks is 15 mm , the fin thickness t_c of the main heat exchanger is 0.7 mm , the fin thickness of the auxiliary heat sink t_h is 1 mm . Also, a commercial thermoelectric cooler (TB127-1.4-1.2) was used in the calculation with the following specifications: module area (A_m) is $40 \times 40 \text{ mm}^2$, geometric factor is 0.163 cm and number of thermocouples is 127. The thermoelectric material properties (α , K , R and Z) were calculated using the effective material properties introduced by Lee et al. [15].

Feher's claims that his VTS heat pump puts out about 33.3 W of cooling power (Q_c) at an input power of $P_{in} = 82 \text{ W}$, which correspond to $COP = 0.4$. Also, the temperature difference across the main heat exchanger ($\Delta T_{cooling}$) was about 10 K , which can be translated to Driver's Metabolic Unit (DMU), which is the amount of heat occupants' body needs to release while driving, of about 26 %. To analyze this system, it is assumed that each heat sink faces a flow with linear temperature gradient, which means that the temperature between fins is the average of the inlet and the exit temperatures. The heat exchangers parameters were calculated to match the cooling power and COP of Feher's VTS heat pump employing the heat sink equations found in Ref. [16] and Nusselt number correlations found in Ref. [33]. Then, the six basic equations were solved for the cooling power and the COP at variable input current values (I). The predicted results for both the cooling and heating modes were, finally, compared with Feher's VTS heat pump experimental data, as shown in Table 4.2. Figure 4.3a and b shows a comparison between the present calculations and Feher's output data. In Figure 4.3a, the predicted cooling

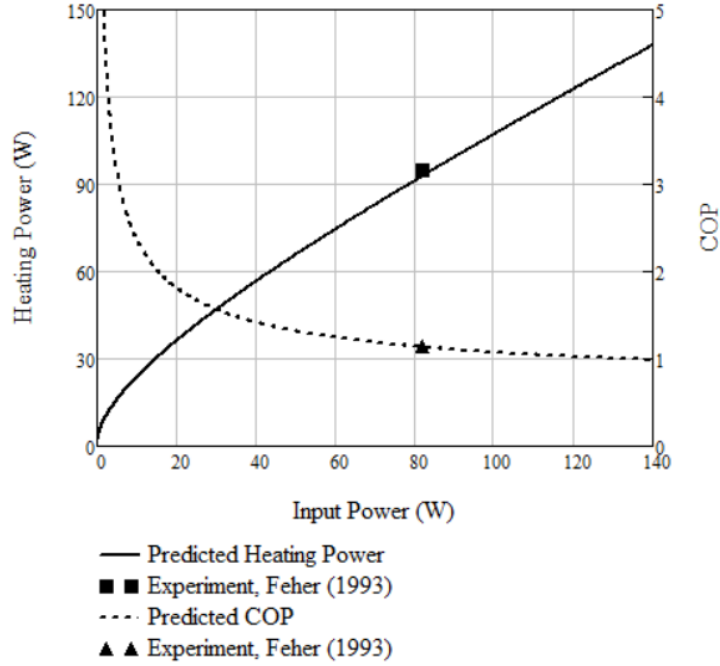
power and COP indicated by the solid and dashed lines, respectively, show fair agreement with the experimental data provided by Feher referred to by the symbols (at input power of 82 W). Similarly, Figure 4.3b illustrates the heating power and COP versus input power compared against Feher's heat pump data for the heating mode with good accuracy. The predicted data showed also acceptable agreement with Feher's data when the flow rate was increased from 6 cfm to 8 cfm, where the predicted COP raised, consequently, from 0.4 to about 0.45 with a small drop in the cooling temperature difference from 9.9 K to 7.9 K. Therefore, since the validity of this prediction (based on Feher's heat pump data) is obtained, this paves the way to a new compression with the optimum design.

Table 4.2 Comparison between Feher's VTS Heat Pump Data and the Present Prediction for Cooling and Heating Modes.

Parameter	Cooling Mode		Heating Mode	
	Feher	Prediction	Feher	Prediction
$T_{amb} (K)$	300.4	300.4	257.04	257.04
$P_{in}(W)$	82	82	82	81.48
$I(A)$	6.3	6.3	6.3	6.05
$Q_c / Q_h(W)$	33.3	33.22	94.6	89.23
$T_c(K)$	NA	277.54	NA	255.45
$T_h(K)$	NA	320.61	NA	322.11
$\frac{\Delta T_{cooling}}{\Delta T_{heating}} (K)$	10	9.91	24.2	27.06
COP	0.406	0.406	1.15	1.106
DMU(%)	26.6	26.5	75.7	71.4
PD (W/cm²)	0.18	0.18	0.526	0.496
Inputs: $V_c = 6 \text{ cfm}, V_h = 18 \text{ cfm}, A_{s,c} = 90 \times 100 \text{ mm}^2, A_{s,h} = 90 \times 200 \text{ mm}^2, b_c = 10 \text{ mm}, b_h = 20 \text{ mm}, t_c = 0.7 \text{ mm}, z_c = 2.8 \text{ mm}, n_c = 25, h_c = 32.78 \text{ W/m}^2\text{K}, h_h = 33.172 \text{ W/m}^2\text{K}, \eta_c h_c A_c = 1.854 \text{ W/K}, \eta_h h_h A_h = 8.083 \text{ W/K}, N_h = 0.229, A_m = 40 \times 40 \text{ mm}^2, n = 127, \alpha_n = -\alpha_p = 210.01 \mu\text{V/K}, \rho_n = \rho_p = 1.038 \Omega\text{cm}, k_n = k_p = 0.016 \text{ W/cmK}, Z = 2.647 \times 10^{-3} \frac{1}{K}$.				



(a)



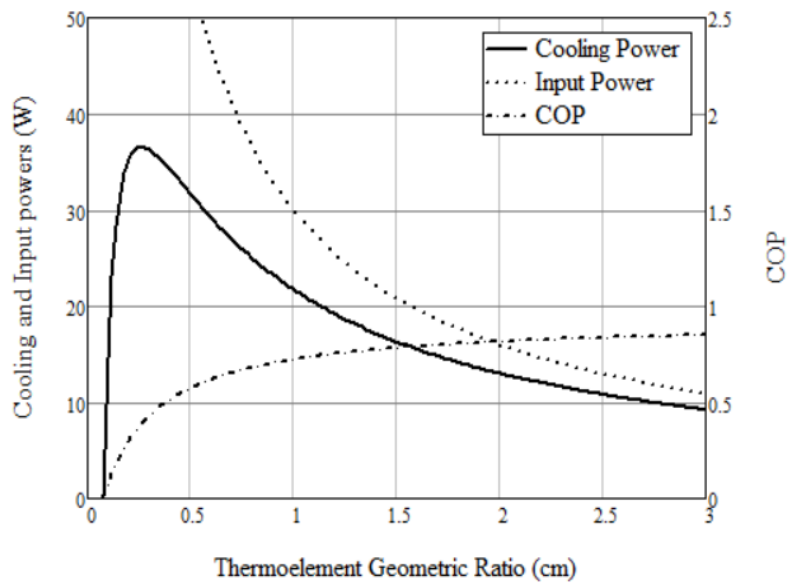
(b)

Figure 4.3 Cooling/heating power and COP versus input power for Feher’s work and present prediction for (a) cooling mode and (b) heating mode.

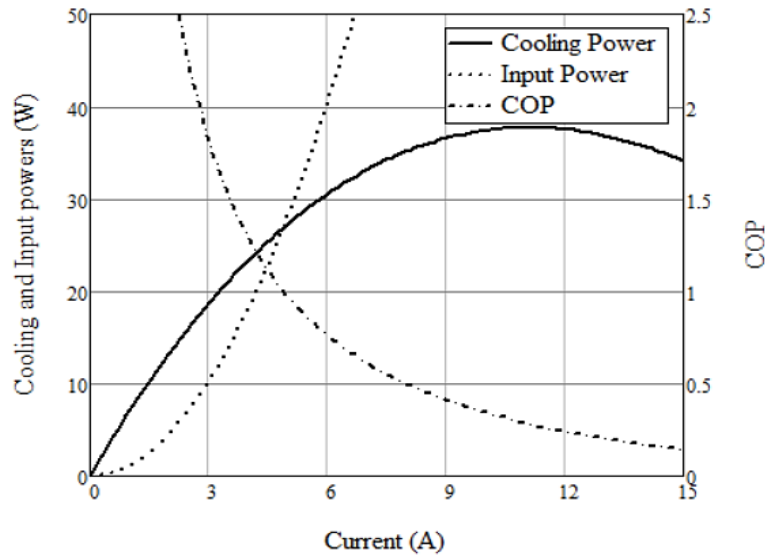
4.3 Feher’s VTS Optimal Design

The optimization method described in CHAPTER III is employed to find the optimal values for the dimensionless parameters (N_l , N_k , Q_c^* , Q_h^* , COP , T_c^* , and T_h^*) iteratively at given N_h , $T_{\infty,in}^*$ and $ZT_{\infty,h,in}$. The same configuration used to predict Feher’s heat pump performance was used in the optimization analysis. Thus, heat sinks parameters represented in N_h , thermoelectric material properties ($ZT_{\infty,h,in}$), and inlet temperatures ($T_{\infty,in}^*$) are all inputs taken from the previous prediction configuration. Then, the dimensionless optimum parameters are converted back to real parameters values by using the same dominant (the thermal resistance, $\eta_h h_h A_h$). The cooling and input powers versus current and thermoelement geometric ratio are shown in Figure 4.4a and b, respectively.

Figure 4.4a was plotted using optimum $N_k = 0.16$, and Figure 4.4b was generated using optimum $N_l = 0.056$. From Figure 4.4a, it is noticeable that the maximum cooling power occurs when the COP is very small and vice versa, so it is important to use midpoints of the optimal current and thermoelement geometric ratio that give reasonable cooling power without dropping the COP to unacceptable low levels. Also, at geometric ratio values larger than about 0.318 cm (at which the maximum cooling power occurs), it is seen that the cooling power starts to decline repedly because the input Joule heating becomes the dominant.



(a)



(b)

Figure 4.4 Cooling and input power versus (a) thermoelement geometric ratio and (b) input current.

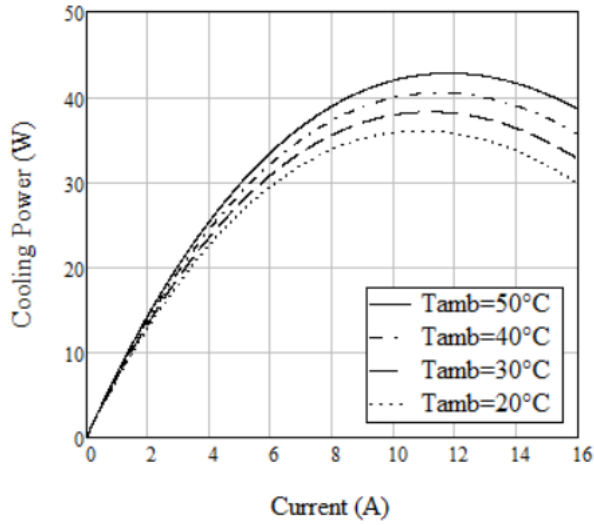
Table 4.3 shows a comparison between the present prediction based on Feher's heat pump data and the optimal design results for the cooling mode. It can be seen that the optimal design has relatively better performance (cooling power and COP) over the old layout. This optimization indicates that if the input current and the geometric ratio are increased to the optimized values, higher performance (COP) would be achieved. In the heating mode, the optimum design calculations did not show significant improvement in performance due to the freezing inlet temperature. In such conditions, an after heater device may be needed to produce warm air to the seat sooner until the interior air temperature rises, resulting in higher COP. However, thermoelectric coolers are considerably more efficient in the heating mode than the cooling mode because the Joule heating term (RI^2) is additive in the heating mode.

Table 4.3 Compression Between Feher’s VTS Heat Pump Predicted Data and Optimal Design.

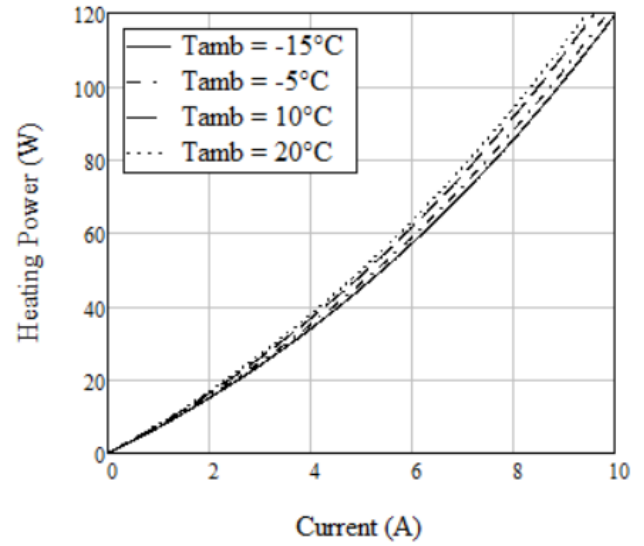
Parameter	Cooling Mode		Heating Mode	
	Prediction (Feher Base)	Optimal Design	Prediction (Feher Base)	Optimal Design
$T_{amb} (K)$	300.4	300.4	257.04	257.04
$ZT_{\infty h, in}$	0.79	0.79	0.68	0.68
$P_{in} (W)$	82.24	80.71	81.48	84.12
$I (A)$	6.45	8.5	6.05	8.45
$G_e (mm)$	1.63	3.18	1.63	3.18
$Q_c/Q_h (W)$	33.22	36.02	89.23	92.27
$T_c (K)$	277.54	275.58	255.45	255.89
$T_h (K)$	320.61	320.88	322.11	327.48
$\Delta T_{cooling} / \Delta T_{heating} (K)$	9.91	10.71	26.06	28.72
COP	0.406	0.446	1.095	1.097
$DMU (\%)$	26.5	28.8	71.4	73.8
$PD (W/cm^2)$	0.18	0.2	0.496	0.513
Inputs: $V_c = 6 \text{ cfm}, V_h = 18 \text{ cfm}, A_{s,c} = 90 \times 100 \text{ mm}^2, A_{s,h} = 90 \times 200 \text{ mm}^2, b_c = 10 \text{ mm}, b_h = 20 \text{ mm}, t_c = 0.7 \text{ mm}, z_c = 2.8 \text{ mm}, n_c = 25, h_c = 32.78 \text{ W/m}^2\text{K}, h_h = 33.172 \text{ W/m}^2\text{K}, \eta_c h_c A_c = 1.854 \text{ W/K}, \eta_h h_h A_h = 8.083 \text{ W/K}, N_h = 0.229, A_m = 40 \times 40 \text{ mm}^2, n = 127.$				

Figure 4.5 shows the change of the cooling/heating power, temperature difference and COP versus the input current at various ambient temperatures for cooling and heating modes. It is clear that as the ambient temperature rises, both the cooling/heating power and the temperature difference will increase further (Figure 4.5a, b, c and d) resulting in higher COPs (Figure 4.5e and f). This is actually an advantage in the cooling mode since the cooling power will drop as the interior of the vehicle temperature cools down responding to opening the windows or activating the HVAC. However, it is a disadvantage in the

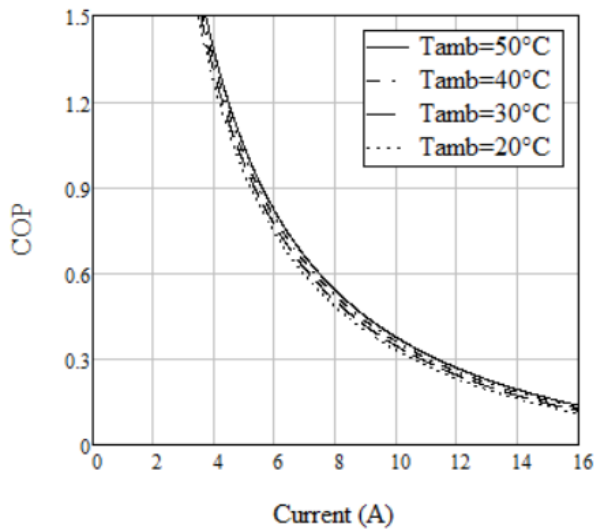
heating mode because as the interior of the vehicle warms due to the engine heat, lower heating from the seat would be desirable.



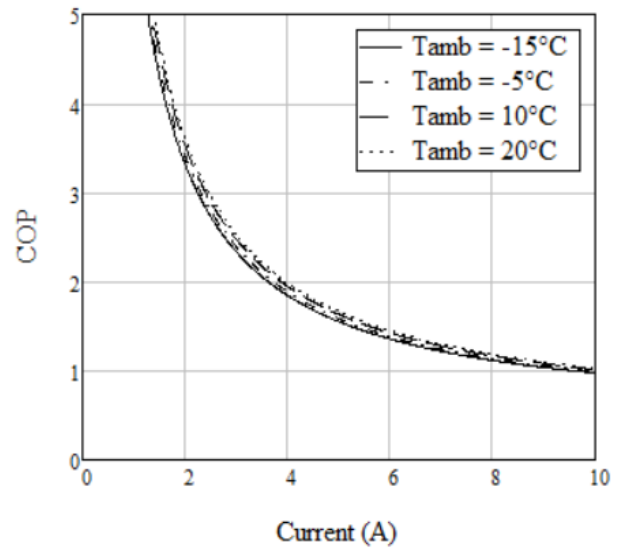
(a)



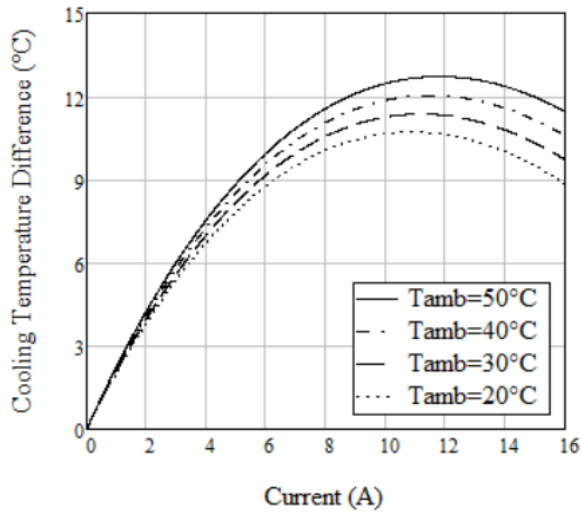
(b)



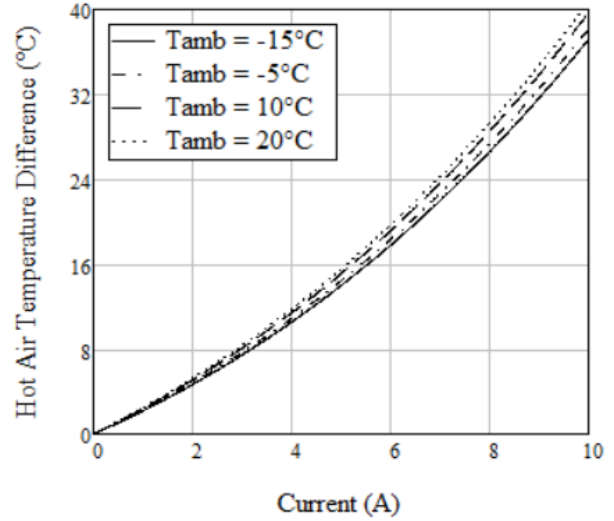
(c)



(d)



(e)



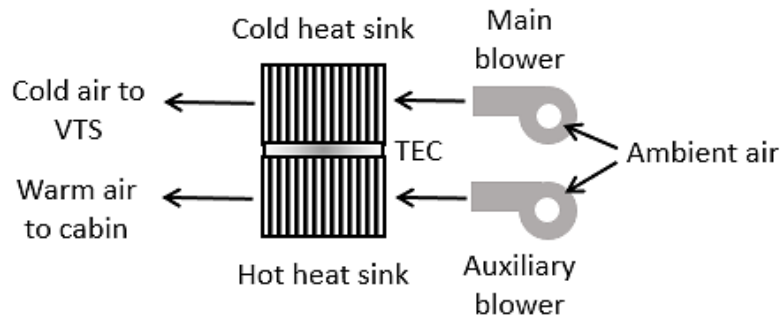
(f)

Figure 4.5 Cooling/heating power, temperature difference and COP versus input current at variable ambient temperature. (a) Cooling power versus input current, (b) heating power versus input current, (c) cooling COP versus input current, (d) heating COP versus input current, (e) cooling temperature difference versus input current and (f) heating temperature.

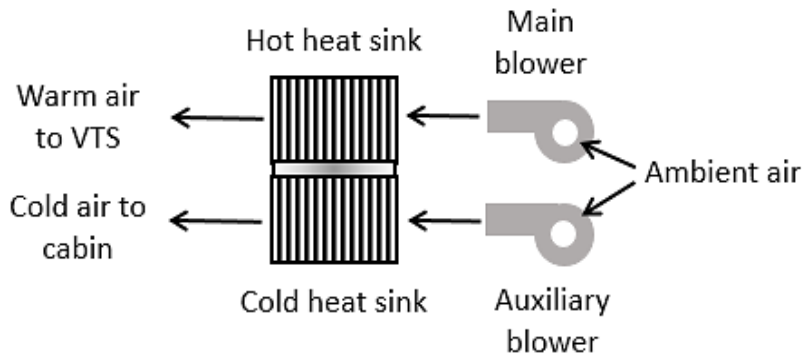
4.4 New Design of the CSCC

In the new model, two thermoelectric heat pumps are used, one of which is installed in the backrest and the other in the seat rest as seen in Figure 4.6. Figure 4.6a and b indicate the cooling and the heating modes, respectively. The conditioned air total flow rate of the old design is divided by two so that each thermoelectric heat pump provides about 3 *cfm* of conditioned air, with a total flow rate of 6 *cfm* for the whole seat. Also, the optimal design of the new system was built based on the same input power used by Feher, but the base area of the heat exchangers was decreased with relatively higher profile length to meet the old design performance. Several key factors were considered when designing the new CSCC:

1. Limited space within the vehicle seat. The new CSCC can be easily installed and fit even very thin car seats.
2. Mounting the new CSCC heat pumps close to the seat surface can guarantee efficient delivery of the conditioned air to the occupant.
3. Also, short and simplified air ducting would be used, which reduces the air duct heat leak, cost and pressure drop which results in reducing the noise and fans input power.



(a)



(b)

Figure 4.6 Schematic of the new CSCC heat pump. (a) cooling mode and (b) heating mode.

Figure 4.7 illustrates the importance of having an efficient plenum venting, so when the occupant is seated (Figure 4.7b), the hot air and the unconsumed cold air (in cooling mode) are allowed to move freely through the plenum to the cabin. The volume flow rate of the hot air vented to the cabin is small compared the total flow rate HVAC, so it should not be disturbing the occupants. In contrast, in the heating mode, the cold air would be the exhaust which will be wasted to the cabin through the outlet vents.

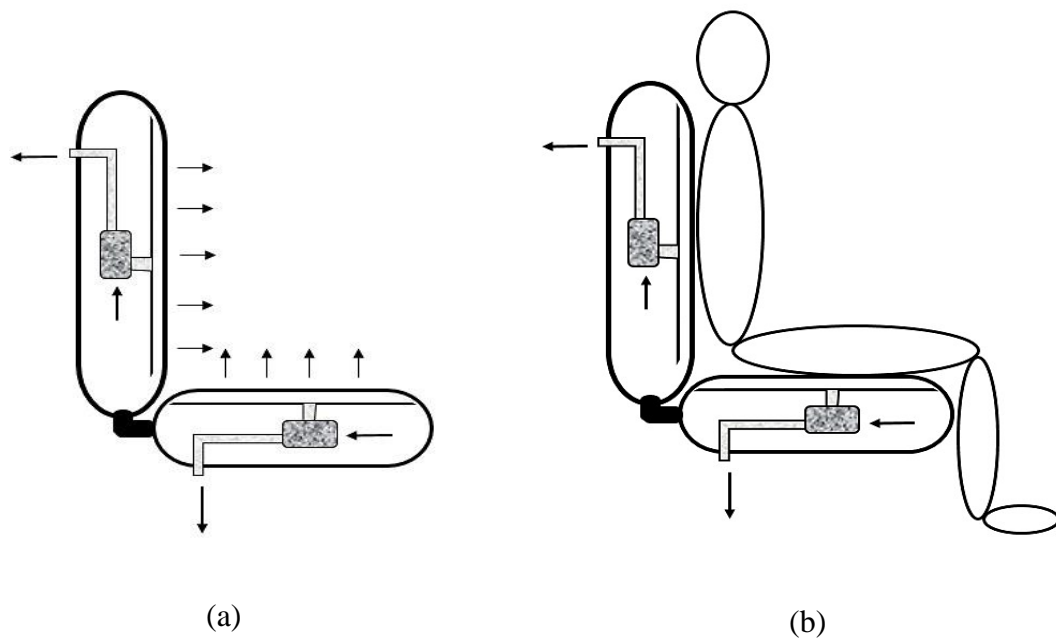


Figure 4.7 Schematic of the new CSCC design. (a) The air flow venting system, (b) the car seat with the occupant seated.

The heat sinks optimization method discussed in CHAPTER III is applied to optimize the cold and hot heat sinks regarding the fin spacing and fin thickness to minimize the thermal resistances ($\eta_c h_c A_c$ and $\eta_h h_h A_h$) and thus to maximize the heat transfer rates. Therefore, after calculating the optimum fin spacing using Equation (1.98), the optimum fin thickness can be optimized to give the maximum heat transfer rate from Equation

(1.99). Figure 4.8 shows the results of heat sinks optimization. In Figure 4.8, the total heat transfer rates for the hot and the cold sides are plotted versus the fin thickness. The flow rates in the heat sinks are regarded as channel flows, so the Nusselt number correlations found in Ref. [35] are used to calculate the convection coefficients.

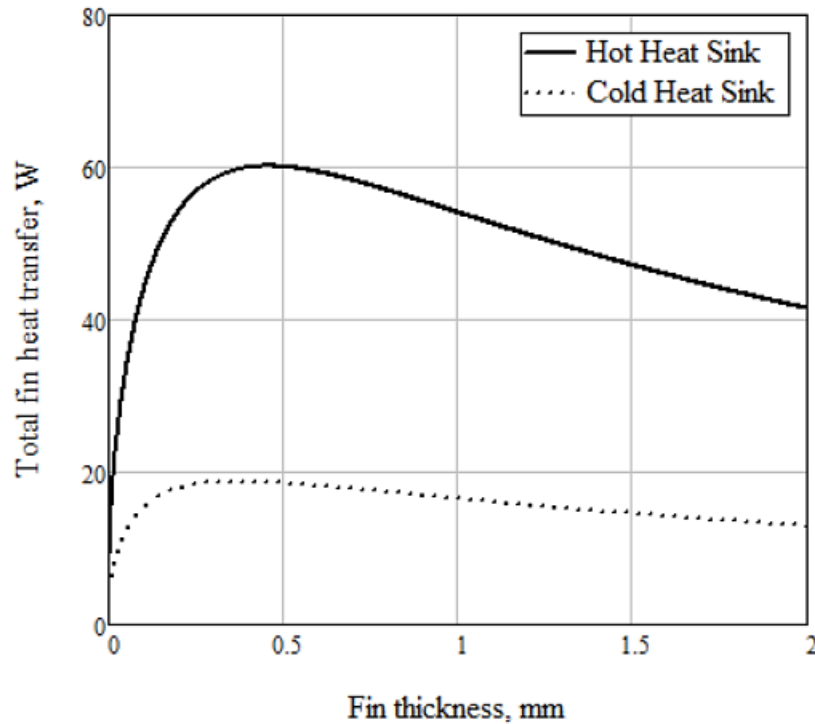
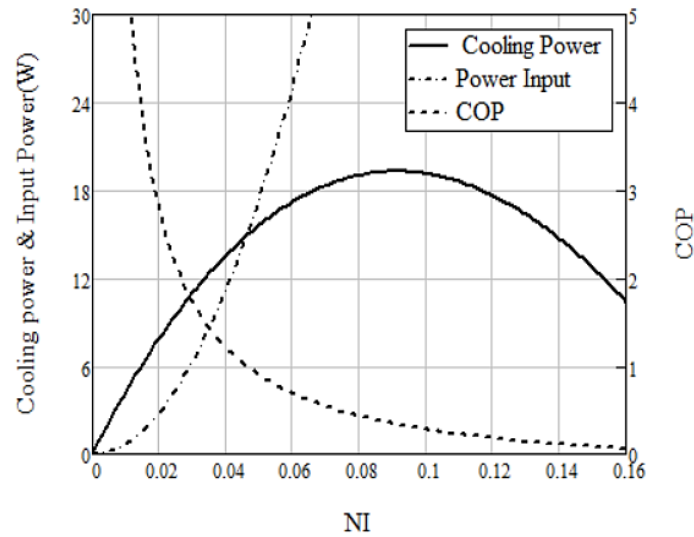


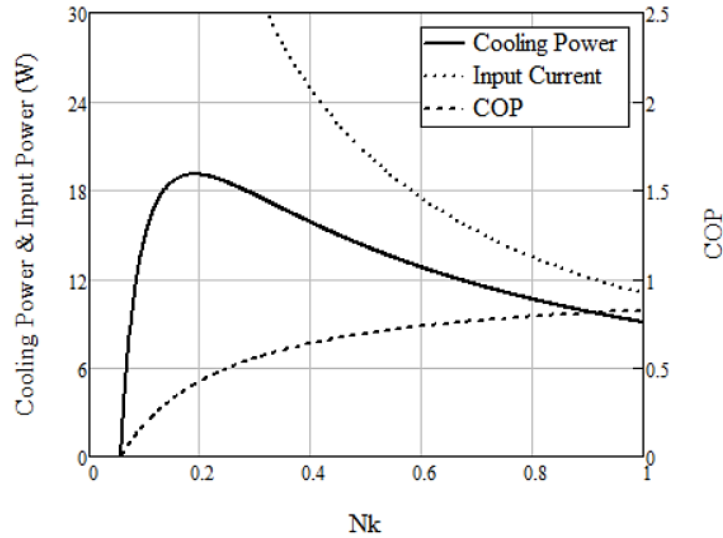
Figure 4.8 Total heat transfer rate versus fin thickness for hot and cold heat sinks.

Finally, the same optimal design method is applied to find the optimum combination of the dimensionless parameters (N_I, N_k) as shown in Figure 4.9. Figure 4.9a was generated with the dimensionless thermal conductance $N_k = 0.219$, while Figure 4.9b was plotted at dimensionless input current $N_I = 0.0775$. In fact, N_k represents the geometry of the thermoelectric device, so once determined, it is permanent, while N_I is the current, which can be adjusted depending on the demand such as transient initial startup (few seconds or minutes) or steady state cooling/heating for a long time (minutes or hours).

Note that the optimization procedure is employed at the same input power used in the Feher's VTS heat pump, so that the performance can be compared against the old design. Similarly, this dimensionless parameters can be converted to the real parameters (thermoelement geometric ratio, number of thermocouples and input current) from the definition of these dimensionless quantities and by using the same thermal conductance $\eta_h h_h A_h$. Usually the number of thermocouples is fixed and the thermoelement geometric ratio is optimized to give the maximum cooling/heating power. Then, using the same number of thermocouples, the optimum input current can be determined by the equivalent procedure.



(a)



(b)

Figure 4.9 Cooling power, input power and COP versus (a) dimensionless input current and (b) and dimensionless thermal conductance.

Results of the new CSCC design are shown in Table 4.4. The goal of the new model is not only to provide occupant comfort during the steady state conditions but also during the startup (transient) period until the car HVAC is in activation. Therefore, the transient operation behavior is equivalently important, which is also studied and its results are shown in Table 4.4. The column titled ‘maximum power’ for the cooling mode in Table 4.4 means that if the current is increased above that value, there will be no much gain in the cooling power. For instance, an increased power consumption of 66.75 W leads to slight gains in the cooling power and temperature difference of 0.25 W and 0.148 K, respectively. However, for heating, the situation is different. We can increase the heating power from 47.91 W to 83 W and temperature differences from 28.806 K to 49.91 K with the current increasing from 4.2 A to 6 A with a pay for the power consumption from 40.57 W to

85.67 W. This may be incorporated as an option into car seat climate control for extreme winter conditions if the car battery is permitted.

Table 4.4 Summary of The New CSCC Optimal Design.

Parameter	Cooling Mode		Heating Mode	
	Max. Power (Transient) $I_{opt} = 4.3 A$	Min. Power (Steady state) $I_{opt} = 1.5 A$	Max. Power (Transient) $I_{opt} = 4.2 A$	Min. Power (Steady state) $I_{opt} = 0.5 A$
$T_{amb} (K)$	300.4	294	257.04	294
$ZT_{\infty h, in}$	0.79	0.772	0.68	0.772
$P_{in}(W)$	40.95	5.04	40.57	0.567
$Q_c/Q_h (W)$	18.61	9.74	47.91	4.17
$\frac{\Delta T_{cooling}}{\Delta T_{heating}} (K)$	11.064	5.792	28.806	2.507
COP	0.454	1.93	1.18	7.35
$DMU(\%)$	14.9	7.8	38.3	3.3
$PD (W/cm^2)$	1.163	0.609	2.994	0.261
Inputs: $V_c = 3 cfm, V_h = 8 cfm, A_{s,c} = 40 \times 40 mm^2, A_{s,h} = 40 \times 40 mm^2, b_c = 20 mm, b_h = 25 mm, t_c = 0.36 mm, z_c = 1.848 mm, n_c = 18, t_h = 0.45 mm, z_c = 1.248 mm, n_c = 23, h_c = 52.89 W/m^2K, h_h = 84.68 W/m^2K, Nu_c = 6.88, Nu_h = 7.45, A_m = 40 \times 40 mm^2, G_e = 1.59 mm, n = 127$				

Note that the data listed in Table 4.4 are for only one thermoelectric heat pump (backrest or seat rest). Thus, to obtain the whole seat performance, the cooling/heating power, input power, and DMU should be multiplied by two. The new design performance for the entire seat is compared with the old model performance (based on Feher's data) and with the optimal design of the VTS heat pump as shown in Table 4.5. This comparison indicates that the new optimal design of CSCC has the advantage over the two other models regarding the performance with significant size reduction from $200mm \times 90mm \times 50mm$ to approximately $40mm \times 40mm \times 52mm$ for each heat pump.

Table 4.5 Comparison of the New CSCC Optimal Design with Feher's VTS Heat Pump Predicted Data and its Optimal Design.

Parameter	Cooling Mode			Heating Mode		
	Prediction (Feher Base)	Optimal Design	New Design	Prediction (Feher Base)	Optimal Design	New Design
$T_{amb} (K)$	300.4	300.4	300.4	257.04	257.04	257.04
$P_{in}(W)$	82.24	80.71	81.9	81.48	84.12	81.14
$Q_c/Q_h (W)$	33.22	36.02	37.22	89.23	92.27	95.82
$\Delta T_{cooling} / \Delta T_{heating} (K)$	9.91	10.71	11.064	26.06	28.72	28.806
COP	0.406	0.446	0.454	1.095	1.097	1.18
$DMU(\%)$	26.5	28.8	29.8	71.4	73.8	38.3
$PD (W/cm^2)$	0.18	0.2	1.16	0.496	0.513	2.995

Furthermore, this dimensionless technique can determine the optimal parameters for the different dimensionless figure of merit (ZT) values. It is found that as the ZT value changes, the optimal design parameters (optimal geometric ratio and input current) will accordingly change. Table 4.6 indicates the cooling mode performance of the air-to-air VTS heat pump with different ZT value and at the same input power. As seen from this table, as the $ZT_{\infty h, in}$ values increase the performance of the heat pump in terms of the cooling power and COP improve. For instance, at $ZT_{\infty h, in} = 2$ the cooling power and COP raised up significantly to about 30.494 W and 0.759, respectively, compared to the present work ($ZT_{\infty h, in} = 0.79$).

Table 4.6 Optimal Design Performance for Different ZT Values for Cooling Mode.

Parameter	$ZT_{\infty h, in} = 0.79$ (PRESENT)	$ZT_{\infty h, in} = 1$	$ZT_{\infty h, in} = 1.5$	$ZT_{\infty h, in} = 2$
$P_{in}(W)$	40.95	39.126	40.126	40.153
$G_{e, opt}(mm)$	1.59	1.513	1.353	1.237
$I_{opt}(A)$	4.3	4.5	5	5.2
$T_c(K)$	281.02	278.08	272.535	268.672
$T_h(K)$	327.457	327.936	330.845	332.513
$Q_c(W)$	18.61	21.452	26.78	30.494
$\Delta T_{cooling}$	11.064	12.751	15.919	18.126
COP	0.454	0.548	0.666	0.759
$DMU(\%)$	14.9	17.2	21.4	24.4
$PD(W/cm^2)$	1.163	1.341	1.674	1.906
Inputs: $T_{\infty c, in} = 300.4 K$, $T_{\infty h, in} = 300.4 K$ $V_c = 3 cfm$, $V_h = 8 cfm$, $A_{s, c} = 40 \times 40 mm^2$, $A_{s, h} = 40 \times 40 mm^2$, $b_c = 20 mm$, $b_h = 25 mm$, $t_c = 0.36 mm$, $z_c = 1.848 mm$, $n_c = 18$, $t_h = 0.45 mm$, $z_h = 1.248 mm$, $n_h = 23$, $h_c = 52.89 W/m^2K$, $h_h = 84.68 W/m^2K$, $Nu_c = 6.88$, $Nu_h = 7.45$, $A_m = 40 \times 40 mm^2$, $n = 127$.				

Similarly, the thermoelectric heat pump performance showed significant improvement in the heating mode as the figure of merit values increased as seen in Table 4.7. In other words, the power consumption can be significantly reduced with equivalent heating levels. For instance, at $ZT = 2$, the car seat climate control can provide heating power and air temperature difference similar to the present design (47 W and 28°C, respectively) at input power of 30.5 W. This results shows a remarkable gain in the power consumption by roughly 25 %. Such high performance indicates that if new materials with higher ZT values are designed or discovered in the future, the thermoelectric CSCC can be very competitive with other climate control systems in the automotive industry. Moreover, this also can help the future designers of temperature controlled seats by providing a clear vision for the performance of future designs.

Table 4.7 Optimal Design Performance for Different ZT Values in Heating Mode.

Parameter	$ZT_{\infty h,in} = 0.68$ (PRESENT)	$ZT_{\infty h,in} = 1$	$ZT_{\infty h,in} = 1.5$	$ZT_{\infty h,in} = 2$
$P_{in}(W)$	40.57	40.31	40.53	40.46
$G_{e,opt}(mm)$	1.59	1.513	1.353	1.237
$I_{opt}(A)$	4.2	4.66	5.04	5.24
$T_c(K)$	253.57	251.29	248.72	246.87
$T_h(K)$	307.08	312.04	317.87	321.81
$Q_h(W)$	47.91	52.17	57.7	61.44
$\Delta T_{heating}$	28.806	32.48	35.92	48.25
COP	1.18	1.29	1.423	1.519
$DMU(\%)$	38.3	41.7	46.16	49.15
$PD(W/cm^2)$	2.994	3.26	3.57	3.84
Inputs: $T_{\infty c,in} = 257.04 K$, $T_{\infty h,in} = 257.04 K$ $V_c = 8 cfm$, $V_h = 3 cfm$, $A_{s,c} = 40 \times 40 mm^2$, $A_{s,h} = 40 \times 40 mm^2$, $b_c = 25 mm$, $b_h = 20 mm$, $t_c = 0.45 mm$, $z_c = 1.248 mm$, $n_c = 23$, $t_h = 0.36 mm$, $z_h = 1.84 mm$, $n_c = 18$, $h_c = 81.55 W/m^2K$, $h_h = 52.89 W/m^2K$, $Nu_c = 7.45$, $Nu_h = 6.88$, $A_m = 40 \times 40 mm^2$, $n = 127$.				

4.5 Experimental Validation of the New Design

One of the goals of this study is to experimentally validate the accuracy of the optimal design analytical model. Therefore, the experimental setup discussed in CHAPTER III is implemented to evaluate the performance of the new design. The theoretical results, which were calculated utilizing the effective material properties with the basic heat balance equations (3.5 - 3.10) were compared against the new design performance data obtained experimentally in this work to validate the present work. The experimental junction temperatures were obtained from the extrapolation of the thermocouples temperature reading at the aluminum blocks, while the analytical junction temperatures were calculated from solving the six heat balance equations at given initial values. This comparison is made at given constant air flow rates at the cold and the hot heat sinks and variable input current at the thermoelectric cooler module for both heating and cooling modes.

4.6 Cooling Mode Experimental Validation

Figure 4.10 illustrates the comparison between the experimental and the theoretical junction temperatures for the cooling mode as a function of the applied current. The analytical modeling includes many conceptual and experimental features such as the fin and heat sinks efficiencies, Nusselt number correlations, the effective material properties of the TEC module and the uncertainties of the temperature measurements and their extrapolation. Nevertheless, the comparison of the calculated cold and the hot junction temperatures indicate, interestingly, good agreement with the experimental data except for high values of input current, where the errors between the experimental and predicted values start to grow up slightly. This is usually due to the use of the effective material

properties which are temperature dependent and were selected at the room temperature of 30°C, but in reality the thermoelectric material properties depend on temperature and have different values at higher operating temperatures.

The experimental values of the junction temperatures were inserted into the thermoelectric ideal equations to calculate the heat fluxes at the cold and the hot junctions. Figure 4.11 shows the comparison between the experimental and theoretical cooling power (refers to Figure 4.11a) and the coefficient of performance COP (refer to Figure 4.11b) at variable input power with fair agreement. These values were obtained using the measured junction temperatures with the thermoelectric ideal equations. The cold and hot air inlet temperatures of 22.2 °C and 22.7 °C, respectively, were used as the average temperature measured during the experiment.

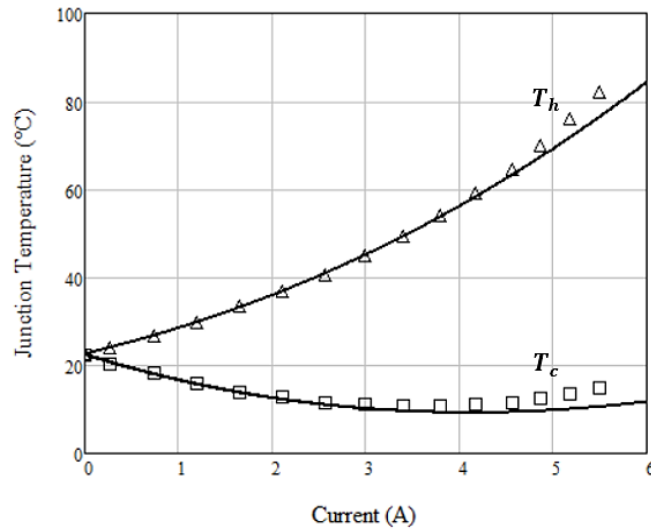
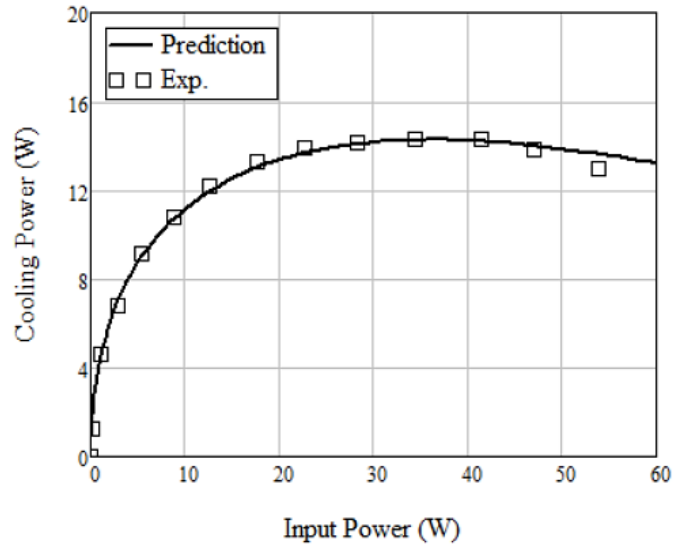
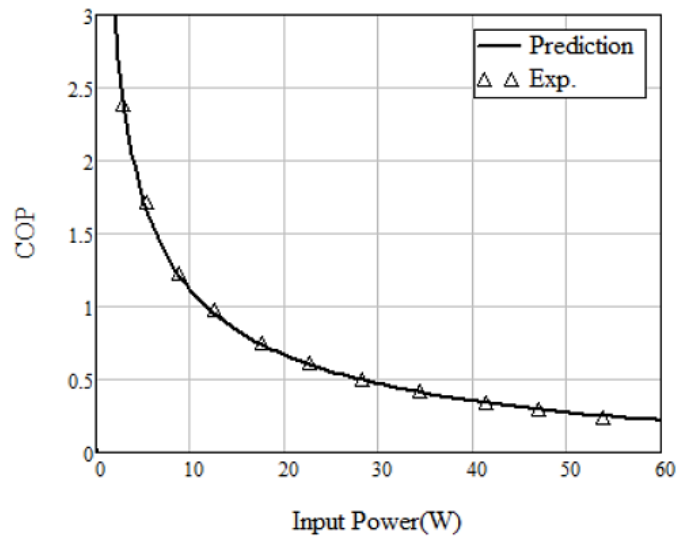


Figure 4.10 Cold and hot junction temperatures versus current. The symbols are measurements, and the lines are predictions.



(a)



(b)

Figure 4.11 Comparison between experimental and analytical (a) cooling power and (b) COP vs. input power.

One of the current optimal design goals was to obtain the maximum possible COP at a given input power of roughly 40 W for each heat pump by optimizing the dimensionless input current (N_I) and the thermal conductance (N_k). Table 4.8 shows a

comparison between the optimal design with the optimized heat sinks, the experiment and the prediction (with and without aluminum blocks) at the same input power. It is clear that the aluminum blocks have a negative effect on the overall performance as they increase the thermal resistances (R_c and R_h) at the two sides of the module. The predicted results indicate that the heat pump COP increases by about 14.6 % as the aluminum blocks are eliminated from the system calculations. Also, using the optimized heat sinks can reduce the thermal resistances at the hot and the cold sides and, thus, improves the heat transfer resulting in higher cooling power and COP. It is important to remember that the tested TEC module has a different thermoelement geometric ratio than the optimum design with optimized heat sinks, which also contributes in some improvement in the system performance.

Table 4.8 Comparison between the Experiment, Prediction, and Optimum Design results for the cooling mode.

Description	R_c (K/W)	R_h (K/W)	N_I	I_m (A)	N_k	G_e (mm)	\dot{Q}_c (W)	COP
Experiment	0.622	0.577	0.134	4.46	0.398	1.7	14.05	0.351
Prediction	0.622	0.577	0.13	4.32	0.398	1.7	14.23	0.356
Prediction (W/O aluminum blocks)	0.538	0.493	0.112	4.36	0.34	1.7	16.32	0.408
Optimal design (W/O aluminum blocks and with optimal heat sinks)	0.744	0.338	0.0775	4.33	0.219	1.59	18.129	0.439
Given: $T_{\infty c, in} = 22.2^\circ C$, $T_{\infty h, in} = 22.7^\circ C$, $\dot{V}_c = 3CFM$, $\dot{V}_h = 8CFM$, $P_{in} = 40W$, $ZT_{\infty h, in} = 0.79$, and $n = 127$.								

Furthermore, Figure 4.12 compares the experimental and predicted cold air temperature difference and COP with the optimal design performance at different input

powers. This figure also shows the improvement in the performance when the aluminum blocks are removed and using the optimized thermoelectric module and heat sinks. One of the reasons for the significant disparity in the cold air temperature difference between the optimum values and the predicted results is because of the different heat sinks fin spacing. The cold heat sink used in the experiment has smaller fin spacing compared to the optimum heat sink, which results in increasing the air velocity between fins. This, in fact, add more heat from the ambient air to the cold heat sink not allowing it to cool down farther. On the other hand, the optimum cold heat sink has wider fin spacing leading to lower heat sink temperatures and higher cold air temperature differences.

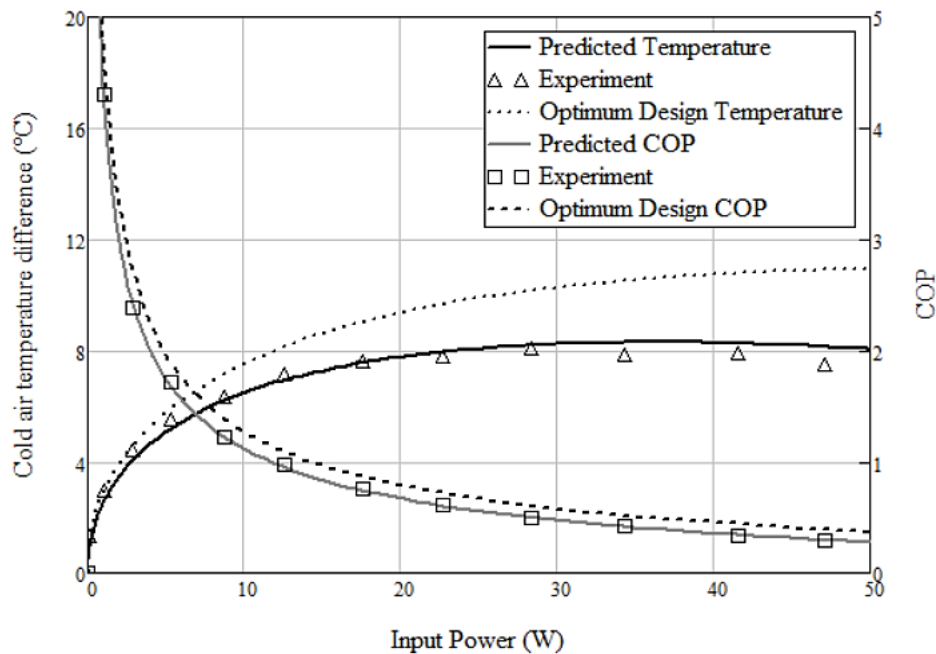


Figure 4.12 For cooling mode, a comparison between experiment and predicted COP and cold air temperature difference vs. input power.

4.6.1 Heating Mode Experimental Validation

As discussed earlier, one of the thermoelectric devices advantages is that they can provide temperature difference on their two sides, which can be used as a source of cooling

and heating depending on the surrounding conditions. The heating mode for the thermoelectric heat pump can be achieved simply by reversing the direction of the applied current. Therefore, the same experimental setup (maintaining the same volume flow rates at the two heat sinks) was used to validate the theoretical model of the heating mode. The cold and hot junction temperatures were measured at variable input current, and their extrapolation values were compared against the analytical junction temperatures, as shown in Figure 4.13 with good agreement.

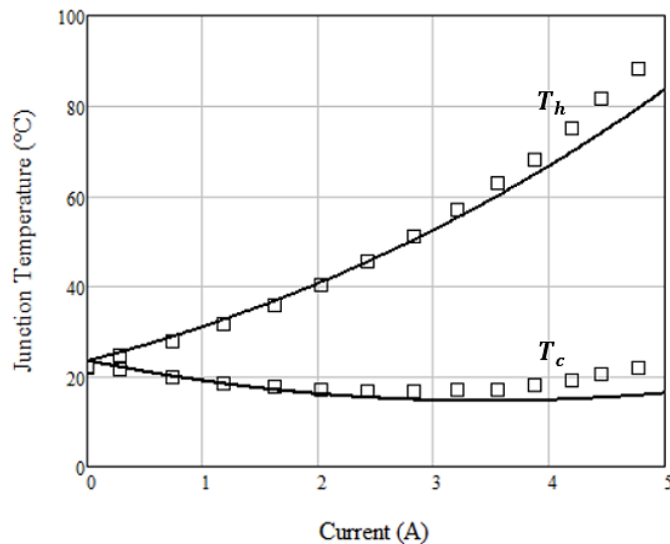
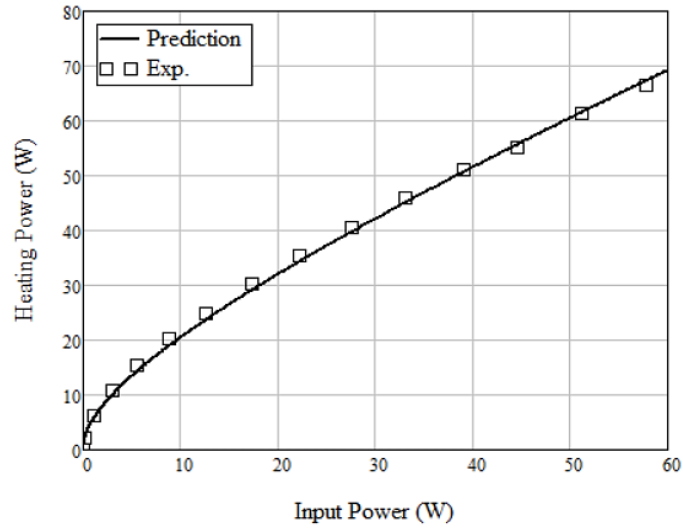


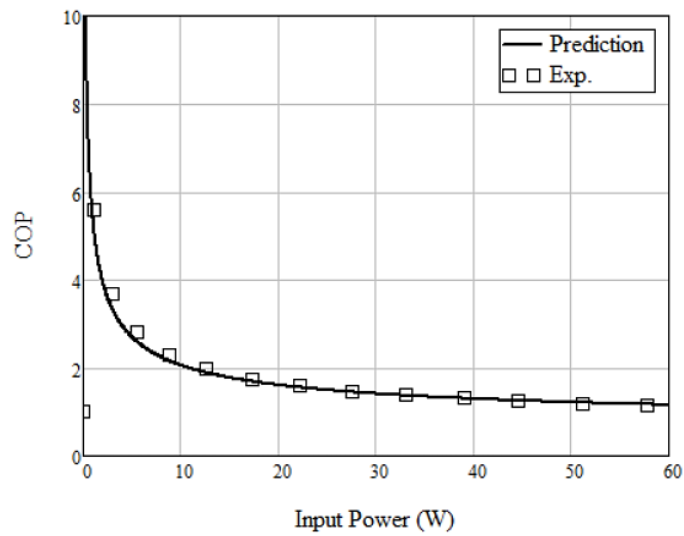
Figure 4.13 Hot and cold junction temperatures versus current. The symbols are measurements, and the lines are predictions.

The experimental values of the heating power are also compared with theoretical results at different input power values as shown in Figure 4.14a. This comparison indicated a very good agreement although with small errors in the junction temperatures between the experiment and the prediction. This is usually because the theoretical and experimental junctions' temperature differences across the thermoelectric device have equal values even at higher input current values. Similarly, Figure 4.14b shows the experimental and

analytical values of the COP as a function of the input power with a very good agreement as well.



(a)



(b)

Figure 4.14 Comparison between experimental and analytical (a) heating power and (b) COP as a function of input power.

Table 4.9 shows a comparison between the experimental, predicted and the optimal design data for the heating mode and at an equalized input power of 40 W. Similar to the cooling mode, the aluminum blocks work negatively, as the performance improves when they are removed from the calculations. However, the heating power shows a small drop when using the optimized heat sinks compared to the predicted heating power when the aluminum blocks are removed. This decline is associated with the different heat sinks with dissimilar fin spacing as discussed in the previous section.

Table 4.9 Comparison between the Experiment, Prediction, and Optimum Design results for the heating mode.

Description	R_c (K/W)	R_h (K/W)	N_l	I_m (A)	N_k	G_e (mm)	\dot{Q}_h (W)	COP
Experiment	0.622	0.591	0.13	4.21	0.408	1.7	51.31	1.28
Prediction	0.622	0.591	0.131	4.26	0.408	1.7	51.68	1.29
Prediction (W/O aluminum blocks)	0.538	0.507	0.113	4.29	0.35	1.7	53.53	1.34
Optimal design (W/O aluminum blocks and with optimal heat sinks)	0.69	0.351	0.0775	4.09	0.219	1.59	51.58	1.28
Given: $T_{\infty c, in} = 23.3^\circ C$, $T_{\infty h, in} = 23.19^\circ C$, $\dot{V}_c = 8CFM$, $\dot{V}_h = 3CFM$, $P_{in} = 40W$, $ZT_{\infty h, in} = 0.79$, and $n = 127$.								

In addition, the experimental, analytical and optimal design comparison of hot air temperature difference at various input powers is shown in Figure 4.15. It was expected that at higher values of the input power, the temperature difference would show larger discrepancies as a result of employing the effective material properties. However, in general, the comparison indicates fair agreement close to the optimal operating condition. In other words, at the optimal input power of 40 W, the error between the predicted and

the experimental values was around 3%. Also, when using the optimized heat sinks, the optimal design performance shows a relatively small improvement in the hot air temperature difference. Figure 4.15 also compares the experimentally obtained and the analytically predicted COP against the optimal design values. The accuracy of the predicted data was better even at higher input power values.

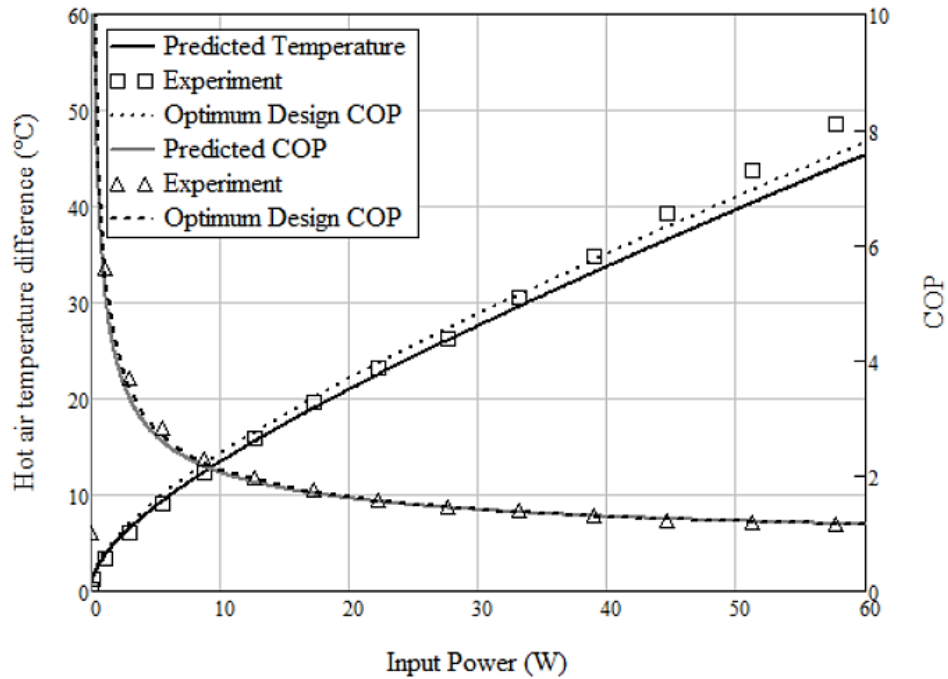


Figure 4.15 For heating mode, a comparison between experiment and prediction COP and hot air temperature difference vs. input power.

CHAPTER V

CONCLUSIONS AND FUTURE WORK

5.1 Conclusions

One of the objectives of the present work was to investigate the optimal design of a thermoelectric cooler applied for a car seat climate control (CSCC). This optimization utilizes a newly developed optimization theory with the dimensional technique to simultaneously obtain the optimum combination of the dimensionless applied current N_I and the dimensionless thermal conductance N_k to determine the optimum cooling/heating power and COPs suitable for a temperature controlled seat. The optimal design of Feher's heat pump was analyzed maintaining the same input parameters and overall geometry. The optimized results indicated an increase in the COP by about 10% in the cooling mode compared with Feher's design.

Then, a new thermoelectric CSCC design which consists of two heat pumps installed at the backrest and the seat rest was presented. In addition to obtaining the optimum thermoelectric geometric ratio, the new model provides also the optimum input current values for the transient (short time) and steady state (long time) operating conditions. The new design performance for the whole seat was utilized and compared against Feher's VTS and its optimal design. This comparison indicated that with a

significant size reduction and very slight increase in the overall height of the system, the optimized results of the new design showed comparable performance.

The second aim of this study was to experimentally validate the analytical performance results of the thermoelectric heat pump. Thus, based on the optimal design parameters of the thermoelectric module and the heat sinks, two experiments (cooling and heating modes) were conducted to validate the present theoretical model. The effective material properties of the commercial thermoelectric module were obtained using the manufacturer-provided maximum parameters in order to reduce the errors associated with the assumptions used in the thermoelectric ideal equations. Once the effective material properties are obtained, the performance of the thermoelectric system was analytically evaluated and compared with the experimental data. Although the present model was constructed based on the simple thermoelectric ideal equation, the analytical results showed very good agreement with the experiment at most of the operating conditions for both cooling and heating modes.

One of the critical factors that can improve the performance of thermoelectric systems is the appropriate thermal design and optimization. At present, the commonly used technique to optimize and evaluate the performance of thermoelectric systems for different applications is through experiments or advanced simulation software, which are usually costly and time-consuming for designers. The present work represents a simple theoretical approach that may provide the temperature controlled seats designers with an uncomplicated guideline that can contribute in moving this feature from optional to standard vehicle equipment.

5.2 Future Work

First, to efficiently deliver the conditioned air to the occupant body through the seat surface and to reject the waste air to the vehicle cabin, it would be essential to design and optimize the air ducting system. Properly designed air ducts can also reduce the pressure drop which can decrease the blowers power consumption and improve the overall efficiency of the system.

Second, in the current design, the wasted conditioned air can be recirculated into the fan by a recirculating duct instead of completely consumed at the end of the seat channels. This option can be verified through experimental measurements. However, preliminary calculations indicate that much lower power consumption can be achieved with equivalent cooling/heating.

Finally, validation with real car seat tests would be necessary to determine the levels of comfort that this design is able to provide.

REFERENCES

- [1] R. Chein and G. Huang, "Thermoelectric cooler application in electric cooling," *Appl Therm Eng*, no. 24, pp. 2207-17, 2004.
- [2] H. J. Goldsmid, Introduction to thermoelectricity, Heidelberg, Germany: Spriner, 2010.
- [3] D. M. Rowe, Thermoelectric handbook: micro to nano, New York: Taylor & Francis, 2006.
- [4] N. Kempf and Y. Zhang, "Design and optimization of automotive thermoelectric generators for maximum fuel efficiency improvement," *Energy Conversion and Management*, no. 121, pp. 224-231, 2016.
- [5] C. T. Hsu, G. Y. Huang, H. S. Chu, B. Yu and D. J. Yao, "Experiments and simulations on low-temperature harvesting," *Appl Energy*, no. 88, pp. 1291-7, 2011.
- [6] D. Kraemer, "Modeling and optimization of solar thermoelectric generators for terrestrial applications," *Solar Energy*, no. 86, pp. 1338-1350, 2012.
- [7] L. E. Alkire and W. H. Carter, "Ventilation Systems for Vehicles," *U.S. Patent 1*, pp. 439,681, December 26, 1922.
- [8] L. H. Johnson, "Heating and Cooling Employing Aerated Car Seats," *U.S. Patent*, no. US3127931, 1964.
- [9] C. Malvicino, S. Mola, A. Zussino and J. Wolowicz, "The Seat Thermal-Hygrometric Performance Measurement and Its Correlation With Perceived Comfort," *SAE Technical Paper*, no. doi:10.4271/2001-01-3432, 2001.
- [10] D. F. Gallup and a. et, "Thermally Conditioned Vehicle Seat," Delphi Technologies, Inc, Troy, MI. US7238101, 2007.
- [11] L. E. Bell, "Thermoelectric Heat exchanger," Gentherm Incorporated, Northville, MI. US RE44,272, 2013.
- [12] Gentherm. [Online]. Available: <http://www.gentherm.com/>. [Accessed 2016].
- [13] H. Lee, "Optimal design of thermoelectric devices with dimensional analysis," *Applied Energy*, vol. 106, pp. 79-88, 2013.

- [14] H. Lee, A. Atta and S. Weera, "Performance prediction of commercial thermoelectric cooler modules using the effective material properties," *Journal of Electronic Materials*, vol. 44, no. 6, pp. 2157-2165, 2015.
- [15] T. J. Seebeck, "Magnetic polarization of metals and minerals," *Abhandlungen der Königlich Akademie der Wissenschaften zu Berlin* ed, Berlin, Germany, 1822.
- [16] G. S. Nolas, J. Sharp and H. J. Goldsmid, "Thermoelectrics," Springer, Heidelberg, Germany, 2001.
- [17] H. Lee, *Thermal Design: Heat Sinks, Thermoelectrics, Heat Pipes, Compact Heat Exchangers, and Solar Cells*, Hoboken: John Wiley & Sons, Inc, 2010.
- [18] H. Lee, *Thermoelectrics: Design and Materials*, 1 edition, John Wiley, ISBN-13: 978-1118848951, Nov, 2016, p. 464 pages.
- [19] L. Hicks and M. Dresselhaus, "Effect of quantum-well structures on the thermoelectric," *Physical Review B*, vol. 47, no. 19, pp. 12727-12731, 1993.
- [20] L. D. Hicks and M. S. Dresselhaus, "Thermoelectric figure of merit of a one-dimensional conductor," *Physical Review B*, vol. 47, no. 24, pp. 16631-16634, 1993.
- [21] L. Onsager, "Reciprocal Relations in Irreversible Processes. I.," *Physical Review*, vol. 37, no. 4, pp. 405-426, 1931.
- [22] H. Lee, "The Thomson effect and the ideal equation on thermoelectric coolers," *Energy*, vol. 56, pp. 61-69, 2013.
- [23] E. J. Sandoz-Rosado, "Investigation and Development of Advanced Models of Thermoelectric Generators for Power Generation Applications," Rochester Institute of Technology, Master Thesis UMI Number: 1469748, Rochester, 2009.
- [24] A. Elarusi, H. Fagehi, A. Attar and H. Lee, "Theoretical Approach to Predict the Performance of Thermoelectric Generator Modules," *Journal of Electronic Materials*, doi: 10.1007/s11664-016-4948-9, 2016.
- [25] S. L. L. Weera, "Analytical performance evaluation of thermoelectric modules using effective material properties," Master's Theses. Paper 483, 2014.
- [26] "TETECHNOLOGY, INC" 2016. [Online]. Available: <http://www.tetech.com/>.
- [27] S. Feher, "Thermoelectric Air Conditioned Variable Temperature Seat (VTS) and Effect Upon Vehicle Occupant Comfort, Vehicle Energy Efficiency, and Vehicle Environmental Compatibility," *SAE Technical Paper 931111*, 1993.
- [28] S. Feher, "Stirling Air Conditioned Variable Temperature Seat (SVTS) and Comparison with Thermoelectric Air Conditioned Variable Temperature Seat (VTS)," *SAE Technical Paper 980661*, 1998.

- [29] M. Menon and H. H. Asada, "Iterative learning control of shape memory alloy actuators with thermoelectric temperature regulation for a multifunctional car seat," in *American Control Conference*, USA, 2006.
- [30] H.-S. Choi, S. Yun and K.-i. Whang, "Development of a temperature-controlled car-seat system utilizing thermoelectric device," *Applied Thermal Engineering*, vol. 27, no. 17, pp. 2841-2849, 2007.
- [31] M. Vinoth and D. Prema, "Automated car safety cooling system using thermoelectric cooler," in *International conference on computation of power, energy, information and communication (ICCPECI)*, Chennai, 2014.
- [32] H. DU, Y. P. Wang, X. H. Yuan, Y. D. Deng and C. Q. Su, "Experimental Investigation of a Temperature-Controlled Car Seat Powered by an Exhaust Thermoelectric Generator," *Journal of Electronic Materials*, vol. 45, no. 3, pp. 1529-1539, 2015.
- [33] M. H. Makhmalbaf, "Experimental study on convective heat transfer coefficient around a vertical hexagonal rod bundle," *Heat and Mass Transfer*, vol. 48, no. 6, pp. 1023-1029, 2012.
- [34] P. Teertstra, M. Yovanvich, J. Culham and T. Lemczyk, "Analytical forced convection modeling of plate fin heat sinks," in *Fifteenth Annual IEEE Semiconductor Thermal Measurement and Management Symposium*, San Diego, CA, USA, 1999.
- [35] W. Zhimin and C. K. Fah, "The optimum thermal design of microchannel heat sinks," in *Electronic Packaging Technology Conference*, 1997.
- [36] M. Yamanashi, "A new approach to optimum design in thermoelectric cooling systems," *Journal of Applied Physics*, vol. 80, no. 9, pp. 5494-5502, 1996.
- [37] X. C. Xuan, "Optimum design of a thermoelectric device," *Semiconductor Science and Technology*, vol. 17, no. 2, pp. 114-119, 2002.
- [38] Y. Pan, B. Lin and J. Chen, "Performance analysis and parametric optimal design of an irreversible multi-couple thermoelectric refrigerator under various operating conditions," *Applied Energy*, vol. 84, no. 9, pp. 882-892, 2007.
- [39] A. Attar, H. Lee and S. Weera, "Optimal design of automotive thermoelectric air conditioner (TEAC)," *Journal of Electronic Materials*, vol. 43, no. 6, pp. 2179-2187, 2014.
- [40] A. Attar and H. Lee, "Designing and testing the optimum design of automotive air-to-air thermoelectric air conditioner (TEAC) system," *Energy Conversion and Management*, vol. 112, no. 0196-8904, pp. 328-336, 2016.
- [41] A. Attar, H. Lee and S. Weera, "Experimental validation of the optimum design of an automotive air-to-air thermoelectric air conditioner (TEAC),," *Journal of Electronic Material*, vol. 44, no. 6, pp. 2177-2185, 2015.

- [42] Y. W. Chang, C. C. Chan, M. T. Ke and S. L. Chen, "Thermoelectric air-cooling module for electronic devices," *Applied Thermal Engineering*, vol. 29, pp. 2731-2737, 2009.
- [43] D. Liu, F. Y. Zhao, H. X. Yang and G. F. Tang, "Thermoelectric mini cooler coupled with micro thermosiphon for CPU cooling system," *Energy*, vol. 83, pp. 29-36, 2015.
- [44] H. S. Huang, Y. C. Weng, S. L. Chang, S. L. Chen and M. T. Ke, "Thermoelectric water-cooling device applied to electronic equipment," *International Communications in Heat and Mass Transfere*, vol. 37, pp. 140-146, 2010.
- [45] S. B. Riffat, S. A. Omer and X. Ma, "A novel thermoelectric refrigeration system employing heat pipes and a phase change material: an experimental investigation," *Renewable Energy*, vol. 23, no. 2, pp. 313-323, 2001.
- [46] M. Cosnier, G. Fraisse and L. Luo, "An experimental and numerical study of a thermoelectric air-cooling and air-heating system," *International Journal of Refrigeration*, vol. 31, no. 6, pp. 1051-1062, 2008.
- [47] D. Zhao and G. Tan, "Experimental evaluation of a prototype thermoelectric system integrated with PCM (phase change material) for space cooling," *Energy*, vol. 68, pp. 658-666, 2014.
- [48] Y. J. Dai, R. Z. Wang and L. Ni, "Experimental investigation and analysis on a thermoelectric refrigerator driven by solar cells," *Solar Energy Materials and Solar Cells*, vol. 77, no. 4, pp. 377-391, 2003.
- [49] A. Elarusi, A. Attar and H. Lee, "Optimal Design of a Thermoelectric Cooling/Heating System for Car Seat Climate Control (CSCC)," *Journal of Electronic Materials*, no. the paper was accepted and under publication, 2016.